

**STOCHASTIC MODELING OF EQUILIBRIUM SPEED-DENSITY  
RELATIONSHIP FOR NON-LANE-BASED HETEROGENEOUS TRAFFIC**

by

Md. Yusuf Ali

MASTER OF SCIENCE IN CIVIL ENGINEERING (TRANSPORTATION)



Department of Civil Engineering

BANGLADESH UNIVERSITY OF ENGINEERING AND TECHNOLOGY,  
DHAKA, BANGLADESH

July, 2021

**STOCHASTIC MODELING OF EQUILIBRIUM SPEED-DENSITY RELATIONSHIP  
FOR NON-LANE-BASED HETEROGENEOUS TRAFFIC**



A thesis submitted to the Department of Civil Engineering,  
Bangladesh University of Engineering and Technology, Dhaka, Bangladesh  
in partial fulfillment of the requirements for the degree of

**MASTER OF SCIENCE IN CIVIL ENGINEERING (TRANSPORTATION)**

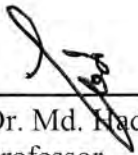
by

Md. Yusuf Ali

Department of Civil Engineering  
BANGLADESH UNIVERSITY OF ENGINEERING AND TECHNOLOGY  
Dhaka, Bangladesh  
July, 2021

The thesis titled 'Stochastic Modeling Of Equilibrium Speed-Density Relationship For Non-Lane-Based Heterogeneous Traffic', submitted by Md.Yusuf Ali, Roll No: 0417042425 (F), Session: April 2017 has been accepted as satisfactory in partial fulfillment of the requirement for the degree of Master of Science in Civil Engineering (Transportation) on July 10, 2021.

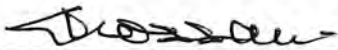
### BOARD OF EXAMINERS



---

Dr. Md. Nadiuzzaman  
Professor  
Department of Civil Engineering  
Bangladesh University of Engineering and Technology (BUET)  
Dhaka 1000, Bangladesh

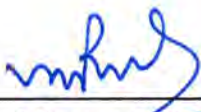
Chairman



---

Dr. Md. Delwar Hossain  
Professor and Head  
Department of Civil Engineering  
Bangladesh University of Engineering and Technology (BUET)  
Dhaka 1000, Bangladesh

Member  
(Ex-officio)



---

Dr. Md. Mizanur Rahman  
Professor  
Department of Civil Engineering  
Bangladesh University of Engineering and Technology (BUET)  
Dhaka 1000, Bangladesh

Member



---

Dr. Mohammed Russedul Islam  
Associate Professor  
Department of Civil Engineering  
Military Institute of Science and Technology

Member  
(External)

## DECLARATION

It is hereby declared that this thesis or any part of it has not been submitted elsewhere for the award of any degree or diploma.

Md. Yusuf Ali

July 10, 2021

Md. Yusuf Ali

***DEDICATED***

*To*

*My Parents and Wife*

## **ACKNOWLEDGEMENT**

I am deeply indebted to and want to express my utmost gratitude to my thesis supervisor, Dr. Md. Hadiuzzaman, Professor, Department of Civil Engineering, BUET, for his guidance, generous help, constructive comments, invaluable suggestions what has made it possible to prepare this concerted thesis. I would like to thank Nazmul Haque, Lecturer, DUET for his untiring support throughout the progress of the thesis work. His endurance, consistent efforts, ceaseless inspiration have helped me to work diligently for the completion of this research work. Without his continuous support and guidance, this thesis would not have materialized.

I want to thank the Department of Civil Engineering, BUET for providing me an opportunity to work on this contemporary thesis work.

I am grateful to my family, friends, and colleagues for their constant encouragement and cooperation in pursuing my goals.

## ABSTRACT

In traffic flow theory, fundamental diagrams (FDs) address the relationship among three variables: flow, speed and density. Among them, equilibrium speed-density relationship explains the speed dynamics in road incorporating two important parameters, i.e., free-flow speed and jam density. This speed-density relationship is widely used for designing strategies related to traffic control and management. The analysis of real time traffic dynamics largely depends upon the output from the fundamental diagram where the congestion occurs. Fundamental diagram is the relation between traffic speed and density which comes from the driver's speed choices under capricious car following distances. About eighty-five years ago Greenshields proposed a seminal linear relationship between speed and density. Later, a number of researchers have devoted to reviewing or improving such a simplified relationship. But these models are mainly deterministic in nature which cannot addresses the randomness of traffic behavior i.e. driver's behavior. Therefore, the randomness makes speed-density relation to view as a stochastic process. Additionally, most of the existing speed-density model are applicable for traffic having strict lane discipline along with homogeneous traffic stream. They are not being formulated, calibrated and validated for non-lane-based heterogeneous traffic (prevails in many south Asian countries) with unpredictable randomness. Moreover, these models cannot calibrate the jam density or shockwave speed in case of an incomplete dataset (e.g. collected traffic data includes only free-flow traffic regime). Furthermore, human decisions about lane change, gap acceptance, and acceleration and deceleration process affect the equilibrium speed–density relationship. Thus, a highly adaptive and robust FD model is required, which can incorporate non-lane-based heterogeneous behavior of traffic and randomness.

This study aims to develop such a stochastic speed-density model to better represent empirical observations from non-lane based heterogeneous traffic and provide a base for a stochastic prediction of traffic dynamics. It will be more acceptable if such a model is formulated with both mathematical elegance and empirical accuracy. The mathematical elegance of the model mainly depends upon a single equation (single-regime) with physically meaningful parameters and empirical accuracy comes from the model fitness. For this study, video data of several days have been collected using high-resolution camera from the study corridor i.e. Tongi Diversion Road, a section of the Dhaka-Mymensingh Highway (N3), containing non-lane based heterogeneous traffic at five locations (mainline, on-ramp close to mainline, off-ramp close to mainline, on-ramp and off-ramp) considering the geometric

variation. The collected traffic flow data is then extracted by using pixel-based heterogeneous traffic flow measurement technique. Lane based homogeneous traffic data is also collected from I-80 Berkeley at five different locations to prove the robustness of the proposed model. This data is used to develop the stochastic speed-density model choosing the best transfer function from various transfer function i.e hardlimit, heaviside, saturation, pureline. Among them the best fit saturation function is chosen based on the goodness of fit ( $R^2$ ).

The data is split in different composition like 50-50, 60-40, 70-30, 75-25, 80-20, 85-15, 90-10 in training and testing data set respectively. Among the above composition the 80-20 split division gives better results in terms of goodness of fit ( $R^2=0.96259$ ). Four types of hidden layer number (2, 3, 4, 5, 6) are considered since it gives flexibility of the speed-density curve for fitting this curve properly. It is seen from the analysis hidden layer number 5 gives better results. Three types of optimization algorithm named Bayesian regularization, Scaled conjugate gradient, Levenberg-Marquardt (LM) is exercised. Among them LM algorithm performs well. Additionally, it takes less memory and time to fit. This study also analyses the effect of time aggregation 20 seconds, 1, 2, 3, 5, 6 minutes and it can be concluded that 5 min minutes yields better performance. The proposed model is then compared with other prominent existing model i.e. ANFIS, 5 PL model. The study analysis dictates that ANN model performs well than other model. From this study, three new equations have been developed for free-flow speed ( $V_f$ ), jam density ( $\rho_j$ ) and capacity ( $C$ ). The model is further used to develop a tool named **Fundamental DiagRam CalibrAtion using Machine LEarning (FRAME)** which can calibrate the speed-density relationship automatically.



## TABLE OF CONTENTS

<b>DECLARATION</b>	<b>IV</b>
<b>ACKNOWLEDGEMENT</b>	<b>VI</b>
<b>ABSTRACT</b>	<b>VII</b>
<b>TABLE OF CONTENTS</b>	<b>IX</b>
<b>LIST OF FIGURES</b>	<b>XIII</b>
<b>LIST OF TABLES</b>	<b>XV</b>
<b>LIST OF ABBREVIATIONS</b>	<b>XVI</b>
<b>CHAPTER 1 INTRODUCTION</b>	<b>1</b>
1.1 Background	1
1.2 Problem Statement	3
1.3 Specific Objectives	5
1.4 Thesis Structure	5
<b>CHAPTER 2 LITERATURE REVIEW</b>	<b>7</b>
2.1 Introduction	7
2.2 Significance of Fundamental Diagram Models	7
2.3 Deterministic Single-Regime Models	8
2.3.1 Model of Greenshields	10
2.3.2 Logarithmic Greenberg Model	12
	ix

2.3.3 Underwood Exponential Model	13
2.3.4 Drake Model	14
2.3.5 Pipe-Munjaj Generalized Model	15
2.3.6 Drew Model	16
2.3.7 Newell Model	17
2.3.8 Modified Greenshields Model	18
2.3.9 Payne's Model in FREFLO(Free-Flow)	19
2.3.10 Kerner and Konhauser's Model	20
2.4 Deterministic Multi-Regime Models	21
2.5 Stochastic Speed-Density Models	24
2.6 Motivation of the Work	24
<b>CHAPTER 3 FRAMEWORK OF STOCHASTIC MODELING</b>	<b>26</b>
3.1 Introduction	26
3.2 Artificial Neural Network	26
3.2.1 History of Artificial Neural Systems Development	26
3.2.2 Neuron Modeling for Artificial Neural Systems	27
3.2.3 Models of Artificial Neural Networks	29
3.2.3.1 Feedforward Network	29
3.2.4 Supervised and Unsupervised Learning	30
3.2.5 Neural Network Learning Rules	32
3.3 Optimization Algorithm	33

3.4 Flow Chart for Proposed Model	33
3.5 ANN Methodology for the Proposed Model	35
3.6 Fundamental Diagram for Incomplete Data Set	41
3.7 Developing a Tool to Calibrate Speed-density Diagram Automatically	41
<b>CHAPTER 4 DATA COLLECTION AND PROCESSING</b>	<b>43</b>
4.1. Introduction	43
4.2 Data Collection Location	43
4.3. Data Processing	48
4.4 Data Extraction Technique and Quality Assurance	48
4.5 Extracted Data	52
<b>CHAPTER 5 CALIBRATION RESULTS AND MODEL VALIDATION</b>	<b>53</b>
5.1 Introduction	53
5.2 Effects of Different Parameters in Proposed Model	54
5.2.1 Effect of Size of Training and Testing Data Sets	54
5.2.2 Effect of Hidden Layer Number	55
5.2.3 Effect of Training Algorithm	56
5.2.4 Effect of Number of Epoch	57
5.2.5 Effects of Time Aggregation Level on Speed-density Relationship	58
5.3 Model Validation Result	60
5.3.1 Comparison with Single Regime Models	60
5.3.2 Comparison with Multi-Regime Models	65

5.4 Proposed Model Performance for Non-Lane Based Traffic Condition	66
<b>CHAPTER 6 CONCLUSION AND RECOMMENDATION</b>	<b>71</b>
6.1 Introduction	71
6.2 Key Findings	72
6.3 Application of Stochastic Speed-Density Model	74
6.4 Limitations and Recommendations for Further Research	76
<b>REFERENCES</b>	<b>77</b>
<b>APPENDIX A-1: RESULTS OF THE PROPOSED MODEL</b>	<b>82</b>
<b>APPENDIX A-2: GRAPHICAL REPRESENTATION OF MODEL PERFORMANCE</b>	<b>90</b>
<b>APPENDIX A-3: EXTRACTED TRAFFIC DATA</b>	<b>110</b>

## LIST OF FIGURES

Figure 1:1 The scattering effects of the fundamental relationship from Berkeley I-80 observations	3
Figure 2:1 Plot of single-regime deterministic speed-density models	10
Figure 2:2 Performance of Greenshields model against empirical data (Wang, 2010)	11
Figure 2:3 Performance of Greenberg model against empirical data (Wang, 2010)	12
Figure 2:4 Performance of Underwood model against empirical data (Wang, 2010)	13
Figure 2:5 Performance of Drake model against empirical data (Wang, 2010)	14
Figure 2:6 Performance of Pipe-Munjaj model against empirical data (Wang, 2010)	15
Figure 2:7 Performance of Drew model against empirical data (Wang, 2010)	16
Figure 2:8 Performance of Newell model against empirical data (Wang, 2010)	17
Figure 2:9 Performance of modified Greenshield model against empirical data (Wang, 2010)	18
Figure 2:10 Performance of Payne model against empirical data (Wang, 2010)	19
Figure 2:11 Performance of Kerner and Konhauer model against empirical data (Wang, 2010)	20
Figure 2:12 Performance of Edie model against empirical data (Wang, 2010)	22
Figure 2:13 Performance of modified Greenberg model against empirical data (Wang, 2010)	22
Figure 2:14 Performance of three-regime linear model against empirical data (Wang, 2010)	23
Figure 2:15 Performance of two regime model against empirical data (Wang, 2010)	23
Figure 3:1 General symbol of neuron consisting of processing node and synaptic connections (McCulloch and Pitts, 1943)	28
Figure 3:2 Single-layer feedforward network: (a) interconnection; and (b) scheme and block diagram Feedforward network is used during the simulation of the proposed model	30
Figure 3:3 Block diagram for explanation of basic learning modes: (a) supervised learning; and (b) unsupervised learning	31
Figure 3:4 Flow diagram of proposed model using neural network	34
Figure 3:5 Automatic speed-density diagram calibrating tool	42
Figure 4:1 Data collection point along study corridor (Source: Google Map)	45
Figure 4:2 Illustration of layout of study site I-80, Berkeley (not to scale)	46
Figure 4:3 Detailing of camera setting for data collection	47

Figure 4:4 Flow chart of data extraction methodology	49
Figure 4:5 Screenshot of data extraction trajectory	50
Figure 4:6 Screenshot of area selection for data extraction	51
Figure 4:7 Screenshot of vehicles detection and counting block	51
Figure 4:8 Screenshot of tracked binary image for illumination of vehicles	52
Figure 5:1 Effect of time aggregation level on speed-density relationship at location on ramp	59
Figure 5:2 Comparison of different model with proposed model observed from mainline	62
Figure 5:3 Comparison of different model with proposed model observed from mainline near to on-ramp	63
Figure 5:4 Comparison of different model with proposed model observed from off ramp	64
Figure 5:5 Comparison of different model with proposed model observed from on-ramp	65
Figure 5:6 Graphical representation of different model performances at I-80 on- mainline near to off-ramp	66
Figure 5:7 Graphical representation of proposed model performance for non-lane based heterogeneous traffic at (a) main line close to on- ramp; (b) off- ramp; (c) on-ramp; (d) main line close to off- ramp; and (e) main line	69

## LIST OF TABLES

Table 2.1 Deterministic single-regime speed-density models	9
Table 2.2 Deterministic multi-regime speed-density models	21
Table 4.1 Data collected from study corridor	52
Table 5.1 Effect of different composition of training dataset on fitness of data ( $R^2$ values) for different scenarios	55
Table 5.2 Effect of hidden layer number on fitness of data ( $R^2$ values) for different scenarios	56
Table 5.3 Performance comparison among different algorithm to fit the data in terms of fitness value ( $R^2$ )	57
Table 5.4 Effect of different interval of time aggregation	59
Table 5.5 Performance comparison among different model in estimation of fundamental diagram parameter	61
Table 5.6 Performance evaluation of the proposed model for non-lane based heterogeneous traffic condition	70

## LIST OF ABBREVIATIONS

ANN	Artificial Neural Network
ANFIS	Adaptive Neuro Fuzzy Interface System
BGS	Background Subtraction
BR	Bayesian Regularization
BRT	Bus Rapid Transit
FD	Fundamental Diagram
FRAME	Fundamental Diagram Calibration using Machine Learning
GUI	Graphical User Interface
ITS	Intelligent Transportation System
LM	Levenberg- Marquardt
LOS	Level Of Service
MAE	Mean Absolute Error
MAPE	Mean Absolute Percentage Error
ME	Mean Error
MPE	Mean Percentage Error
MRT	Mass Rapid Transit
MSE	Mean of Squared Error
RMSE	Root Mean of Squared Error
SCG	Scaled Conjugate Gradient
SC	Scenario
SINN	Single Input Neural Network
TDM	Travel Demand Management
TSM	Transportation System Management



# CHAPTER 1

## INTRODUCTION

### 1.1 Background

Recently, it has been very challenging to ensure sustainable transportation system with boosting user safety, increasing social mobility, repairing outdated and decaying transportation facilities, curbing down carbon dioxide emission and energy consumption, cutting down the chronic traffic congestion. These type of problems remind us the importance of a well-functioning transportation system to strengthen long term competitiveness of any country. Core of this challenge is highway traffic congestion which influences the mobility of the road network inside the metropolitan areas and reduces the social efficiency.

Treatment of highway traffic congestion is generally known as “Congestion Management Strategies”. The main purpose of this management is to increase mobility through lower cost policy-based improvement and technology based solutions. Generally, there are three ways of congestion management strategies: (i) Travel Demand Management (TDM); (ii) Transportation System Management (TSM); and (iii) Intelligent Transportation System (ITS) (Wang, 2010).

The idea of Travel Demand Management (TDM) is to modify current travel patterns through a variety of policy based strategies such as VMT (Vehicle Mile Travel) fee, gas tax, promoting high occupancy vehicle and public transit, ride matching and car sharing, telecommunicating and advanced traveler information. To be more straightforward, the more your travel, the more you have to pay. With the help of this, the recurring congestion due to morning and evening commuters could be shifted to both public transit and non-motorized modes. Moreover, congestion can also be minimized by adapting variation in work hours. Transportation System Management (TSM) and Intelligent Transportation System (ITS) are generally traffic control based strategies. The aim of the traffic control strategy is to maximize number of vehicles allowed on roadway and shorten the travel time to reach destination. To control highways traffic there are two types of control principles: (i) Proactive control; and (ii) Passive control. The passive control is performed through traffic control devices on public streets or highways approaching grade crossings with railroad tracks including advance warning signs, pavement markings and street lighting system. Though traffic condition changes throughout a road section, the passive control system remains same. The essence of proactive control system is

to predict traffic congestions (geographic location) and acting advance of a future condition. Therefore, proactive traffic control needs to predict future traffic flow situation but no prediction is involved in passive control.

A key way to understand the mechanism of traffic congestion formation and dissipation is through mathematical models which cover essential traffic dynamics with predictive power. A mathematical model is a simplified description of a complex system that helps in numerical calculations and quantitative predictions. The prime impetus for traffic modeling is to give proficient learning experiences which will raise awareness and understanding to facilitate one to make educated decisions in suitable transportation management strategies. Usually, there are two approaches to making predictions: (i) Deterministic; and (ii) Stochastic. In a determinist approach, a given input to the deterministic model will always produce exactly same result no matter how many times one replicates the simulation. However, the output of a stochastic model is always represented by probabilistic distributions instead of a fixed value (Wang, 2010). The deterministic models were considered incomplete for this task, thus stochastic models which incorporate randomness are required in order to serve this purpose.

In traffic theory, fundamental diagrams (FDs) address the relationship among three variables: flow, speed and density. Among them, equilibrium speed-density relationship explains the speed dynamics in road incorporating two important parameters, i.e. free-flow speed and jam density. This speed-density relationship is widely used for designing strategies related to traffic control and management. Most of the existing speed-density model are applicable for traffic having strict lane discipline along with homogeneous traffic stream. They are not being formulated, calibrated and validated for non-lane-based heterogeneous traffic (prevails in many south Asian countries) with unpredictable randomness. Moreover, these models cannot calibrate the jam density or shockwave speed in case of an incomplete dataset (e.g. collected traffic data includes only free-flow traffic regime). Furthermore, human decisions about lane change, gap acceptance, and acceleration and deceleration process affect the equilibrium speed–density relationship. Thus, a highly adaptive and robust FD model is required, which can incorporate non-lane-based heterogeneous behavior of traffic and randomness. Since human makes decisions based on complex reasoning and it becomes challenging to formulate an appropriate model for it, making the application of Artificial Neural Network (ANN) systems justified in developing the relationship.

Bangladesh is an emerging economic country in the world. Construction of various capacity augmentation projects like mass rapid transit (MRT), bus rapid transit (BRT), expressway are going on. Traffic management system for these transport projects requires a real time traffic prediction. For example, ramp metering may be needed for traffic management of the expressway during the peak hour. Therefore, a reliable dynamic speed-density model is warranted for this traffic management. This study focuses on developing models to use in traffic management schemes like ramp metering.

## 1.2 Problem Statement

The stochastic speed-density relationship model is largely motivated by the prevailing randomness exhibited in empirical observations that mainly comes from drivers, vehicles, roads, and environmental conditions. Traffic observations depict a spreading effect which is readily seen if speed is plotted against density as shown in Figure 1.1. It is this intrinsic property of transportation system observation which shows that deterministic models should be considered deficient. The basic mechanism behind the observed scattering phenomenon is frequently the effect of a large number of factors (i.e. driver behaviors, highway geometries, and vehicle characteristics) which influence the plot but are not modeled explicitly.

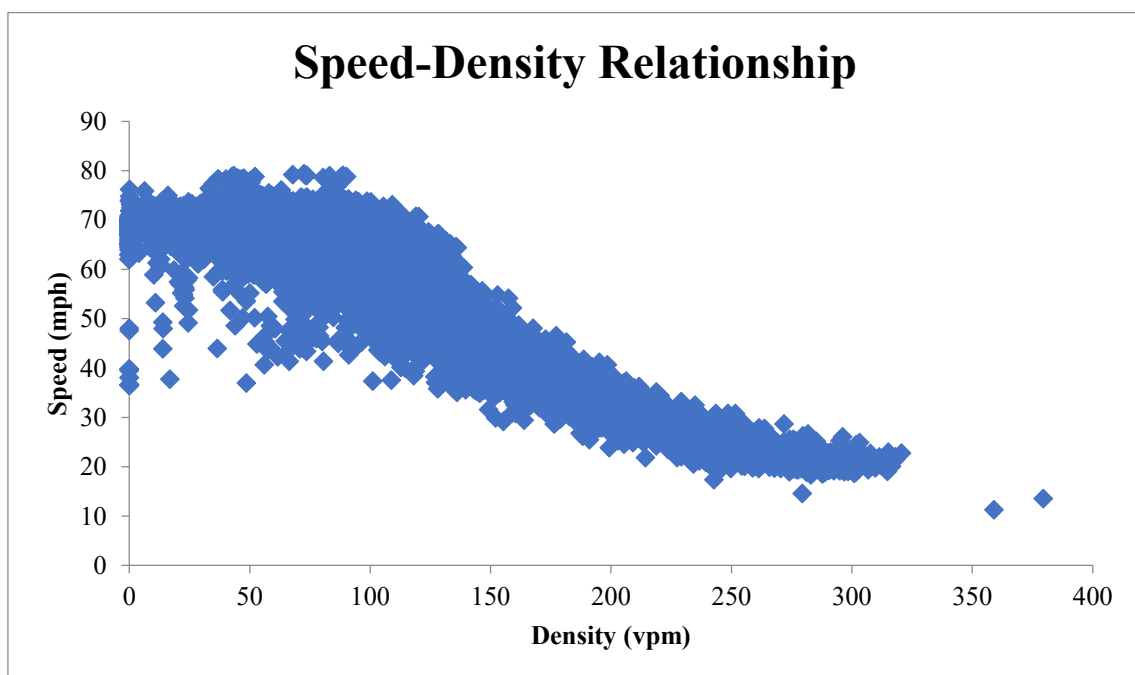


**Figure 1:1 The scattering effects of the fundamental relationship from Berkeley I-80 observations**

The research problem is obvious when one takes an in-depth look at more empirical speed-density plots and their corresponding mean-variance curve. These observations are randomly selected from mainline traffic data collected at stations from test bed I-80 Berkeley (PeMS, 2017)

It can be observed that the empirical plots exhibit a widely scattered speed-density relationship with as much randomness (or uncertainty). General deterministic families of models which especially express a 'pair-wise' relation between speed and density are not adequate to include the traffic speed variance and elucidate some complex phenomenon such as capacity drop, traffic hysteresis etc. In particular, speed-density models in a deterministic sense, either single or multi-regimes, have a 'pair-wise' relationship; that is, a density value corresponds to a fixed corresponding speed value according to the deterministic formulas. By studying empirical observations from I-80, Berkeley, the existence of another scenario was verified as there is a distribution of traffic speed at a certain density level due to the stochastic nature of traffic flow; this is in contrast to the 'pair-wise' pattern from deterministic models. In this conditions, there are mathematical arguments showing that a deterministic model represents the mean of a similar stochastic model (Rouse and Douglas , 1991). However, the mean alone is not enough to explain dynamic traffic behaviors. Using a stochastic speed-density model to replace a deterministic speed-density model is justified by this argument and investigations of empirical observations provide solid evidence to support the argument that at any density level there is a distribution of speeds instead of a single traffic speed given by deterministic model.

To address the question as to why stochastic speed-density model is wanted, let's think about modeling the outcome when dice are thrown. In principle, a complex deterministic model can predict the outcome, the trajectory of dice moving in the air and the tumbling and bouncing can be modeled in great detail, including the many imperfections of the dice and the table. A very simple stochastic model with the six possible outcomes having equal probability usually works better. This is because most parameters of the deterministic model are not known, and the process of throwing cannot be controlled in sufficient detail. This example reveals that it should usually be possible to reduce scattering effects (deviations between measurements and predictions by deterministic models) either by modeling more factors, or by excluding the scatter inducing factors experimentally. Thus, a stochastic speed-density model is favorable in capturing traffic dynamics and the randomness involved inherently in a transportation system.

The validity of the proposed stochastic speed-density model has been verified by empirical observations and its performance was compared with existing deterministic models.

### **1.3 Specific Objectives**

This study is concerned with the development of a stochastic model of speed-density relationship. The specific objectives are:

- I. Formulation of an analytical speed-density relationship for non-lane based heterogeneous traffic.
- II. Calibration and validation of the formulation using field data collected from the study road segment.
- III. Comparison of the newly developed model with the previous state-of-art models in terms of different measures of performances.
- IV. Determining the free-flow speed, jam density and capacity of the road segment from the calibrated ANN parameters.
- V. Developing a tool to calibrate speed-density diagram automatically.

The outcome of this research will contribute to design appropriate roadway geometry and automatic traffic control strategies along with continuous monitoring.

### **1.4 Thesis Structure**

This thesis is divided into six chapters and an appendix.

Chapter 1 presents the background of the study and describes the specific objectives of the study along with the problem statement.

Chapter 2 reviews the literature addressing different models used in estimation of fundamental traffic flow parameter.

Chapter 3 introduces research approaches the framework this study, a step-by-step plan of the model and the mathematical formulations behind the models.

Chapter 4 details the data collection, processing and extraction of the data required for this study.

Chapter 5 presents the calibration results analysis and proposed model validation comparing with existing various model.

Chapter 6 summarizes the findings, recommendations and application of this study along with the limitations.

Appendix A-1 attaches the results for five scenarios of data split in different training- testing composition with various hidden layer.

Appendix A-2 attaches the graphical presentation for five scenarios of data split in different training- testing composition with various hidden layer.

Appendix A-3 attaches the collected data for non-lane based heterogeneous traffic from study corridor.

## CHAPTER 2

### LITERATURE REVIEW

#### 2.1 Introduction

The objective of this chapter is to provide a review of the modeling efforts regarding the speed-density relationship which leads to a fundamental diagram of traffic flow. This review is to help us understand why the stochastic speed-density model is desired when compared to the existing deterministic models.

#### 2.2 Significance of Fundamental Diagram Models

Spatiotemporal modeling and specification of traffic speed-density patterns are keys to freeway traffic monitoring and management that generate technological advancements for intelligent transportation systems. The traffic flow fundamental diagram has been considered as the foundation of traffic flow theory. It addresses the relationship among three fundamental parameters of traffic flow: flow (vehs/h), speed (km/h), and density (vehs/km) of a traffic stream. For example, the study on traffic flow dynamics relies on input from the flow-density relationship to understand how a perturbation propagates among vehicles (Lighthill and Whitham, 1955); a highway capacity analysis makes use of the speed-flow relationship to determine the level of service that the highway provides (Transportation Research Board, 2010). Hence, sound mathematical models which better represent these relationships build a solid foundation for traffic flow analysis and efficient traffic control. Among the three ‘pair-wise’ relationships (e.g. speed-density, flow-density, and speed-flow), the speed-density relationship appears to be fundamental since it draws direct connection to everyday driving experience, i.e. how a driver’s speed choice is influenced by the presence of other vehicles in their vicinity.

Such an observation has encouraged many speed-density models for a path-breaking attempt by Greenshields eighty-five years ago (Greenshields, 1935). These efforts revealed a path toward two, somehow competing, goals: mathematical elegance and empirical accuracy. On the other hand, a speed-density model that possesses the following attributes is always preferred: (i) it is in a reasonably simple functional form (Greenshields, 1935); (ii) it works over the entire density range (i.e. single regime in one equation); and (iii) it involves physically

meaningful parameters. For example, the Greenshields model consists of such a simple, linear equation that it is frequently used for illustrative and pedagogical purposes. Meanwhile, analytical studies of traffic flow evolution often require a functional relationship between flow and density and such a function is expected to have derivatives (Lighthill and Whitham, 1955). A mathematically elegant speed-density model can be used to derive such a function. On the other hand, the approximation of the model to empirical observations is always a concern. The literature survey in the next section clearly shows such a direction. Departing from the Greenshields model, a number of models referred to Table 2.1 are proposed with varying degrees of success in terms of empirical accuracy. Note that these models are still in a single equation form (i.e. single regime) and hence preserve mathematical elegance. Further improvements referred to Table 2.2 are made by decomposing the speed-density relationship into multiple pieces for better fitting. In this case, mathematical elegance gradually gives way to empirical accuracy. (Transportation Research Board, 2010) gives a family of empirical equations of the speed-flow relationship. Whether single or multi-regime, deterministic models essentially describe average system behaviors. Actually, speed-density relationship is real-time dynamic flow in traffic management system (Hadiuzzman et al., 2018). But, in a live transportation system, a solely deterministic model is unlikely to include the prevalent dynamical randomness effects (or uncertainties) that have been observed empirically. The speed-density curve varies at the congested region due to the dynamics behavior of vehicle and selection of safety headways (Gaddam and Rao, 2019)

### **2.3 Deterministic Single-Regime Models**

There has been a fairly large number of efforts devoted to revise and improve Greenshields model: an over-simplified relationship. Among these pursuits, other single regime models include Greenberg (1959), Underwood (1961), Drake et al. (1967), Drew (1968), Pipes (1967), Newell (1961), Castillo and Benitez (1995), Jayakrishnan et al. (1995), Kerner and Konhauser (1994), Aerde (1995) and MacNicholas (2008). Table 2.1 lists the well-known single-regime deterministic models.



**Table 2.1 Deterministic single-regime speed-density models**

Single-regime models	Functions	Parameters
Greenshields (1935)	$v = v_f \left( 1 - \frac{\rho}{\rho_j} \right)$	Where, $v_f$ = Free-flow speed
Greenberg (1959)	$v = v_m \log \frac{\rho_j}{\rho}$	$v_m$ = Maximum Speed
Underwood (1961)	$v = v_f \exp \left( -\frac{\rho}{\rho_o} \right)$	$\rho_o$ = Optimal Density
Drake et al. (1967)	$v = v_f \exp \left( -\frac{1}{2} \left( \frac{\rho}{\rho_o} \right)^2 \right)$	
Drew (1968)	$v = v_f \left[ 1 - \left( \frac{\rho}{\rho_j} \right)^{n+\frac{1}{2}} \right]$	$\rho_j$ = Jam Density
Pipes (1967)	$v = v_f \left( 1 - \left( \frac{\rho}{\rho_j} \right)^n \right)$	n= Number of Order
Wu and Rakha (2009 ),	$\rho = (v_o - v) \frac{C}{v_o^2}$	
Kühne (1984)	$V = V_f \left\{ 1 - \left( \frac{\rho}{\rho_m} \right)^{n1} \right\}^{n2}$	$\rho_m$ = Critical density a, b, $\theta$ = Shape Parameters
Five- parameter logistic (5PL) model (2014)	$V(\rho, \theta) = v_b + \frac{v_f - v_b}{\left( 1 + \exp \left( \frac{\rho - \rho_t}{\theta_1} \right) \right) \theta_2}$	

**Table 2.1: Deterministic single-regime speed-density models (Contd.)**

Single-regime models	Functions	Parameters
Gaddam et al. (2019)	$v = v_f \left[ \frac{e^{-\left(\frac{\rho}{\rho_m}\right)^{1+a}} - e^{-\left(\frac{\rho_f}{\rho_m}\right)^{1+a}}}{1 - e^{-\left(\frac{\rho_f}{\rho_m}\right)^{1+a}}} \right]^b$	

Some of selected model from the above the models are plotted in a graph to visualize the difference among those model.

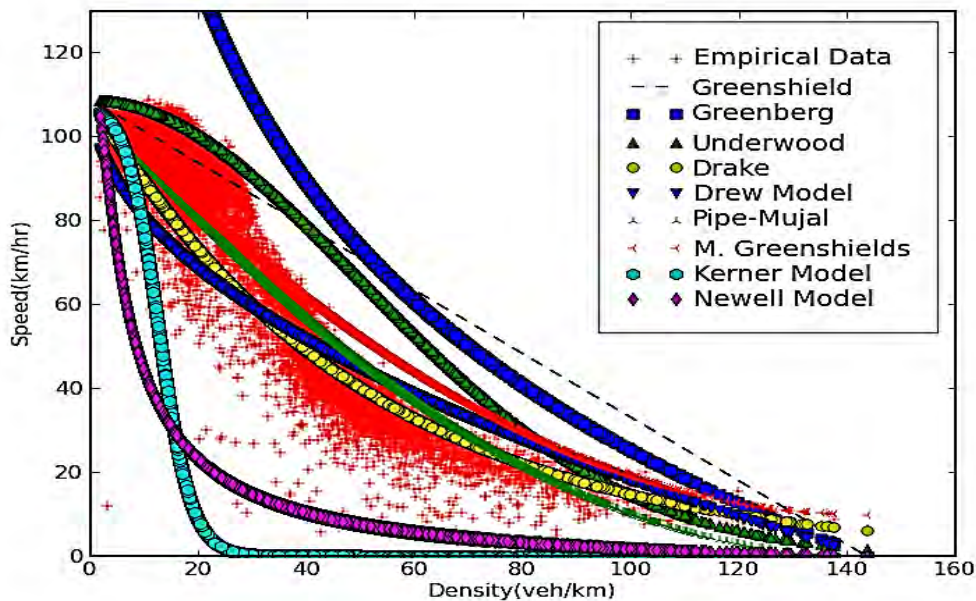


**Figure 2.1 Plot of single-regime deterministic speed-density models (Wang, 2010)**

### 2.3.1 Model of Greenshields

It has been almost eighty-five years since Greenshields seminal paper: “Study of Traffic Capacity” in 1935 (Greenshields, 1935). Attaching empirically derived curves to a fitted linear model of the speed-density relationship started a new era of transportation science and engineering. Due to its strong empirical nature, the efforts to find a perfect theory to explain these particular shapes mathematically never cease, but only limited success has been obtained. Figure 2.2 shows the performance of Greenshields against the empirical data.

Consider the seminal linear speed-density by Greenshields in Equation 2.1: there are only seven data points collected from one lane in a two-way rural road in which six of the data points are below 60 mi/hr and the seventh data point was taken from a different road (Hall et al., 1992). Seven data points are not enough to generate a whole picture of a speed-density model.

$$v = v_f \left( 1 - \frac{\rho}{\rho_j} \right) \quad (2.1)$$

Where  $v_f$  denotes free flow speed and  $\rho_j$  is jam density. Usually,  $v_f$  is relatively easy to estimate from empirical data and mostly lies between speed limit and highway design speed.

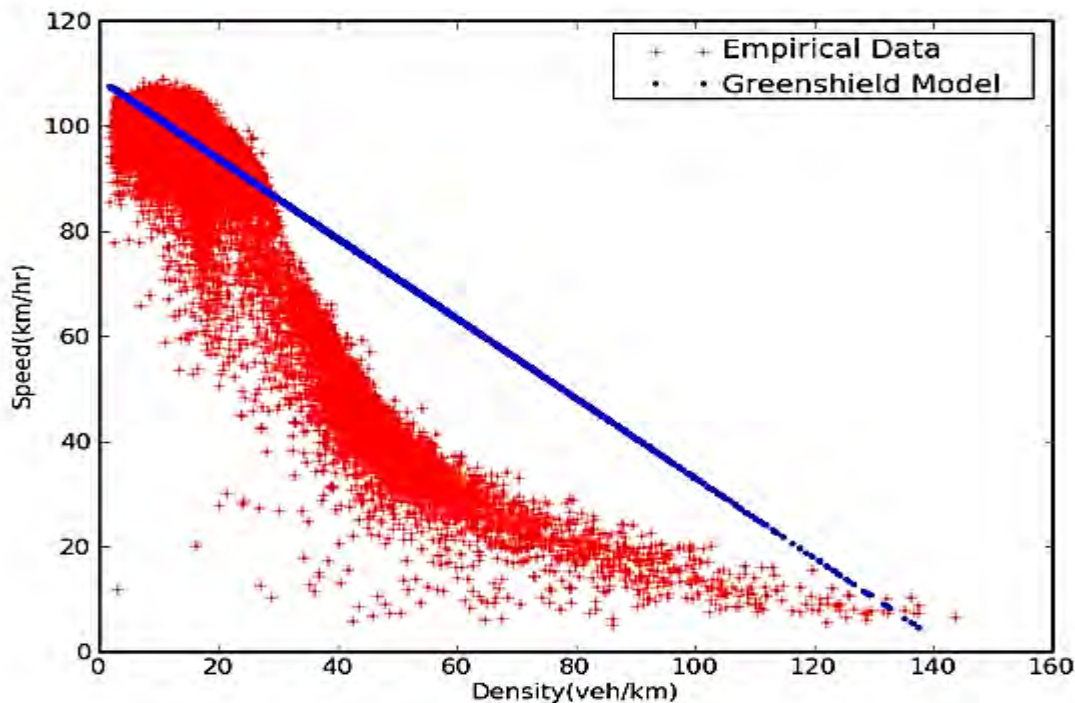


**Figure 2:2 Performance of Greenshields model against empirical data (Wang, 2010)**

But  $\rho_j$  is not easy to observe; however, an approximate value of 185-250 vehicle/mile is a reasonable range (May, 1990).

### 2.3.2 Logarithmic Greenberg Model

The Greenberg model gained popularity because it bridged the gap analytically from a macroscopic stream model to a microscopic car-following model (Gazis et al., 1959). However, the main criticism of this model is its inability to predict speed at lower densities, because as density approaches zero, speed tends to increase to infinity.

$$v = v_m \log \frac{\rho_j}{\rho} \quad (2.2)$$

$v_m$  is optimum speed which is not directly observable but can be determined by experiences. The Greenberg model tends to overestimate empirical observations over the whole density range; this has been verified in Figure 2.3 which shows the performance of the Greenberg model against empirical observations.

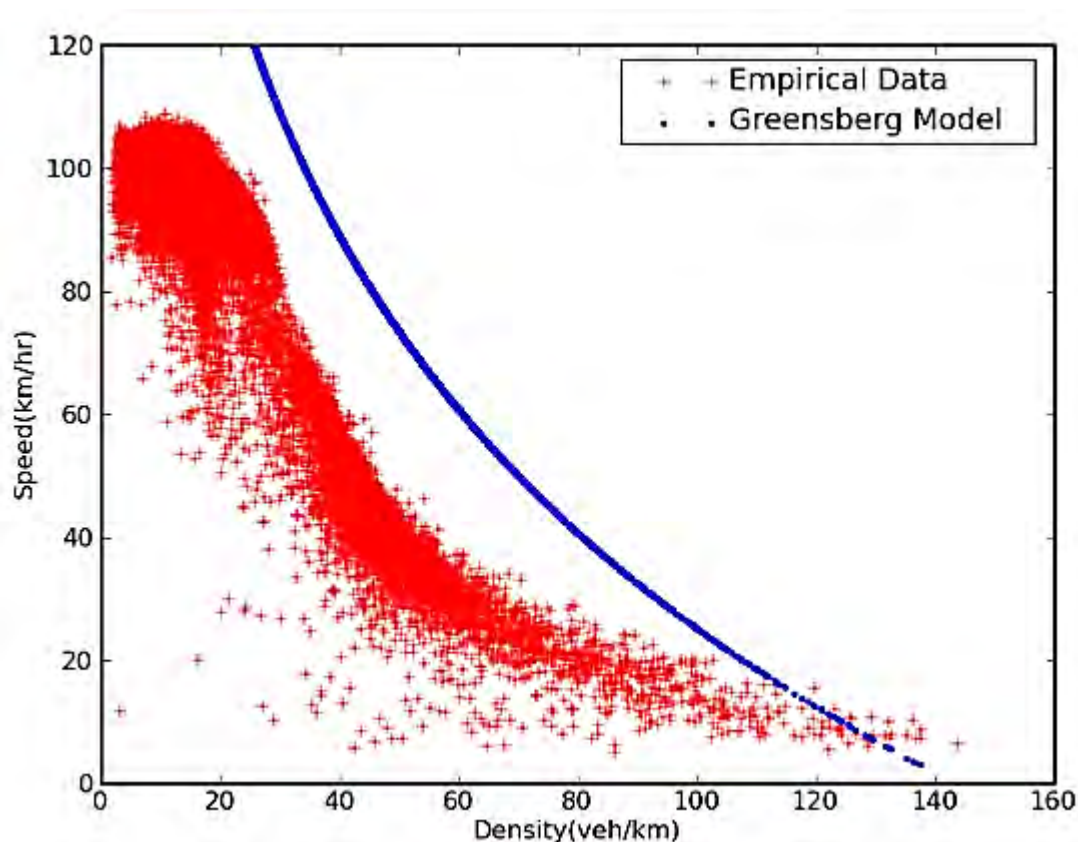


**Figure 2:3 Performance of Greenberg model against empirical data (Wang, 2010)**

Obviously, model parameters can be adjusted to make them fit empirical data better, but it will not fundamentally change the performance.

### 2.3.3 Underwood Exponential Model

Later, Underwood derived an exponential model that attempted to overcome the limitation of the Greenberg model (Underwood, 1961). The performance of the Underwood model is plotted against empirical observations referring to Figure 2.4 which shows that the Underwood model tends to underestimate free-flow phase but overestimate congested portion.

$$v = v_f \exp\left(-\frac{\rho}{\rho_o}\right) \quad (2.3)$$

$\rho_o$  is the density at which maximum flow or capacity is reached. Generally, the Underwood model performs better than previous deterministic models in fitting results to empirical data.

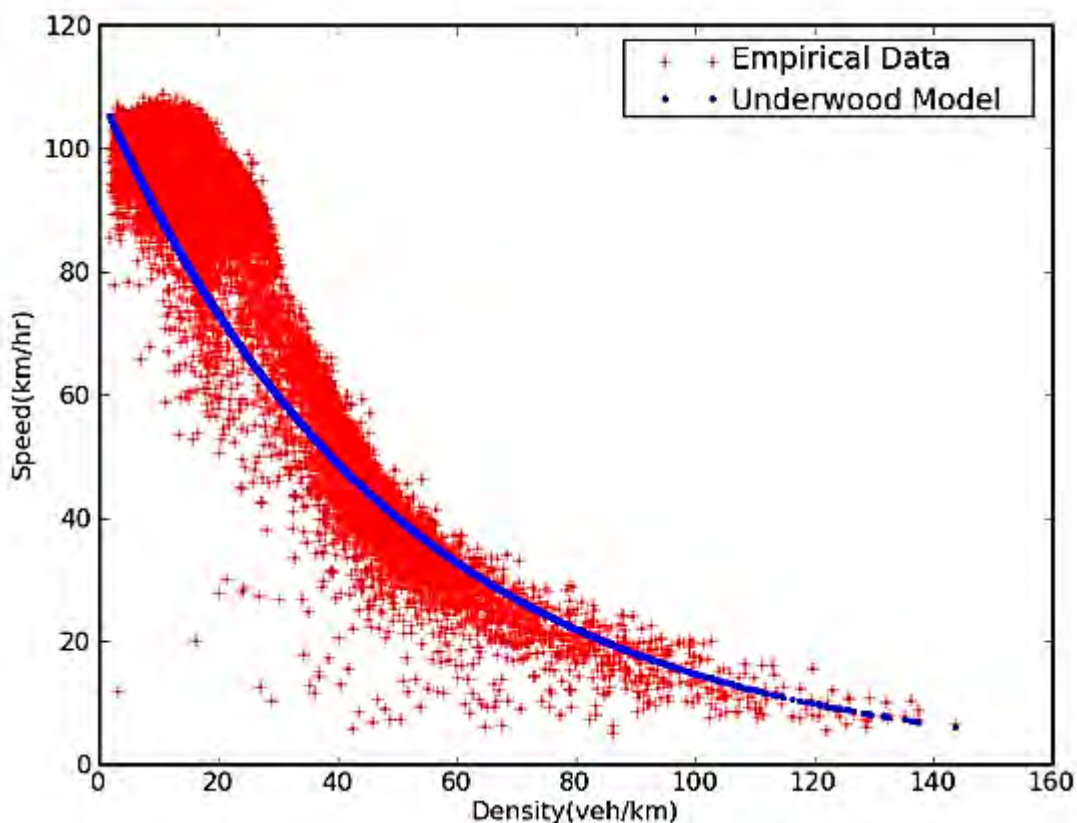


**Figure 2:4 Performance of Underwood model against empirical data (Wang, 2010)**

The rationale behind this is that speed-density observations over a long time period tends to show an exponential shape rather than linear or logarithmic. This explains the performance differences among the single-regime family of compared models. The main drawback of the

Underwood model is that speed becomes zero only when density reaches infinity. Hence, this model cannot be used for predicting speeds at high densities.

### 2.3.4 Drake Model

The Drake model (Drake et al., 1967) works in a manner opposite to the Underwood model. It tends to overestimating the free-flow region while underestimate the congested region. This can be verified from Figure 2.5 which shows the relative performance of the Drake model plotted against empirical observations.

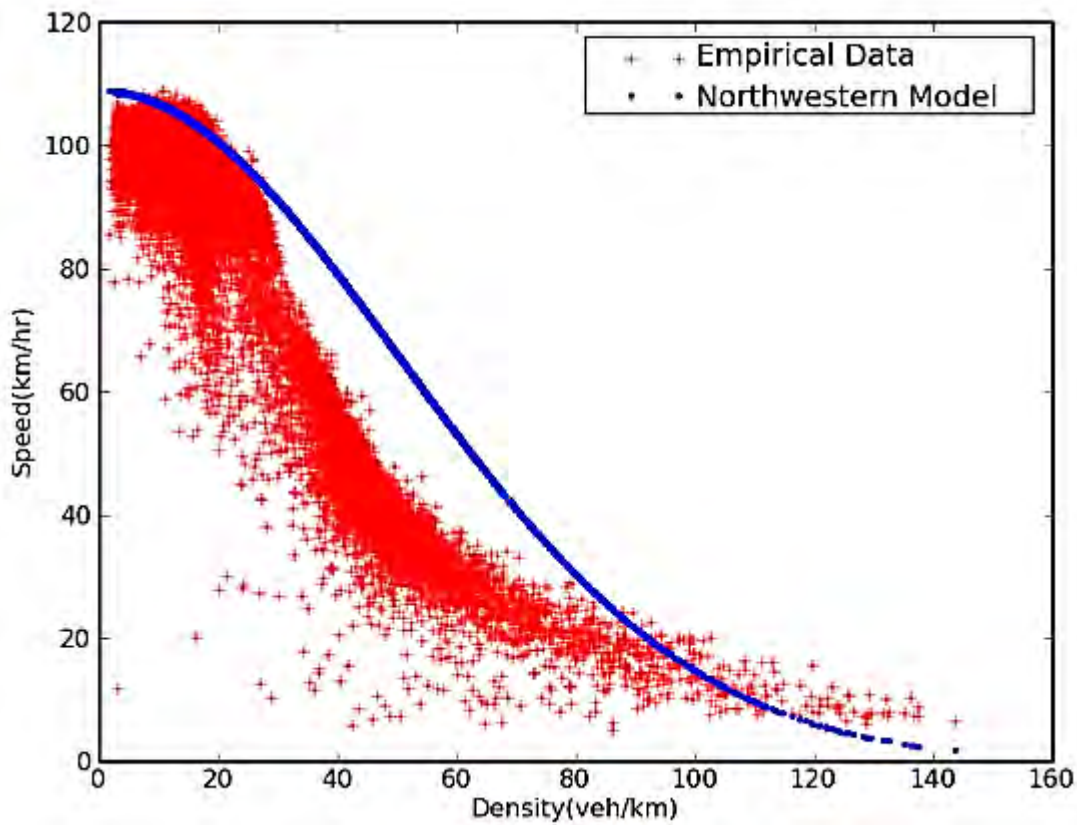


**Figure 2:5 Performance of Drake model against empirical data (Wang, 2010)**

Wong and Wong (2002) applied the modified Drake model to all user classes and developed a multi-class traffic flow model which extends LWR with heterogeneous driver populations.

$$v = v_f \exp \left( -\frac{1}{2} \left( \frac{\rho}{\rho_0} \right)^2 \right) \quad (2.4)$$



### 2.3.5 Pipe-Munjal Generalized Model

The Pipes-Munjal model resembles Greenshields model.

$$v = v_f \left( 1 - \left( \frac{\rho}{\rho_j} \right)^n \right)^m \quad (2.5)$$

By varying the values of  $n$ , a family of models can be developed; i.e., a Green shield model is obtained by letting  $n = 1, m = 1$ . The performance of Pipes-Munjal model is shown in Figure 2.6 against empirical speed-density data.

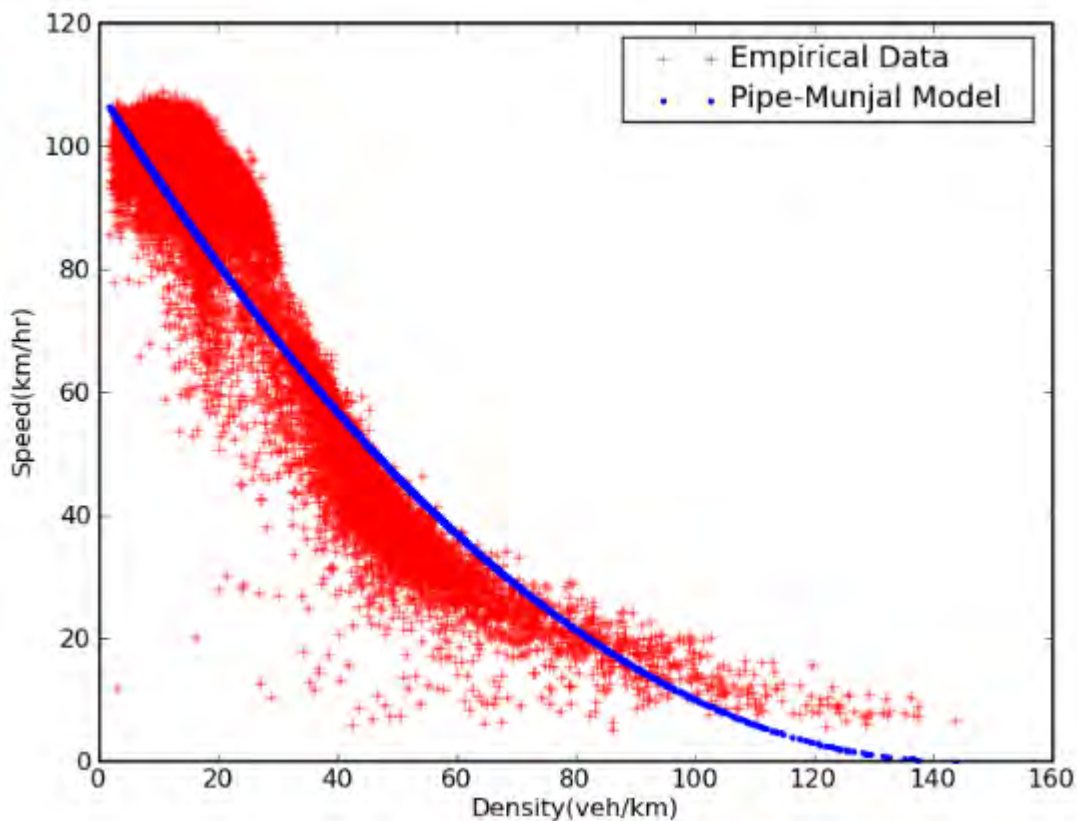


Figure 2:6 Performance of Pipe-Munjal model against empirical data (Wang, 2010)

### 2.3.6 Drew Model

Drew (1968) tends to underestimate speed at a free-flow phase, but it overestimates the speed in the congested phase.

$$v = v_f \left[ 1 - \left( \frac{\rho}{\rho_j} \right)^{n+\frac{1}{2}} \right] \quad (2.6)$$

The performance of the Drew model is plotted against empirical data referred to Figure 2.7.

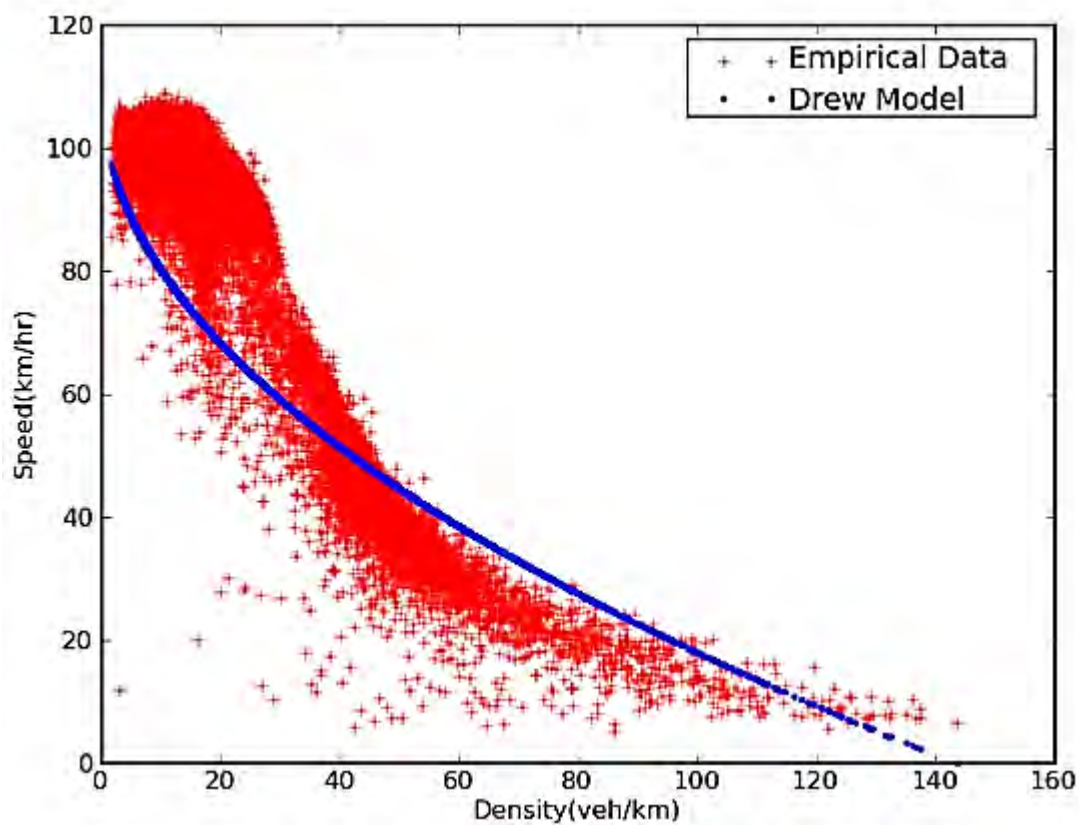


Figure 2:7 Performance of Drew model against empirical data (Wang, 2010)



### 2.3.7 Newell Model

Newell (1961) is given by

$$v = v_f \left[ 1 - \exp\left\{-\frac{\lambda}{v_f} \left(\frac{1}{k} - \frac{1}{k_j}\right)\right\}\right] \quad (2.7)$$

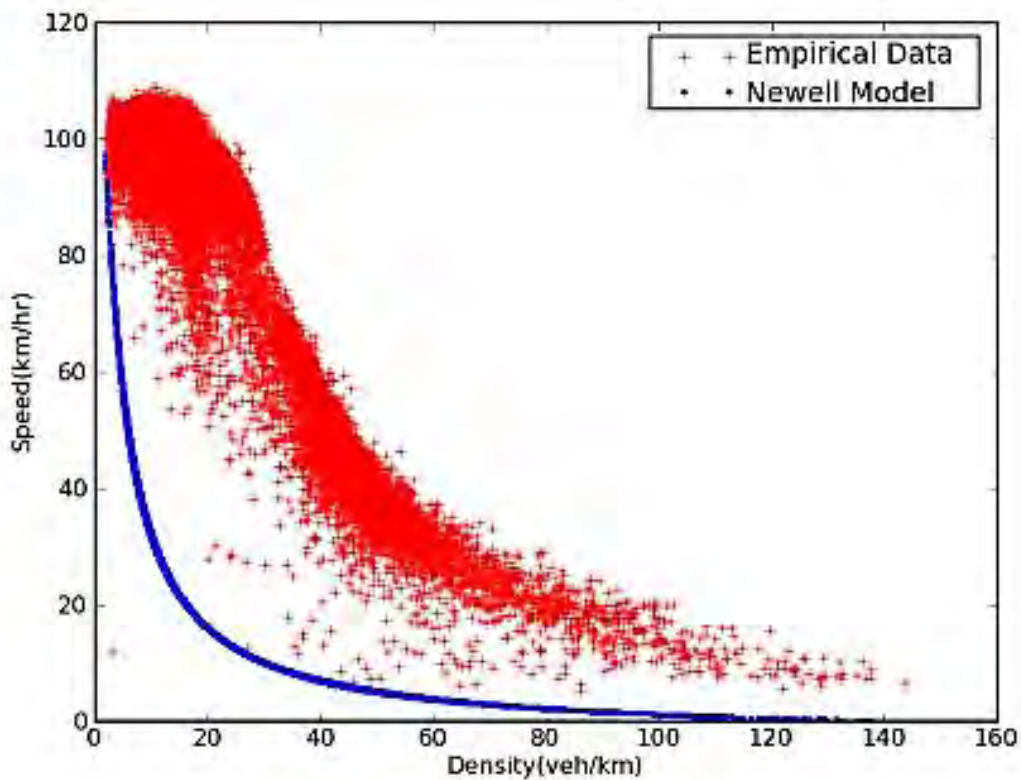


**Figure 2:8 Performance of Newell model against empirical data (Wang, 2010)**

in which  $\lambda$  is the slope of spacing-speed curve at  $v = 0$ . Another form of Newell's steady state speed-density curve of the car-following models is given by

$$v = v_f \left[ 1 - \exp\left\{\frac{\lambda}{v_f} (1 - k_j(x_{i-1} - x_i))\right\}\right] \quad (2.8)$$

The performance of the model is dependent on the choice of parameter  $\lambda$ .

### 2.3.8 Modified Greenshields Model

Dynamic Network Assignment-Simulation Model for Advanced Roadway Telematics – Planning version (DYNASMART-P) uses a modified Greenshields model for traffic propagation (Qin and Hani, 2004) the functional form is given by

$$v = v_0 + (v_f - v_0)\left(1 - \frac{k}{k_j}\right)^\alpha \quad (2.9)$$

in which  $v_0$  is a user-specified minimum speed,  $v_f$  is free-flow speed,  $k_j$  is jam density and  $\alpha$  is user-specified parameter. There are two types of the modified Greenshields family models available. The first type is a two-regime model in which constant free-flow speed is specified for the free-flow regime and Modified Greenshields model is specified for the congested-flow regime. The second type applies the Modified Greenshields model for both free and congested-flow regimes. The general performance of the modified Greenshields model is shown in Figure 2.9 with  $\alpha = 2$ .

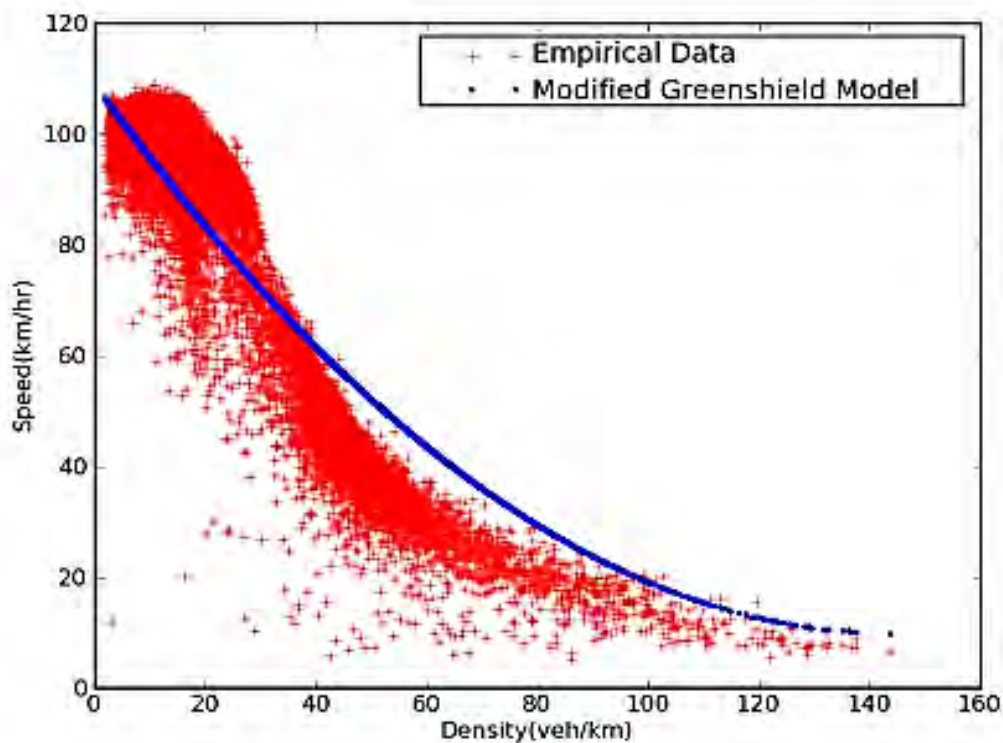


**Figure 2:9 Performance of Modified Greenshield model against empirical data (Wang, 2010)**

### 2.3.9 Payne's Model in FREFLO(Free-Flow)

Payne adopted the speed-density curve given by the following expression

$$v_e = \min\{88.5, 88.5[1.94 - 6(\frac{k}{143}) + 8(\frac{k}{143})^2 - 3.93(\frac{k}{143})^3]\} \quad (2.9)$$

in which  $k$  is traffic density (veh/km) and  $v$  is traffic speed (km/hr) for the simulation program FREFLO. The Payne speed-density model is mostly used for simulation purposes. Its performance compares to empirical data is plotted in Figure 2.10, it works as the Modified Greenberg model in a multi-regime family. Jingang et al. (2002) derived a nonlinear traffic flow stability criterion using wave front expansion technique; the Payne's model was applied to the numerical tests for high-order model stability analysis.

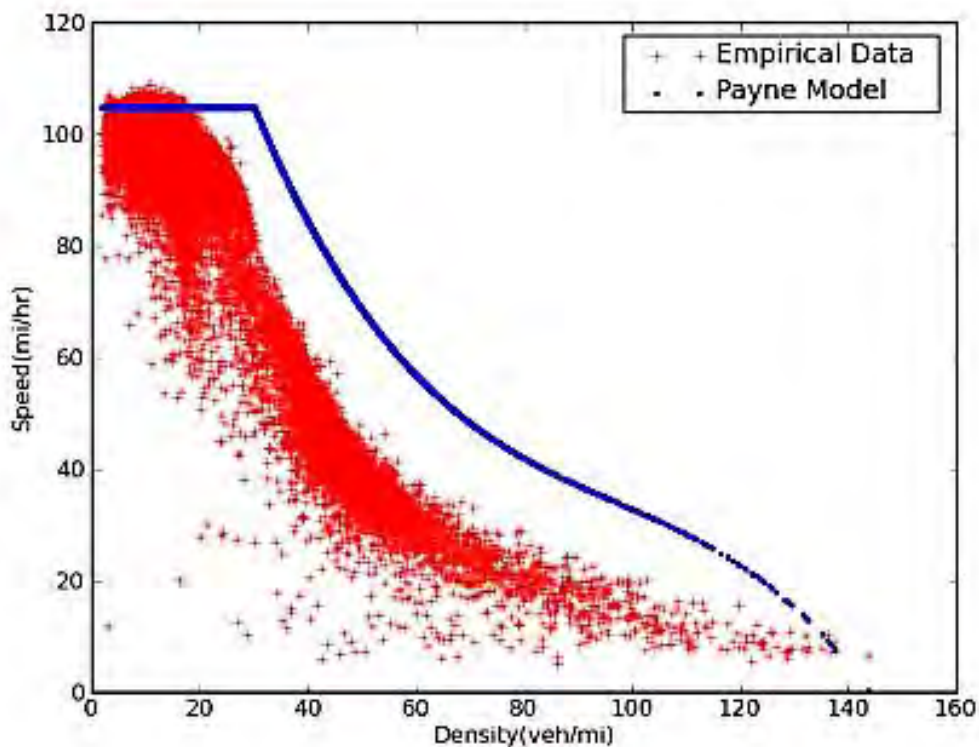


Figure 2:10 Performance of Payne model against empirical data (Wang, 2010)

### 2.3.10 Kerner and Konhauser's Model

Kerner and Konhauser (1994) used this speed-density relationship in their computational test for cluster effects in initially homogeneous traffic flow.

$$v_e = v_f \left( \frac{1}{1 + \exp\left(\frac{\frac{k}{k_m} - 0.25}{0.06}\right)} - 3.72 \times 10^{-6} \right) \quad (2.10)$$

The performance of the Kerner model is plotted against empirical data in Figure 2.11.

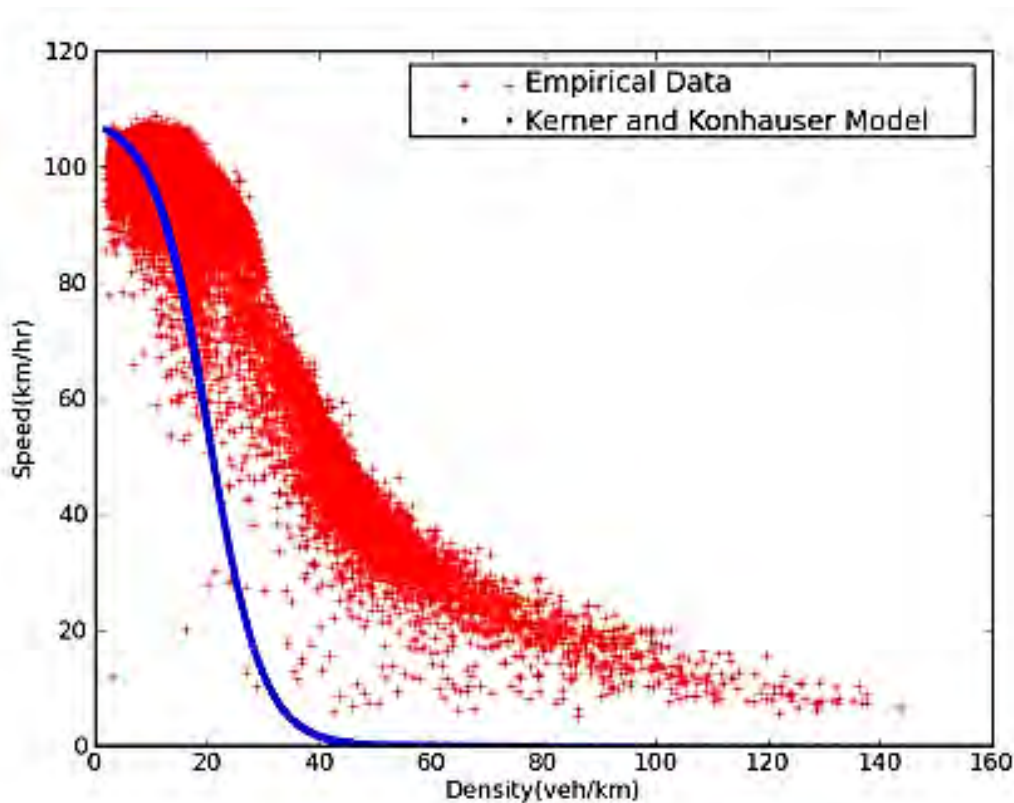


**Figure 2:11 Performance of Kerner and Konhauser model against empirical data (Wang, 2010)**

From Figure 2.11, it is not difficult to tell that the Kerner model does not match empirical data well. This model was used for numerical purposes. Chang-Fu et al. (2007) used this equilibrium speed-density relationship to investigate phase diagrams of speed gradient model with on-ramp effect in a mixed traffic.

## 2.4 Deterministic Multi-Regime Models

When people realized that single-regime model cannot fit the empirical data consistently either in a free-flow regime or in a congested regime, multi-regime came into play. Multi-regime models usually include two or three regimes including: two-regime models such as Edie Model, two-regime model (May, 1990), multi-regime model by cluster analysis (Lu and Jie, 2005), the modified Greenberg (May, 1990), and three-regime models (May, 1990).

**Table 2.2 Deterministic multi-regime speed-density models**

Multi-regime models	Free-flow regime	Transitional-flow regime	Congested-flow regime
Eddie (1961)	$v = 54.9 \exp^{-\frac{\rho}{163.9}}$ ( $\rho \leq 50$ )	–	$v = 26.8 \ln\left(\frac{162.5}{\rho}\right)$ ( $\rho \geq 50$ )
Two-regime Model (May 1990)	$v = 60.9 - 0.515\rho$ ( $\rho \leq 65$ )	–	$v = 40 - 0.265\rho$ ( $\rho \geq 65$ )
Modified Greenberg (May 1990)	$v = 48(\rho \leq 35)$	–	$v = 32 \ln\left(\frac{145.5}{\rho}\right)$ ( $\rho \geq 35$ )
Three-regime linear model (May 1990)	$v = 50 - 0.098\rho$ ( $\rho \leq 40$ )	$v = 81.4 - 0.913\rho$ ( $40 \leq \rho \leq 65$ )	$v = 40.0 - 0.265\rho$ ( $\rho \geq 65$ )

Above the table  $\rho$  is in veh/mile. The basic idea of the two-regime model is to use two different curves to model free-flow regime and congested-flow regime. Edie's model is the first multi-regime model using the Underwood model for a free-flow regime and the Greenberg model for congested flow regime. There is a three-regime model which uses three linear curves to model free flow, transitional-flow and congested-flow regimes each being

represented by a Greenshields model. Table 2.2 lists most of the well-known multi-regime speed-density models.

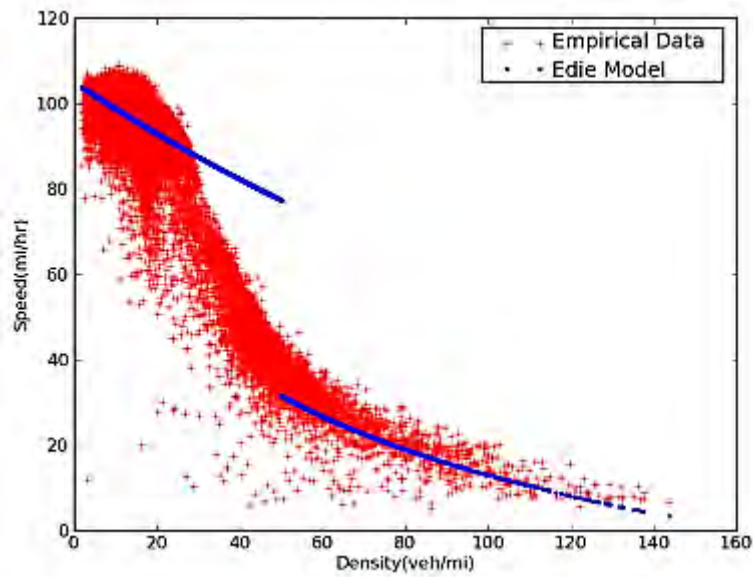


**Figure 2:12 Performance of Edie model against empirical data (Wang, 2010)**

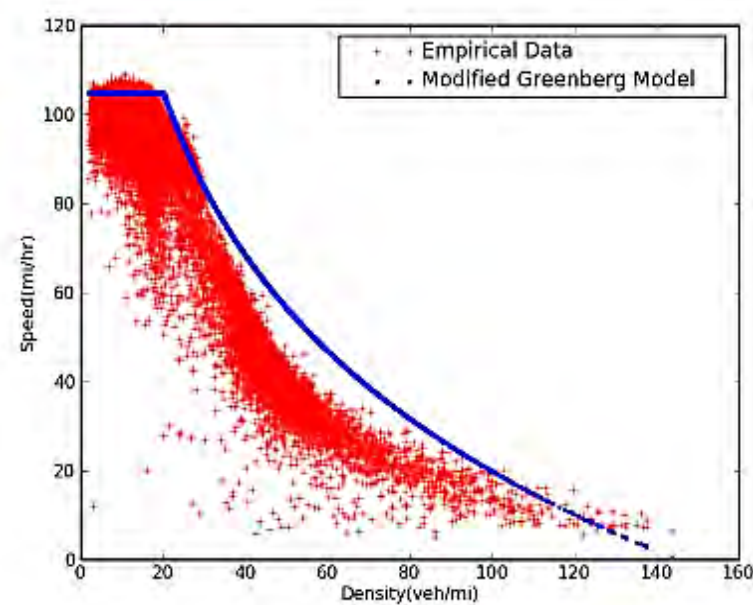


**Figure 2:13 Performance of Modified Greenberg model against empirical data (Wang, 2010)**



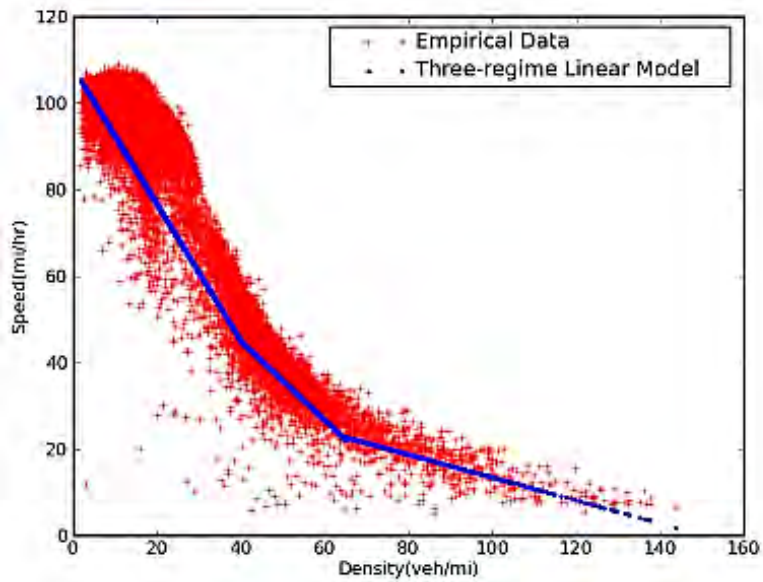


**Figure 2:14 Performance of three-regime linear model against empirical data (Wang, 2010)**

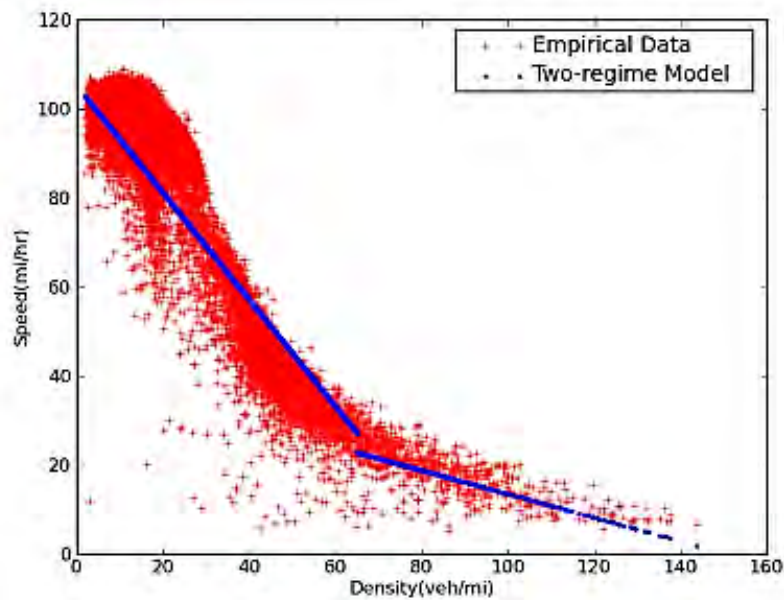


**Figure 2:15 Performance of two regime model against empirical data (Wang, 2010)**

The performance of multi-regime speed- density models is shown in Figure 2.12 to Figure 2.15 (Wang, 2010). Basically, the multi-regime models use a combination of two or three single-regime models piece by piece, the turning points of the curve can be explained by empirical observations, but it is debatable on how to determine the turning points of multi-regime models.

## 2.5 Stochastic Speed-Density Models

The stochastic behavior of a real world traffic system is often difficult to describe or predict exactly when the influence of unknown randomness is sizable. However, it is quite possible to capture the chance that a particular outcome will be observed during a certain time interval in a probabilistic sense. Thus, the interpretation of scattering as measurement error originates from physics. The observations usually differ from model expectations. When the scatter is too large, the model is useless, despite its appropriateness as a stochastic model. A realistic way of dealing with scatter is far from easy and usually leads to highly complicated mathematical models. Model developers are frequently forced to strike a balance between realism and mathematical simplicity. This further degrades the strict application of goodness of fit tests for models with unrealistic stochastic components.

Berry and Belmont (1951) analyzed the distribution of vehicle speeds and travel times from different facilities using empirical data. Soyster and Welson (1973) proposed a stochastic flow-concentration model applied to traffic on hills, this paper may be the first stochastic model regarding flow-concentration relationship which extends the deterministic flow-density relationship by treating the arrival of vehicles to the bottom of the hill and to the top of the hill as Poisson process. Vehicles on the hill represent a birth and death process, a finite number of traffic states is defined which was incorporated into a finite Markov chain with a transition matrix. In recent literature, Kharoufeh and Gautam (2004) derived an analytical expression of the link travel time distribution through stochastic speed processes. Brilon et al. (2005) proposed the concept of a stochastic freeway capacity comparing with the conventional capacity from the speed-flow diagram.

## 2.6 Motivation of the Work

In this chapter, existing both the single-regime and multi-regime speed-density models are reviewed for deterministic domain. Each model's performance against empirical data is also presented. The advantages and limitations of deterministic speed-density models are also discussed in this chapter. Deterministic speed-density models are considered as incomplete because it models the average behavior of the wide-scattering plot (mean). For this reason, a stochastic approach is an essential for a complete speed-density model. From the previous sections of this chapter, it is evident that Underwood model approaches zero speed at infinite density. Hence, it cannot predict the jam density which is an important part of speed-density



model. On the other hand, Greenberg model approaches zero density at infinite speed. As a result, multi-regime piecewise equations (e.g. Edie (1961) model, Modified Greenberg (1990) model) were investigated to predict the parameters accurately by determining free-flow speed and jam density separately. The main controversy for the multi-regime model is to find out the break point. This multi-regime model emphasized on the empirical accuracy but lost mathematical elegance. However, none of these above mentioned models can determine the parameters in case of incomplete data set due to scattering. For this reason, deterministic approach for speed-density should be considered inappropriate for transportation system. The scattering feature can be observed while plotting the speed-density graph of the model. A large number of factors (e.g. driver behaviors, highway geometry, vehicles and environmental conditions) can introduce the scattering effect but these are not directly shown in the model.

The scattering phenomena can be observed in the fundamental diagram due to measurement of errors, the inherent nature of traffic flow or combination of these two. Actually, there are two main sources of randomness (Jia et al., 2008). The first category of randomness come from the data collection procedure and computational process (e.g. inaccurate reading and data round off). This type of randomness is well-understood and can be statistically controlled. Another type of randomness is due to traffic dynamics and lack of knowledge about details of traffic system. For example, driver's behavior on an individual basis; the collective behavior of driver group could be better representative in a distributional law rather than in deterministic terms (Jia et al., 2008).

In recent year all the deterministic single-regime or multi-regime speed-density model has a pairwise relation which determines a fixed speed from a formula for a given density. Several models are shown in Table 2.1 and Table 2.2. This study uses the PeMS data from bed test I-80, Berkeley to represent the lane based homogeneous traffic condition and the analysis shows that multiple traffic speeds corresponding to one density in contrast to pairwise relationship is assumed in deterministic model. This observation motivates to continue further research works considering the randomness along the mathematical elegance and empirical accuracy.

## CHAPTER 3

### FRAMEWORK OF STOCHASTIC MODELING

#### 3.1 Introduction

The detailed modeling framework for the study has been presented in this chapter. The model is proposed using ANN which uses different types transfer function during the run time. After investigating, several types transfer which helps to fit the model with the data properly, one function is proposed best fit in terms of goodness of fit. There are various types of transfer function like hardlimit, logististic, tan-sigmoid, saturation transfer function. Among the above mentioned transfer function saturation is said to be best.

#### 3.2 Artificial Neural Network

An Artificial Neural Network (ANN) is based on a collection of connected units or nodes called artificial neurons, which loosely model the neurons in a biological brain. Each connection, like the synapses in a biological brain, can transmit a signal to other neurons. An artificial neuron that receives a signal then processes it and can gives signal neurons connected to it.

##### 3.2.1 History of Artificial Neural Systems Development

Artificial neural systems development has an interesting history. Since it is not possible to cover this history in depth in a short introductory, only major achievements are mentioned. This glimpse at the field's past milestones should provide the reader with an appreciation of how contributions to the field have led to its development over the years. The historical summary below is not exhaustive; some milestones are omitted and some are mentioned only briefly.

The year 1943 is often considered the initial year in the development of artificial neural systems. McCulloch and Pitts (1943) outlined the first formal model of an elementary computing neuron. The model included all necessary elements to perform logic operations, and thus it could function as an arithmetic- logic computing element. The implementation of its compact electronic model, however, was not technologically feasible during the era of bulky vacuum tubes.

The formal neuron model was not widely adopted for the vacuum tube computing hardware description, and the model never became technically significant. However, the McCulloch and Pitts (1943) neuron model laid the groundwork for future developments .

Hebb (1949) first proposed a learning scheme for updating neuron's connections that we now refer to as the Hebbian learning rule. He stated that the information can be stored in connections, and postulated the learning technique that had a profound impact on future developments in this field. Hebb's learning rule made primary contributions to neural networks theory.

The monograph on learning machines by Nilsson (1965) clearly summarized many of the developments of that time. That also formulates inherent limitations of learning machines with modifiable connections.

Despite the successes and enthusiasm of the early and mid-1960s, the existing machine learning theorems of that time were too weak to support more complex computational problems. Although the bottlenecks were exactly identified in Nilsson's work and the neural network architectures called layered networks were also known, no efficient learning schemes existed at that time that would circumvent the formidable obstacles.

Although the mathematical framework for the new training scheme of layered networks was discovered (Werbos, 1974), it went largely unnoticed at that time. According to the most recent statement (Dreyfus, 1990), the first authors of the optimization approach for multilayer feedforward systems were Bryson and Ho (1969) and Kelley (1960) who obtained a gradient solution for multistage network training. In 1962, Dreyfus used a simple, new recursive derivation based on the chain-rule of differentiation to prove the Bryson-Kelley results and dealt explicitly with the optimal control problem in its discrete-stage form (Dreyfus, 1962). Their work, however, has not been carried to maturity and adopted for neural network learning algorithms.

### **3.2.2 Neuron Modeling for Artificial Neural Systems**

The McCulloch-Pitts model of a neuron is characterized by its formalism and its elegant, precise mathematical definition. However, the model makes use of several drastic simplifications. It allows binary 0,1 states only, operates under a discrete-time assumption, and assumes synchrony of operation of all neurons in a larger network.

Weights and the neurons' thresholds are fixed in the model and no interaction among network neurons takes place except for signal flow.

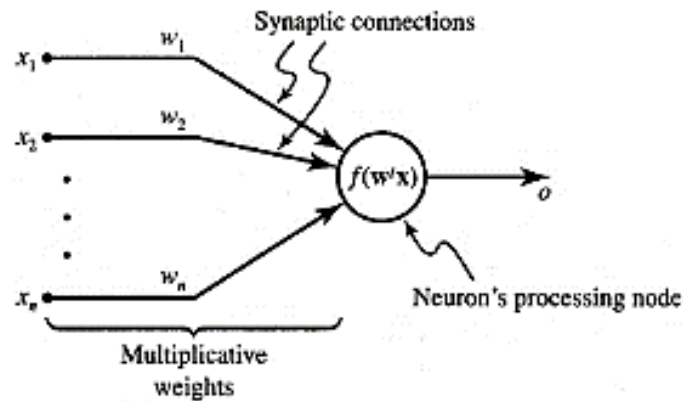


**Figure 3:1 General symbol of neuron consisting of processing node and synaptic connections (McCulloch and Pitts, 1943)**

Thus, it is considered that this model as a starting point for neuron modeling discussion. Specifically, the artificial neural systems and computing algorithms employ a variety of neuron models that have more diversified features than the model just presented below introducing the main artificial neuron models.

Every neuron model consists of a processing element with synaptic input connections and a single output. The data flow of neuron inputs,  $x_i$ , is considered to be unidirectional as indicated by arrows,  $o$  is as a neuron's output data flow. A general neuron symbol is shown in Figure 3.1. This symbolic representation shows a set of weights and the neuron's processing unit, or node. The neuron output data is given by the following relationship:

$$o = f(w^t x) \text{ or}$$

$$o = f\left(\sum_{i=1}^n w_i x_i\right) \quad (3.1)$$

Where  $w$  is the weight vector defined as

$$w = [w_1, w_2, \dots, w_n]^t$$

And  $x$  is the input vector:

$$x = [x_1, x_2, \dots, x_n]^t$$

(All vectors defined in this text are column vectors; superscript  $t$  denotes a transposition.) The function  $f(w_k)$  is often referred to as an activation function. Its domain is the set of activation

values, net, of the neuron model, thus often use this function as  $f(\text{net})$ . The variable net is defined as a scalar product of the weight and input vector.

$$\text{net} = w^t x \quad (3.2)$$

### 3.2.3 Models of Artificial Neural Networks

At this point, knowing the definition of the artificial neural network model, benefit from another definition. The neural network can also be defined as an interconnection of neurons, as defined in (3.1) through (3.2), such that neuron outputs are connected, through weights, to all other neurons including themselves. The network can be feedforward and feedback network discussed in next section.

#### 3.2.3.1 Feedforward Network

Let us consider an elementary feedforward architecture of  $m$  neurons receiving  $n$  inputs as shown in Figure 3.2. Its output and input vectors are, respectively

$$o = [o_1, o_2, \dots, o_m]^t \quad (3.3)$$

$$x = [x_1, x_2, \dots, x_n]^t$$

Weight  $w_{ij}$  connects the  $i$ 'th neuron with the  $j$ 'th input. The double subscript convention used for weights is such that the first and second subscript denote the index of the destination and source nodes, respectively. We thus can write the activation value for the  $i$ 'th neuron as

$$\text{net}_i = \sum_{j=1}^n w_{ij} x_j, \text{ for } i=1,2,\dots,m \quad (3.4)$$

The following nonlinear transformation [Equation (3. 3)] involving the activation function  $f(\text{net}_i)$ , for  $i= 1, 2, \dots, m$ , completes the processing of  $x$ . The transformation, performed by each of the  $m$  neurons in the network, is a strongly nonlinear mapping expressed as

$$o_i = f(w_i^t x), \text{ for } i=1,2,\dots,m \quad (3.5)$$

Where weight vector  $w_i$  contains weights leading toward the  $i$ 'th output node and is defined as follows

$$w_i = [w_{i1}, w_{i2}, \dots, w_{in}]^t \quad (3.6)$$

Introducing the nonlinear matrix operator  $\Gamma$ , the mapping of input space  $x$  to output space  $o$  implemented by the network can be expressed as follows

$$o = \Gamma[Wx] \tag{3.7}$$

Where  $W$  is the weight matrix, also called the connection matrix:

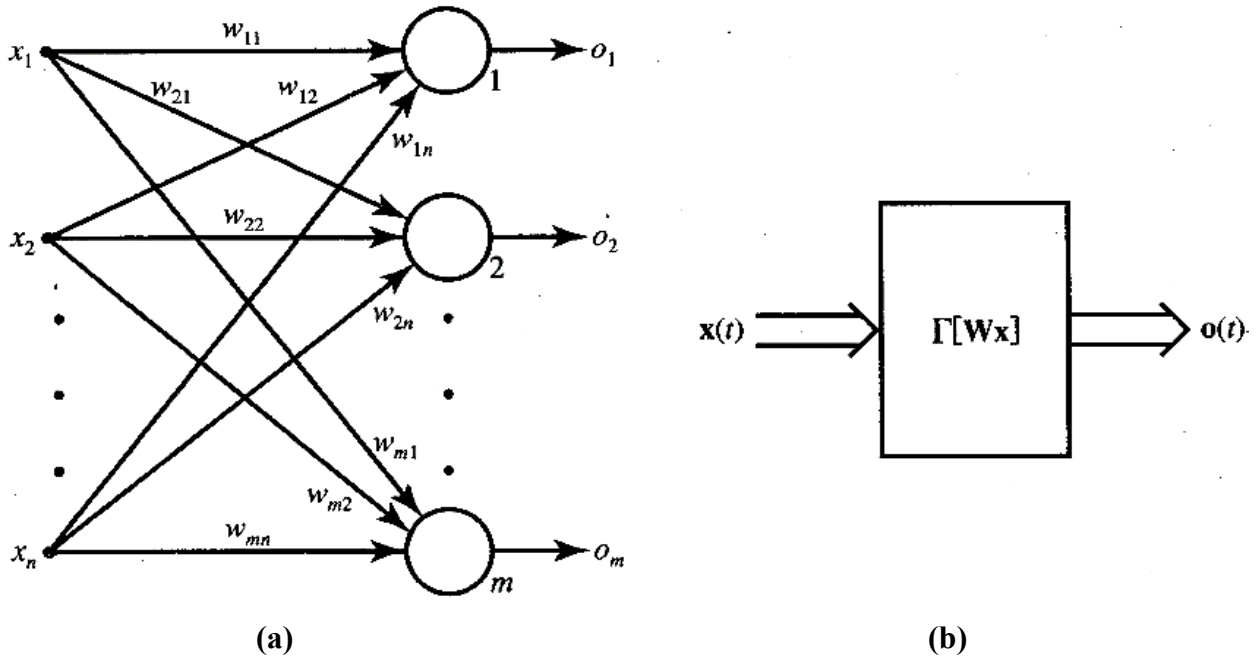


**Figure 3:2 Single-layer feedforward network: (a) interconnection; and (b) scheme and block diagram Feedforward network is used during the simulation of the proposed model**

### 3.2.4 Supervised and Unsupervised Learning

Under the notion of learning in a network, it is considered as a process of forcing a network to yield a particular response to a specific input. A particular response may or may not be specified to provide external correction. Learning is necessary when the information about inputs/ outputs is unknown or incomplete a priori. The majority of the neural networks requires training in a supervised or unsupervised learning mode. Some of the networks, however, can be designed without incremental training. They are designed by batch learning rather than stepwise training.

Batch learning takes place when the network weights are adjusted in a single training step. In this mode of learning, the complete set of input/output training data is needed to determine weights, and feedback information produced by the network which is not involved in developing the network. This learning technique is also called recording. Learning with

feedback either from the teacher or from the environment rather than a teacher, however, is more typical for neural networks. Such learning is called incremental and is usually performed in steps.

The concept of feedback plays a central role in learning. The concept is highly elusive and somewhat paradoxical. In a broad sense it can be understood as an introduction of a pattern of relationships into the cause-and-effect path. There are two different types of learning: learning with supervision versus learning without supervision.

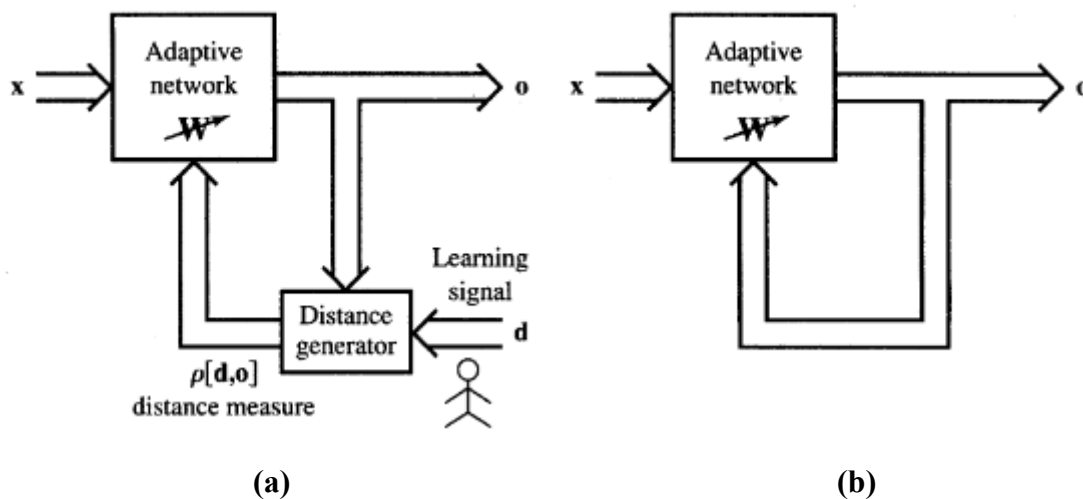


**Figure 3:3 Block diagram for explanation of basic learning modes: (a) supervised learning; and (b) unsupervised learning**

The learning types block diagrams are illustrated in Figure 3.3. In supervised learning it is assumed that at each instant of time when the input is applied, the desired response  $d$  of the system is provided by the teacher. This is illustrated in Figure 3.3(a). The distance  $p[d,o]$  between the actual and the desired response serves as an error measure and is used to correct network parameters externally. Since adjustable weights are assumed, the teacher may implement a reward-and-punishment scheme to adapt the network's weight matrix  $W$ . For instance, in learning classifications of input patterns or situations with known responses, the error can be used to modify weights so that the error decreases. This mode of learning is very pervasive. Also, it is used in many situations of natural learning. A set of input and output patterns called a training set is required for this learning mode.

Unsupervised learning algorithms use patterns that are typically redundant raw data having no labels regarding their class membership, or associations. In this mode of learning, the network must discover for itself any possibly existing patterns, regularities, separating properties, etc.

While discovering these, the network undergoes change of its parameters, which is called self-organization.

We may think of the following analogy. Learning with supervision corresponds to classroom learning with the teacher's questions answered by students and corrected, if needed, by the teacher. Learning without supervision corresponds to learning the subject from a videotape lecture covering the material but not including any other teacher's involvement. The teacher lectures directions and methods, but is not available. Therefore, the student cannot get explanations of unclear questions, check answers and become fully informed. Since supervised learning seems better than unsupervised learning, supervised learning is used during the simulation of the proposed model.

### 3.2.5 Neural Network Learning Rules

The focus of this section will be artificial neural network learning rules. A neuron is considered to be an adaptive element. Its weights are modifiable depending on the input data it receives, its output value, and the associated teacher response. In some cases, the teacher data is not available and no error information can be used, thus the neuron will modify its weights based only on the input and/or output. This is the case for unsupervised learning.

Let us study the learning of the weight vector  $w_i$ , or its components  $w_{ij}$  connecting the  $j$ 'th input with the  $i$ 'th neuron. In general, the  $j$ 'th input can be an output of another neuron or it can be an external input. This section will cover single neuron and single-layer network supervised learning and simple cases of unsupervised learning. Under different learning rules, the form of the neuron's activation function may be different. Note that the threshold parameter may be included in learning as one of the weights. This would require fixing one of the inputs, say  $x_n$ , we will assume here that  $x_n$ , if fixed, takes the value of 1.

The following general learning rule is adopted in neural network studies. (Arnari, 1990): The weight vector  $w_i = [w_{i1}, w_{i2}, \dots, w_{in}]^t$  increases in proportion to the product of input  $x$  and learning signal  $r$ . The learning signal  $r$  is in general a function of  $w_i, x$ , and sometimes of the teacher's signal  $d_i$ .

$$r = r(w_i, x, d_i) \quad (3.8)$$

The increment of the weight vector  $w_i$  produced by the learning step at time  $t$  according to the general learning rule is

$$\Delta w_i(t) = cr [w_i(t), x(t), d_i(t)] x(t) \quad (3.9)$$



where  $c$  is a positive number called the learning constant that determines the rate of learning. The weight vector adapted at time  $t$  becomes at the next instant, or learning step,

$$w_i(t+1) = w_i(t) + cr [w_i(t), x(t), d_i(t)] x(t) \quad (3.10)$$

The superscript convention will be used in this text to index the discrete-time training steps as in Equation (3.10). For the  $k$ 'th step come from (3.10) using this convention

$$w_i^{k+1} = w_i^k + cr [w_i^k, x^k, d_i^k] x^k \quad (3.11)$$

The learning in (3.11) assumes the form of a sequence of discrete-time weight modifications. Continuous-time learning can be expressed as

$$\frac{dw_i(t)}{dt} = crx(t) \quad (3.12)$$

### 3.3 Optimization Algorithm

There are several types of optimization algorithm available such as Gauss-Newton algorithm(GNA), gradient descent algorithm (GDA), Levenberg-Marquardt algorithm(LMA).

The LMA is used software applications for solving generic curve-fitting problems. However, as with many fitting algorithms, the LMA finds only a local minimum, which is not necessarily the global minimum. The LMA is more robust than the GNA and GDA in finding optimal solutions, which means that in many cases it finds a solution even if it starts very far off the final minimum (Gaddam and Rao, 2019). Because LMA interpolates between the Gauss–Newton algorithm (GNA) and the method of gradient descent,

$$[J^T W J + \lambda I] h_{tm} = J^T W (y - \hat{y}) \quad (3.13)$$

Where small values of the damping parameter  $\lambda$  result in a Gauss-Newton algorithm and large value of  $\lambda$  result in a gradient descent algorithm (Gavin, 2020).  $W$  is the weighting matrix,  $J$  is the Jacobian matrix which represents the local sensitivity of the function.

### 3.4 Flow Chart for Proposed Model

ANN approach is adopted in this study to develop speed-density relationship to introduce nonlinearity phenomena rather than conventional approaches. Deterministic models are made of passive data structures. These data structures are normally manipulated by an active procedure. Neural network models show global system behavior observed from local

interactions. Learning process of ANN model follows an input–output mapping and adapts their synaptic weights. Using Neural Fitting tool in MATLAB, ANN models were developed and the details are given in section 3.5. A neural network model consists of processing elements (neurons) and connections (links). The use of models based on neural network approach is efficient and practical as they facilitate their own implementation and learning based on real data. Network is referred as a layered network where hidden units lie between input and output units. Architectural view of proposed model neural network is shown in Figure 3.4. In this study, a two-layer feedforward network trained with Levenberg–Marquardt algorithm is used for analysis of ANN models. Feedforward networks consist of a series of layers, and each subsequent layer has a connection from the previous layer. The final layer produces the network’s output. During the process, different composition data for training and validation were used for analysis of ANN models. The saturation function was used for hidden neuron activation. Mainly, feedforward computation consists of simple run, product and saturation evaluation. Levenberg–Marquardt backpropagation (trainlm) algorithm was used as a network training function which is the fastest backpropagation algorithm. Network performance was measured according to the root mean of squared error (RMSE). In the used network, saturation transfer function was used in the hidden layer and a linear transfer function in the output layer. It can be observed from Table 5.5 that ANN model gives better performance as compared to the other three models in terms of  $R^2$  value.  $R^2$  represents measures of strength of the relationship between dependent and independent variables.

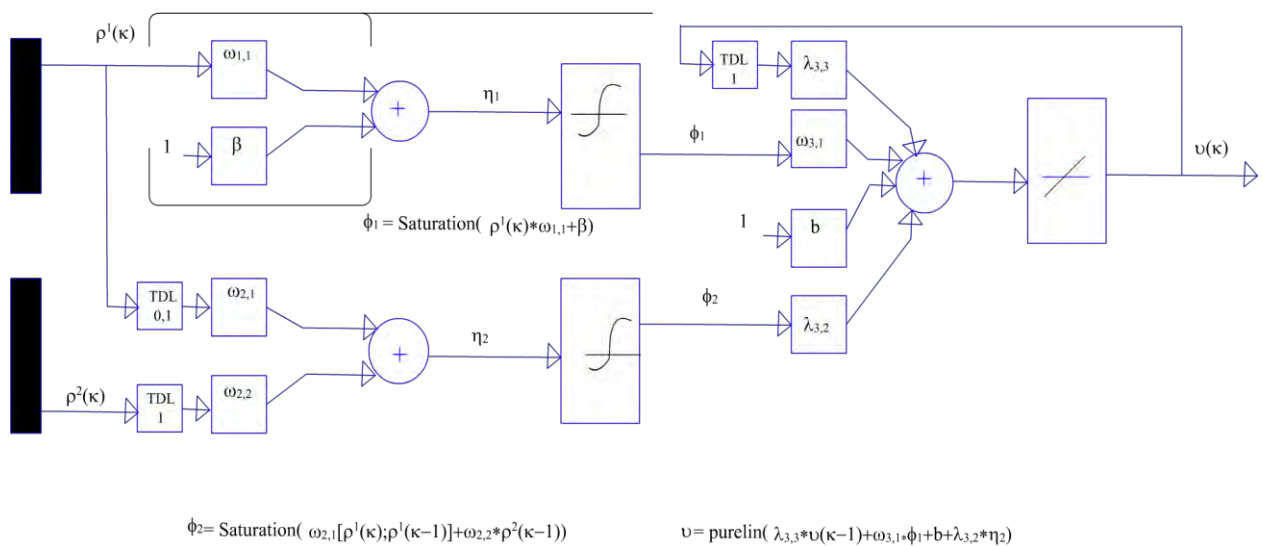


**Figure 3:4 Flow diagram of proposed model using neural network**

### 3.5 ANN Methodology for the Proposed Model

Let, density  $\hat{\rho}_i$  be the normalized input for the NN model  $\mu$ .  $\hat{\rho}_i$  is transmitted through a connection that multiplies its strength by a scalar weight  $\omega$ , to form  $\omega\hat{\rho}_i$ . The product  $\omega\hat{\rho}_i$  is also scalar in nature. A bias  $\beta_n$  is added with  $\omega\hat{\rho}_i$  to form the net input  $\eta$  for each neuron  $n$ . Equation (1) shows the structure of the  $\eta$ .

$$\eta_n = \omega_n \hat{\rho}_i + \beta_n \quad (3.14)$$

Within the neuron  $n$  the net input is pass through a transfer function  $\phi_n(\eta_n)$ . i.e. the  $\phi_n$  can be a tan sigmoid function, pure-linear or log sigmoid etc. For example, the saturation function presented below:

$$\phi_n(\eta_n) = \frac{2|X_n|}{1+|X_n|} \quad (3.15)$$

Afterwards, the output from a transfer function  $\phi_n$  is multiplied with a layer weight  $\lambda_n$  and summed to get a preliminary output. Another bias term  $b$  is added to get the final output. The final output  $\hat{v}$  is obtained from the equation (3.16).

$$\hat{v}_i = \sum_{n=1}^N \lambda_n \phi_n(\eta_n) + b \quad (3.16)$$

$\hat{v}_i$  is the normalized speed which ranges from 0 to 1. Ultimately,  $\hat{v}_i$  is de-normalized to find the estimated speed  $V_i$ .

The scalar weights, layer weights and biases are parameters  $\theta$  and the estimated speed  $V_i$  is dependent on these parameters. Thus, estimated speed  $V_i$  can be expresses as,

$$V_i = \mu_u(\hat{\rho}_i, \theta) \quad (3.17)$$

Where,  $\mu_u$  is the untrained NN model. The tanning algorithm updates  $\theta$  to reduce the overall error in between estimated and observed speed. An error function can determine this error, which can be expresses as follows,

$$R_e = \xi(v_e, \mu_u(\hat{\rho}, \theta)), \hat{\rho} = \{\hat{\rho}_1, \hat{\rho}_2, \hat{\rho}_3, \dots, \hat{\rho}_m\} \text{ and } \forall \hat{\rho}_i \in \mathbb{Z}^{\geq} \quad (3.18)$$

Where,  $R_e$  is response due to error and  $\hat{\rho}$  is the input vector. The simplified form of equation (4) can be expressed as Mean Square Error (MSE) in between  $V_i$  and  $v_e$ . The equation is as follows:

$$R_e = \sum_{i=1}^m \frac{(v_e - \mu_u(\hat{\rho}_i, \theta)_i)^2}{m} \quad (3.19)$$

For obtaining the optimum parameters  $\theta^*$  (scalar weights, layer weights and biases)  $R_e$  is fed into an objective function. A training algorithm is used to minimize the error  $R_e$ . The objective function can be expressed as follows:

$$\theta^* = \arg \min_{\theta \in \mathbb{R}} f \left( \sum_{i=1}^m \frac{(v_e - \mu_u(\hat{\rho}, \theta)_i)^2}{m} \right) \quad (3.20)$$

A trained NN model can be expressed as,

$$V_i = \mu_t(\hat{\rho}, \theta^*) \quad (3.21)$$

Where,  $\mu_t$  is the trained NN model with minimized error  $R_e$ .

### Estimating Fundamental Diagram Parameters

Equation (3.16) can be written as,

$$\hat{v}_i = \sum_{n=1}^N \lambda_n \left( \frac{2|X_n|}{1+|X_n|} \right) + b$$

$$\hat{v}_i = \sum_{n=1}^N \lambda_n \left( \frac{\pm 2 |\omega_n \hat{\rho}_i + \beta_n|}{1 + |\omega_n \hat{\rho}_i + \beta_n|} \right) + b \quad (3.22)$$

De-normalizing the equation (3.22), speed equation can be obtained,

$$V_i = V_{\min} + (V_{\max} - V_{\min}) \left( \sum_{n=1}^N \lambda_n \left( \frac{\pm 2 |\omega_n \hat{\rho}_i + \beta_n|}{1 + |\omega_n \hat{\rho}_i + \beta_n|} \right) + b \right) \quad (3.23)$$

Putting  $\hat{\rho}_i = 0$  in the equation (3.22) becomes

$$\hat{v}_i = \sum_{n=1}^N \lambda_n \left( \frac{\pm 2 |\beta_n|}{1 + |\beta_n|} \right) + b \quad (3.24)$$

De-normalizing the equation (3.24),  $V_f$  the free flow speed can be obtained,

$$V_f = V_{\min} + (V_{\max} - V_{\min}) \left( \sum_{n=1}^N \lambda_n \left( \frac{\pm 2 |\beta_n|}{1 + |\beta_n|} \right) + b \right) \quad (3.25)$$

Similarly, the jam density  $\rho_j$  can be calculated by putting  $V_i = 0$ , in equation (3.23) thus

$$\mu_u(\hat{\rho}_i, \theta) = 0$$

$$V_{\min} + (V_{\max} - V_{\min}) \left( \sum_{n=1}^N \lambda_n \left( \frac{\pm 2 |\omega_n \hat{\rho}_i + \beta_n|}{1 + |\omega_n \hat{\rho}_i + \beta_n|} \right) + b \right) = 0$$

$$V_{\min} + (V_{\max} - V_{\min}) \left( \sum_{n=1}^N \lambda_n \left( \frac{\pm 2 |X_n|}{1 + |X_n|} \right) + b \right) = 0$$

$$\left( \sum_{n=1}^N \lambda_n \left( \frac{\pm 2 |X_n|}{1 + |X_n|} \right) \right) = -\frac{V_{\min}}{(V_{\max} - V_{\min})} - b$$

$$\left( \sum_{n=1}^N \lambda_n \left( \frac{\pm |X_n|}{1 + |X_n|} \right) \right) = -\frac{V_{\min}}{2(V_{\max} - V_{\min})} - \frac{b}{2} \quad (3.26)$$

$$\text{Let, } -\frac{V_{\min}}{2(V_{\max} - V_{\min})} - \frac{b}{2} = C$$

The equation (3.26) becomes

$$\left( \sum_{n=1}^N \lambda_n \left( \frac{\pm |X_n|}{1 + |X_n|} \right) \right) = C$$

Taking the positive (+ve) value i.e  $\omega_n \hat{\rho}_i + \beta_n > 0$

$$\left( \sum_{n=1}^N \lambda_n \left( \frac{X_n}{1+X_n} \right) \right) = C$$

$$\left( \sum_{n=1}^N \lambda_n \left( \frac{X_n+1-1}{1+X_n} \right) \right) = C$$

$$\left( \sum_{n=1}^N \lambda_n \left( 1 - \frac{1}{1+X_n} \right) \right) = C$$

$$\left( \sum_{n=1}^N \lambda_n - \sum_{n=1}^N \frac{\lambda_n}{1+X_n} \right) = C$$

$$\sum_{n=1}^N \lambda_n - C = \sum_{n=1}^N \frac{\lambda_n}{1+X_n}$$

$$\frac{1}{\sum_{n=1}^N \lambda_n - C} = \sum_{n=1}^N \left( \frac{1}{\lambda_n} + \frac{X_n}{\lambda_n} \right)$$

$$\frac{1}{\sum_{n=1}^N \lambda_n - C} - \sum_{n=1}^N \frac{1}{\lambda_n} = \sum_{n=1}^N \frac{X_n}{\lambda_n}$$

Putting  $X_n = \omega_n \hat{\rho}_i + \beta$

$$\sum_{n=1}^N \frac{\omega_n \hat{\rho}_i + \beta_n}{\lambda_n} = \frac{1}{\sum_{n=1}^N \lambda_n - C} - \sum_{n=1}^N \frac{1}{\lambda_n}$$

$$\sum_{n=1}^N \frac{\omega_n}{\lambda_n} \hat{\rho}_i = \frac{1}{\sum_{n=1}^N \lambda_n - C} - \sum_{n=1}^N \frac{1}{\lambda_n} - \sum_{n=1}^N \frac{\beta_n}{\lambda_n}$$

$$\therefore \hat{\rho}_i = \sum_{n=1}^N \frac{\lambda_n}{\omega_n} \left( \frac{1}{\sum_{n=1}^N \lambda_n - C} - \sum_{n=1}^N \frac{1}{\lambda_n} - \sum_{n=1}^N \frac{\beta_n}{\lambda_n} \right) \quad (3.27)$$

De-normalizing the equation (3.27),  $\rho_j$  the jam density can be obtained,

$$\begin{aligned}
\frac{\rho_j - \rho_{\min}}{\rho_{\max} - \rho_{\min}} &= \sum_{n=1}^N \frac{\lambda_n}{\omega_n} \left( \frac{1}{\sum_{n=1}^N \lambda_n - C} - \sum_{n=1}^N \frac{1}{\lambda_n} - \sum_{n=1}^N \frac{\beta_n}{\lambda_n} \right) \\
\rho_j &= \rho_{\min} + (\rho_{\max} - \rho_{\min}) \left( \sum_{n=1}^N \frac{\lambda_n}{\omega_n} \left( \frac{1}{\sum_{n=1}^N \lambda_n - C} - \sum_{n=1}^N \frac{1}{\lambda_n} - \sum_{n=1}^N \frac{\beta_n}{\lambda_n} \right) \right) \\
\therefore \rho_j &= \rho_{\min} + (\rho_{\max} - \rho_{\min}) \left( \sum_{n=1}^N \frac{\lambda_n}{\omega_n} \left( \frac{1}{\sum_{n=1}^N \lambda_n + \frac{V_{\min}}{2(V_{\max} - V_{\min})} + \frac{b}{2}} - \sum_{n=1}^N \frac{1}{\lambda_n} - \sum_{n=1}^N \frac{\beta_n}{\lambda_n} \right) \right) \quad (3.28)
\end{aligned}$$

Similarly, Taking the negative (-ve) value i.e.  $\omega_n \hat{\rho}_i + \beta_n < 0$

$$\left( \sum_{n=1}^N \lambda_n \left( \frac{-X_n}{1+X_n} \right) \right) = C$$

$$\left( \sum_{n=1}^N \lambda_n \left( \frac{X_n + 1 - 1}{1+X_n} \right) \right) = -C$$

$$\left( \sum_{n=1}^N \lambda_n \left( 1 - \frac{1}{1+X_n} \right) \right) = -C$$

$$\left( \sum_{n=1}^N \lambda_n - \sum_{n=1}^N \frac{\lambda_n}{1+X_n} \right) = -C$$

$$\sum_{n=1}^N \lambda_n + C = \sum_{n=1}^N \frac{\lambda_n}{1+X_n}$$

$$\frac{1}{\sum_{n=1}^N \lambda_n + C} = \sum_{n=1}^N \left( \frac{1}{\lambda_n} + \frac{X_n}{\lambda_n} \right)$$

$$\frac{1}{\sum_{n=1}^N \lambda_n + C} - \sum_{n=1}^N \frac{1}{\lambda_n} = \sum_{n=1}^N \frac{X_n}{\lambda_n}$$

Putting  $X_n = \omega_n \hat{\rho}_i + \beta$

$$\sum_{n=1}^N \frac{\omega_n \hat{\rho}_i + \beta_n}{\lambda_n} = \frac{1}{\sum_{n=1}^N \lambda_n + C} - \sum_{n=1}^N \frac{1}{\lambda_n}$$

$$\sum_{n=1}^N \frac{\omega_n}{\lambda_n} \hat{\rho}_i = \frac{1}{\sum_{n=1}^N \lambda_n + C} - \sum_{n=1}^N \frac{1}{\lambda_n} - \sum_{n=1}^N \frac{\beta_n}{\lambda_n}$$

$$\therefore \hat{\rho}_i = \sum_{n=1}^N \frac{\lambda_n}{\omega_n} \left( \frac{1}{\sum_{n=1}^N \lambda_n + C} - \sum_{n=1}^N \frac{1}{\lambda_n} - \sum_{n=1}^N \frac{\beta_n}{\lambda_n} \right) \quad (3.29)$$

De-normalizing the equation (3.29),  $\rho_j$  the jam density can be obtained,

$$\frac{\rho_j - \rho_{\min}}{\rho_{\max} - \rho_{\min}} = \sum_{n=1}^N \frac{\lambda_n}{\omega_n} \left( \frac{1}{\sum_{n=1}^N \lambda_n + C} - \sum_{n=1}^N \frac{1}{\lambda_n} - \sum_{n=1}^N \frac{\beta_n}{\lambda_n} \right)$$

$$\rho_j = \rho_{\min} + (\rho_{\max} - \rho_{\min}) \left( \sum_{n=1}^N \frac{\lambda_n}{\omega_n} \left( \frac{1}{\sum_{n=1}^N \lambda_n + C} - \sum_{n=1}^N \frac{1}{\lambda_n} - \sum_{n=1}^N \frac{\beta_n}{\lambda_n} \right) \right)$$

$$\therefore \rho_j = \rho_{\min} + (\rho_{\max} - \rho_{\min}) \left( \sum_{n=1}^N \frac{\lambda_n}{\omega_n} \left( \frac{1}{\sum_{n=1}^N \lambda_n - \frac{V_{\min}}{2(V_{\max} - V_{\min})} - \frac{b}{2}} - \sum_{n=1}^N \frac{1}{\lambda_n} - \sum_{n=1}^N \frac{\beta_n}{\lambda_n} \right) \right) \quad (3.30)$$



## Estimating Capacity

Capacity is the vital parameter of the traffic flow theory

Capacity can be written

$$C = \frac{1}{4} * \rho_j * V_f$$

$$\therefore \text{Capacity}, C = \frac{1}{4} \left( \rho_{\min} + (\rho_{\max} - \rho_{\min}) \left( \sum_{n=1}^N \frac{\lambda_n}{\omega_n} \left( \frac{1}{\sum_{n=1}^N \lambda_n + \frac{V_{\min}}{2(V_{\max} - V_{\min})} + \frac{b}{2}} - \sum_{n=1}^N \frac{1}{\lambda_n} - \sum_{n=1}^N \frac{\beta_n}{\lambda_n} \right) \right) \right) * \left( V_{\min} + (V_{\max} - V_{\min}) \left( \sum_{n=1}^N \lambda_n \left( \frac{\pm 2|\beta_n|}{1 + |\beta_n|} \right) + b \right) \right)$$

### 3.6 Fundamental Diagram for Incomplete Data Set

Traffic monitoring in urban areas is the fact that road works often result in cables getting broken, and consequently loop detector in the road surface are no longer operation (Li et al., 2014). If the loop detector fails to collect data for any regime i.e. free-flow regime, congested regime, the model should also work. As such we are investigating, first of all, whether it is possible to derive a well-defined fundamental diagram from incomplete dataset. The proposed model is developed in such a way so that it can also work in incomplete dataset.

### 3.7 Developing a Tool to Calibrate Speed-density Diagram Automatically

Fundamental Diagram Calibration using Machine Learning (FRAME) is an application tool developed using MATLAB GUI. The application is capable to work independently under .exe format as well. Figure 3.5 shows the interface of the developed tool. In the middle portion of the interface, there is a 'Load Data File' button. It is provided for uploading traffic data from MS Excel spread sheet. From the uploaded data, the number of data, minimum speed, maximum speed, minimum density, maximum density, average density, average speed will be taken. In the upper right portion of the interface, radio button for different parameters of proposed model. The parameters are transfer function, training algorithm. The available transfer functions are proposed saturation function, Heaviside function, logistic function, pureline function, hardlimit function. The training algorithm are Levenberg-Marquardt, Bayesian Regularization, Scaled Conjugate Gradient. There are also hidden layer option, training-testing data division option. In addition to the 'Load Data File' button, there is a radio button for user to choose various FD models to compare with the proposed model. Several FD

models can be chosen from the three groups of models—Single Regime Models (Greenshields, Greenberg, Underwood, Drew, Pipes-Munjial, 5PL logistic), Multi-Regime Models (Edie, May and Modified Greenberg) and Data driven model (ANFIS). After uploading the aggregated traffic data (measured speed  $v$ , flow  $q$  and density  $k=q/v$ ), selecting FD model, selecting transfer function, training algorithm, hidden layer, the detailed analysis starts automatically after pushing the analyze button. Using  $v$ - $k$  relationship FRAME generates corresponding fitted FD model. It provides the output in left portion of the interface. The outputs are free-flow speed, critical speed, critical density, jam density, capacity, RMSE value and  $R^2$ -value. Later, Speed-density, flow-density and speed-flow scattered plot with fitted model are generated in this portion of the interface.  $R^2$  and root mean square error are computed by FRAME for each selected FD model. Edie model and Two Regime Linear Model utilize separate .m extension file to perform iteration. The least square estimation method is encrypted in the PlotFD.m file to fit different FD structures and graphical interface is feed backed by MATLAB GUI.

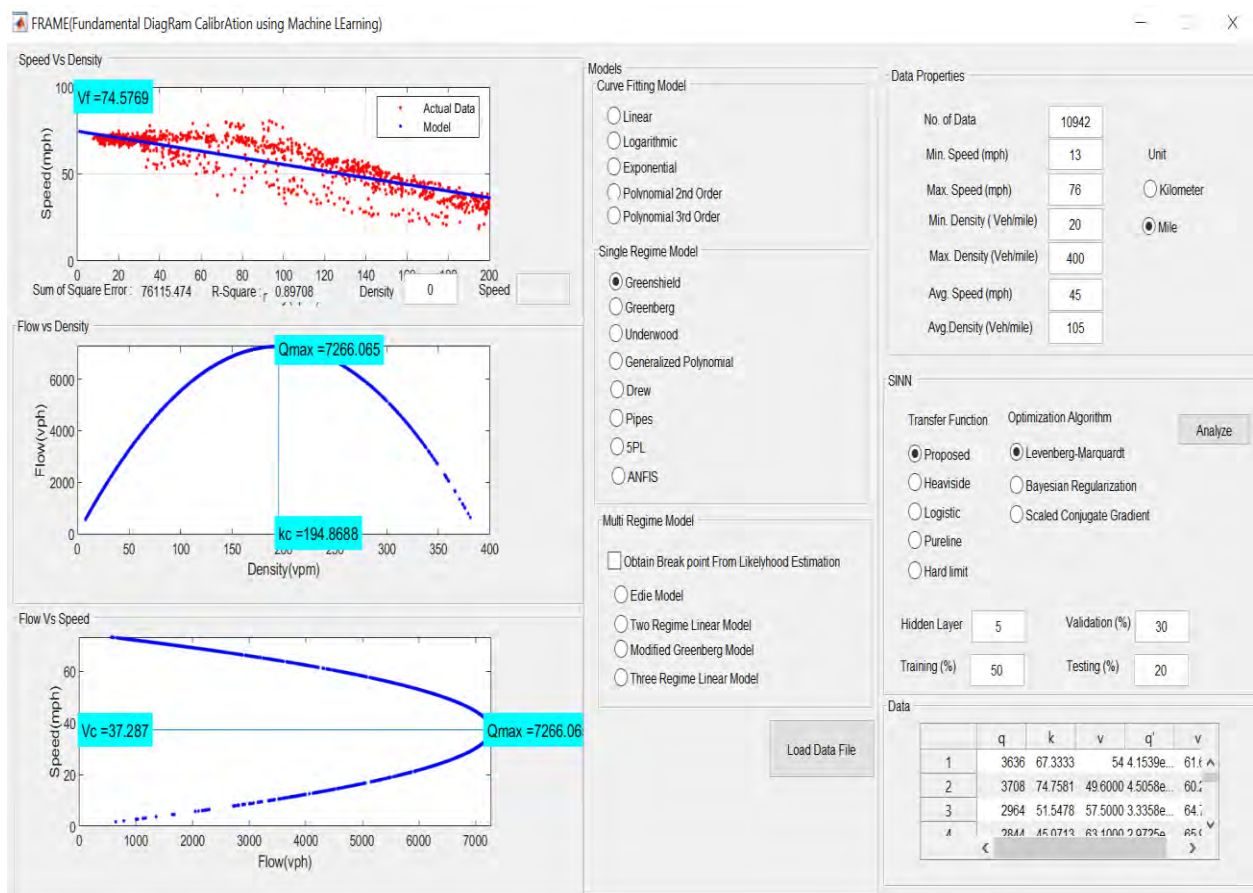


**Figure 3.5: Automatic speed-density diagram calibrating tool**

## CHAPTER 4

### DATA COLLECTION AND PROCESSING

#### 4.1. Introduction

This chapter includes a detailed description of data collection and data analysis methodology. Different models discussed in the previous chapter requires different type of data for calibration and validation. This chapter gives the complete description of the data collection methodology and the way of analysis.

#### 4.2 Data Collection Location

It has been known that speed-density relationships are time and location based. They depend on where observed and for how long it was observed (May, 1990). A fundamental diagram is regarded simply as the functional relationship of the three basic traffic fundamental variables (flow  $q$ , speed  $v$  and density  $k$ ). In particular, speed-density relationships serve as a basis to understand traffic system dynamics in research and engineering practice. Once the speed-density curve is determined at a certain location, the corresponding speed-flow and flow-density relations can easily be obtained. By maximizing the minimum length of segments, the efficiency of the optimization algorithms can be improved.

For on-ramp and off-ramps, the necessity for further research efforts is due to the fact that on-ramp/off-ramp control strategies are important considerations for maintaining highway capacity and a high level of service (LOS). Empirical results show that speed-density curves at on-ramp/off-ramps still attain the exponential relationship but with distinguishable features which differentiate them from basic highway segments. The pattern is relatively consistent but has different free-flow speeds and jam densities due to the various characteristics of the on-ramp/off-ramps or entrance/exit ramps (i.e. ramp geometry, speed limit, elevation, slope, and varying driver behaviors). The results show that the estimation of travel time on traffic network might potentially be improved by removing the assumption that the speed-density curve at on-ramp/off-ramp is the same as on basic highway segments.

The speed-density relationships at different locations of basic freeway segments and ramps also vary. Using a speed-density curve to model a collection of on-ramp/off-ramp will certainly improve the efficiency of on-ramp/off-ramp control algorithms. For this reason, data collection process for model calibration, validation and comparison is based on five different scenarios.

These scenarios represent different driving behavior and consist of main line, main line with interruption from off ramp, main line with interruption from on ramp, off- ramp and on- ramp. Four datasets were collected for each scenario from different locations. One dataset is used for calibration and the other three is used for validation.

For this reason, 5 five data collection points were selected along the study corridor (i.e, non-lane based heterogeneous traffic). The points are shown in the Figure 4.1. These locations are selected as so it represents non-lane based heterogeneous traffic flow characteristics. One of the objectives of the study to fit and evaluate speed-density relationship for non-lane based heterogeneous traffic.

Study corridor used in this research is the Tongi Diversion Road, a section of the Dhaka-Mymensingh Highway (N3) in Bangladesh (shown in Figure 4.1). It is an 8-lane major artery road in Dhaka, which connects the capital city with the Hazrat Shahjalal International Airport (HSIA). The selected 3.26 kilometers (km) long uninterrupted section has one off-ramp, closely followed by an on-ramp. These form one diverge and one merge section along the corridor. There are exactly 4 through lanes on each direction of the test site totaling up to a width of 14.48 meters (m) to 14.94 m in different links. The on-ramps and off-ramps have two lanes each, though lane discipline is absent in the main stream flow and in the ramp flows. From the collected data it can be seen that the traffic stream consists of 40% cars, 12% microbuses or jeeps, 10% motorcycles, 8% buses, 10% utility vehicles and 20% auto-rickshaws. Such geometric and traffic characteristics make the test site an ideal study location for non-lane-based heterogeneous uninterrupted traffic condition. Collection of high-resolution traffic data required for the development of an accurate model is a very challenging task under the existing traffic condition of the study area. This is mainly because loop detectors are unsuitable for the test site due to measurement errors caused by non-lane-based movement of vehicles activating either both or neither of two adjacent detectors. Moreover, traffic cameras for vehicle detection are absent along the corridor. Under these circumstances, video cameras are installed at various locations of the study site to provide traffic data for the research using image processing technique. The locations of video cameras are shown in Figure 4.1.

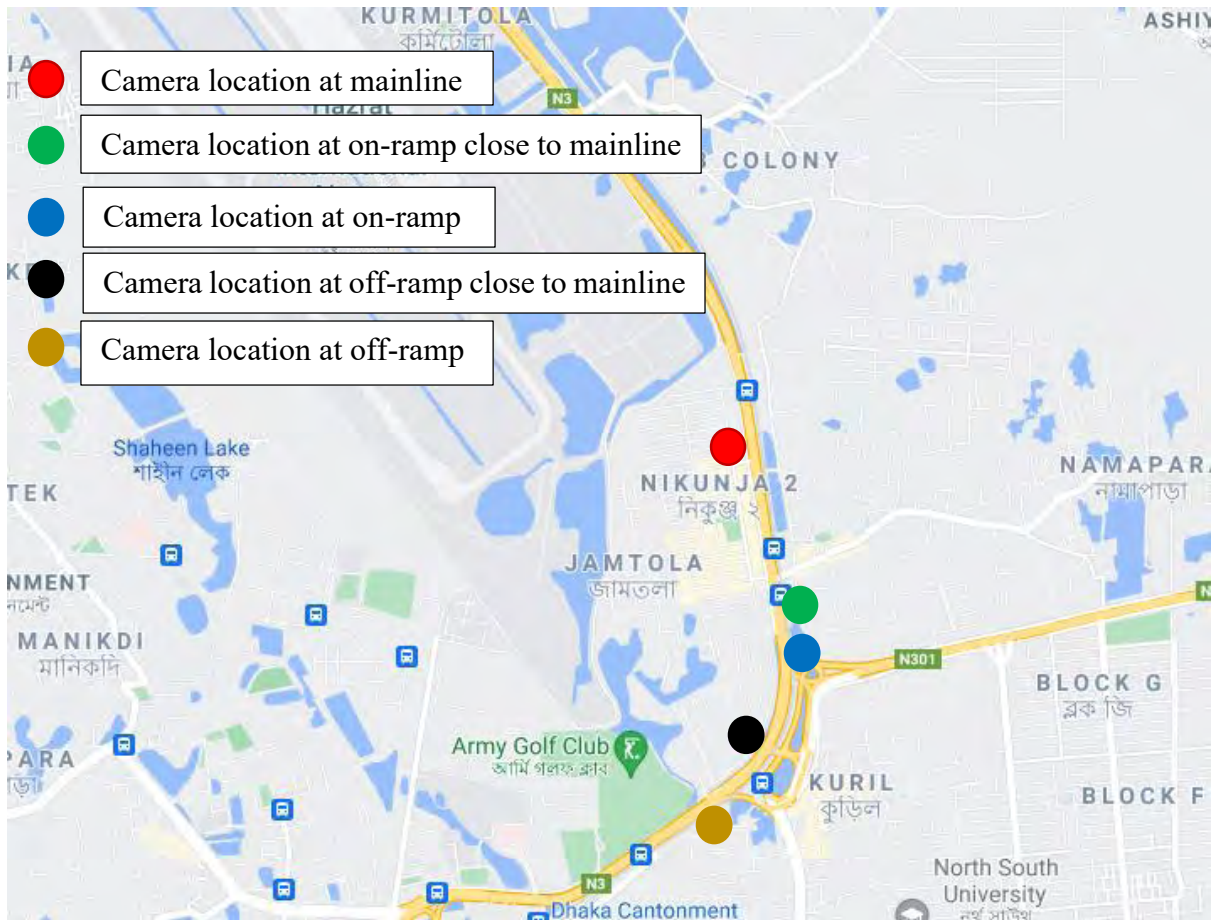


**Figure 4:1 Data collection point along study corridor (Source: Google Map)**

Empirical data is used to develop and validate the proposed model for lane based homogeneous traffic condition to verify the robustness using a secondary data source. These datasets were collected from Caltrans PeMS (2017) which provides flow, speed and density data across different vehicle detector stations in the form of time series data over days of operation. The data used in this study are aggregated over an interval of 5 minutes. The data are collected from I-80 near Berkeley that is a freeway with on-ramps and off ramps. At each location, one year continuous observations were collected. This time interval is long enough for calibration and validation of fundamental diagram. A general setting of I-80 detectors from the study site in Berkeley, California is shown in Figure 4.2.

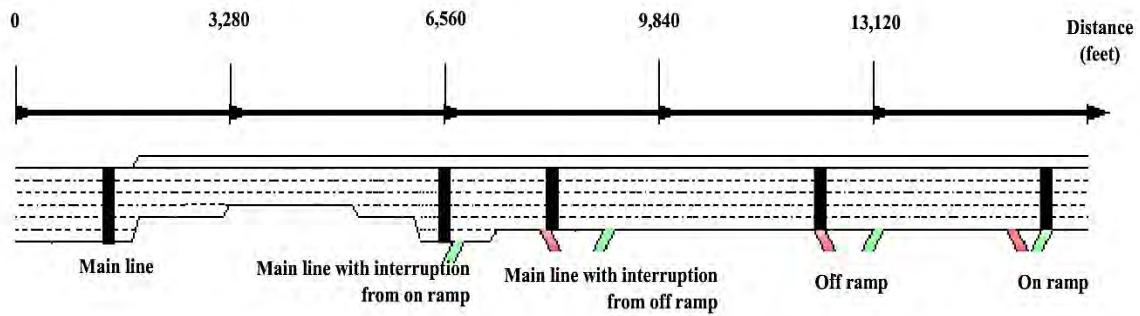


**Figure 4:2 Illustration of layout of study site I-80, Berkeley (not to scale)**

For extracting high resolution traffic data from the video footages of the cameras, an object detection algorithm has been developed based on the Background Subtraction (BGS) technique of image processing (Haddiuzzan, et al., 2017). The developed algorithm can successfully detect non-lane-based movement of vehicles. It can also identify non-motorized traffic, dark car and shadow quite accurately. The algorithm addresses some of the major problems faced in the BGS technique, like the camouflage effect, camera jitter, sudden illumination variation, low camera angle and elevation etc. Video data and vehicle geometry are provided as input to the algorithm and it gives vehicle count and time mean speed at required intervals as the output. For measuring flow, strip based counting method combining successive incremental differentiation is used. On the other hand, for measuring speed, the algorithm segments the whole field of vision and detects the change in center of area of an object in each segment to find the corresponding pixel speed. Then calibrating the pixel distance with the field distance, instantaneous and time mean speeds are obtained, which can easily be converted to space mean speed. The developed algorithm has been proved to give highly accurate traffic data with Mean Absolute Error (MAE) of only 14.01 and 0.88 in flow and speed measurements respectively when compared with actual field measurements. The density of the traffic stream for the research is estimated from the measured flow and speed. The data obtained from each camera is considered representative of the traffic condition of the whole link. The ramps are also equipped with video cameras for collecting data of the merging and diverging traffic. Although the non-lane-based heterogeneous behavior becomes more acute with the increase of traffic volume in the roadway (Hossain, et al., 2016), the test site was videoed from 3:00 PM to 6:00 PM covering both peak and off-peak periods for FD investigation. Two sets of videos were collected for the same time period on 15-16 April, 2019. These videos were processed and the extracted data was filtered for anomalies. Ultimately, 3 hours' data of 15<sup>th</sup> April was used for



calibration of the model parameters and the similar data set from 16<sup>th</sup> April was used for model validation. To ensure better quality of the collected data, the camera height and angle of projection were strictly maintained. As shown in Figure 4.3, the mounting heights of the cameras were at least 20ft to reduce the object details detected by the algorithm and the camera angle was less than 45 degrees to avoid perception problem. However, the angle was not so small as to cause restriction in vision.



**Figure 4:3 Detailing of camera setting for data collection**

Due to the lack of lane discipline and existence of multiple classes of vehicles, extracting heterogeneous traffic data become cumbersome. In this study, BGS, a video image processing algorithm was used to extract individual vehicular speeds and classified volume counts. The detailing process is given in next section.

### **4.3. Data Processing**

All the required non-lane based heterogeneous data for developing the model has been collected by video recording. The extraction of the collected data is necessary for data analysis and developing the desired model. Standard technique (BGS) is applied for extracting the collected data to maintain the quality of data. Video recording is conducted for those location in a certain time to capture the all type traffic flow characteristics. A total of 1800 minutes of video was recorded. In the following chapter data extraction method and technique and data analysis will be discussed.

### **4.4 Data Extraction Technique and Quality Assurance**

The traffic flow and the speed data were extracted from recorded video using two techniques: through pixel-based heterogeneous traffic measurement considering shadow and illumination variation methodology (Haddiuzzan, et al., 2017) using MATLAB coding, and another by manually reviewing the videos by multiple people. In the coding, the area and type of data needed were defined and the coding provided the classified traffic as output. 15-minutes interval was defined in the coding and data extracted from approximately 1800 minutes of recording video. Manual extraction was completed by reviewing the video by playing them at slow speed. The result obtained from both techniques were compared and repeated if there were any significant discrepancies (i.e., difference of  $\pm 20$  vehicles) (Mohamad, 2015).



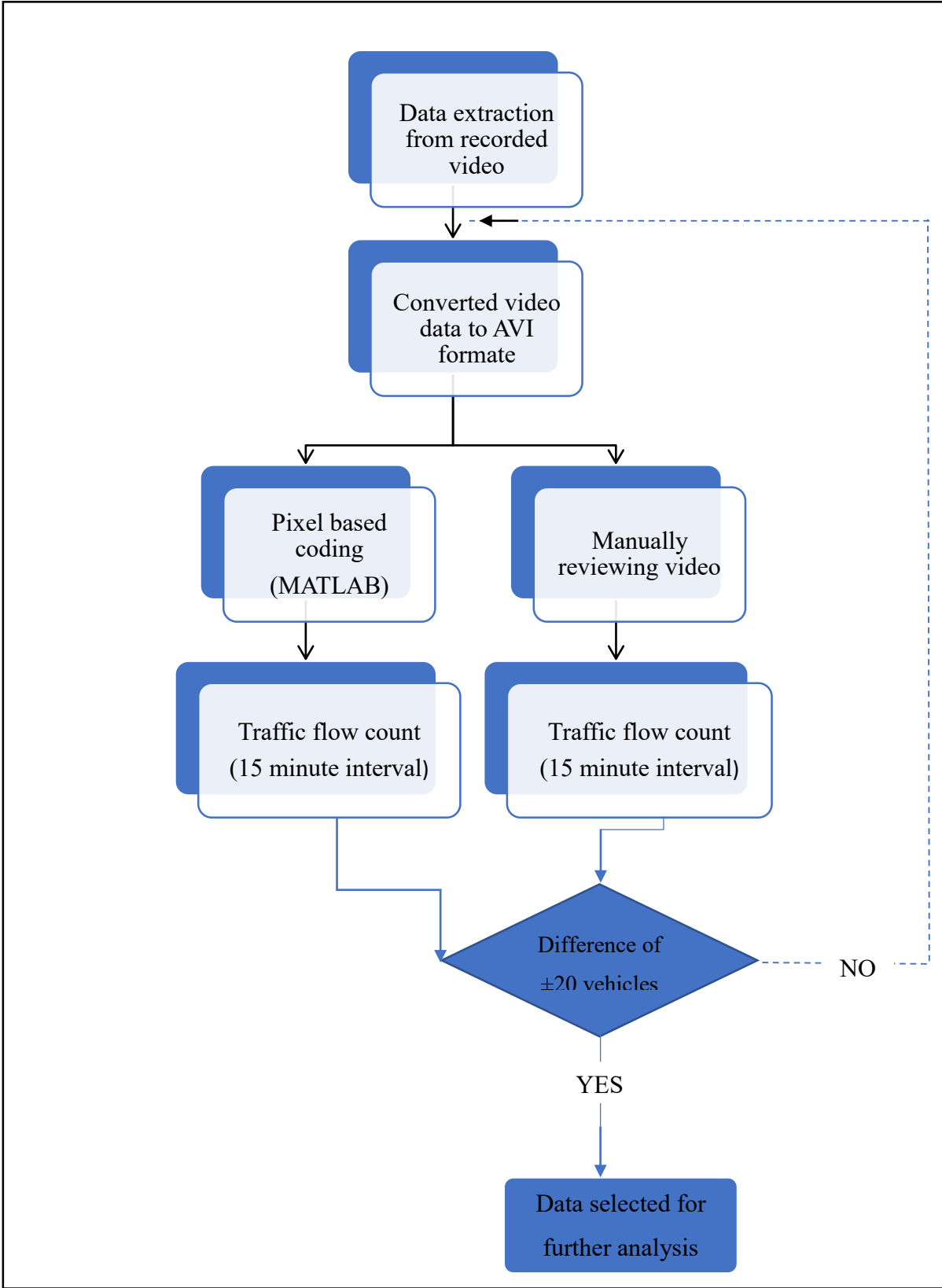
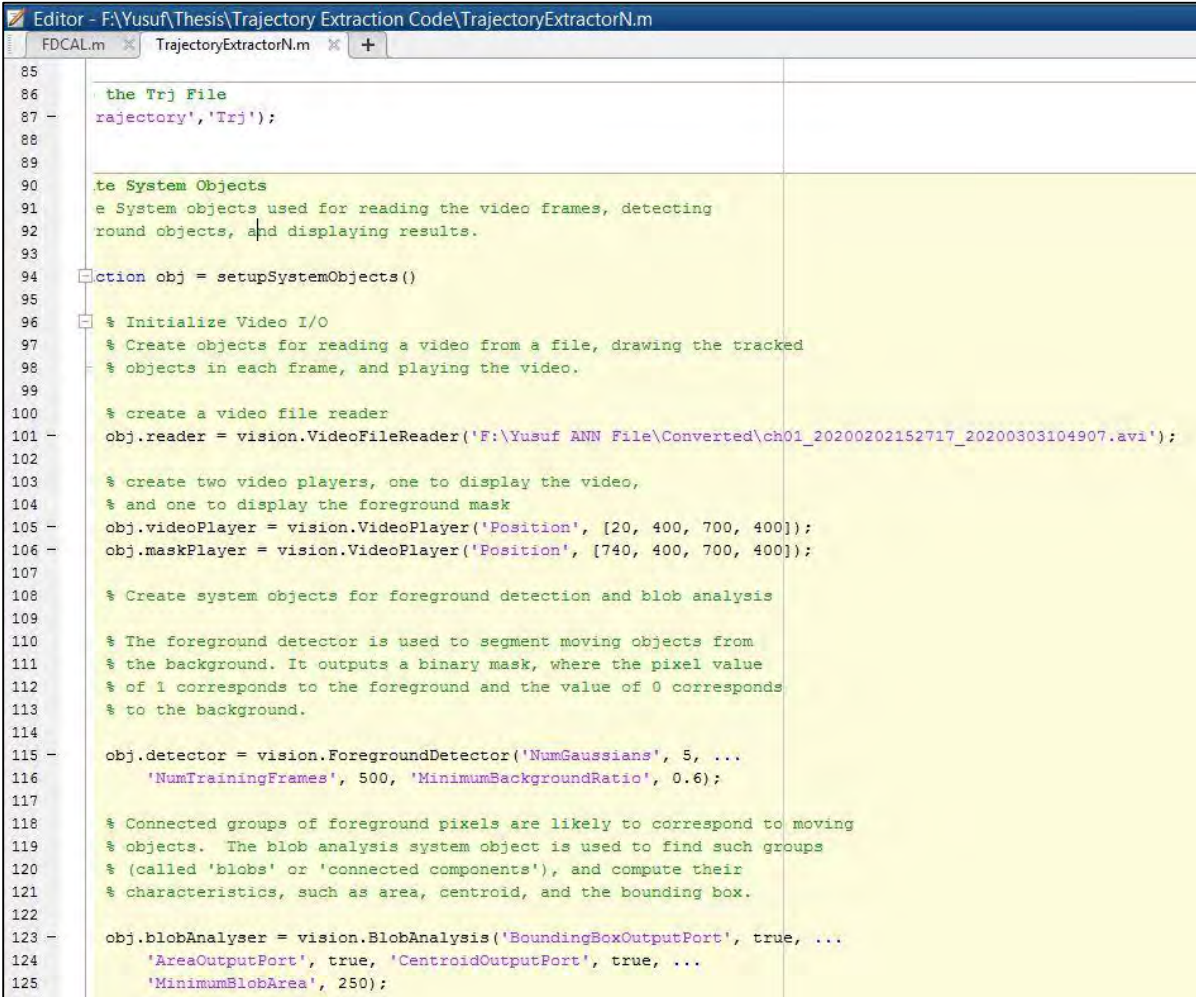


Figure 4:4 Flow chart of data extraction methodology

According to the above described methodology the data was extracted by pixel-based methodology. The screenshot of the coding and data extraction interface is shown in Figure 4.5 to Figure 4.8.



```
Editor - F:\Yusuf\Thesis\Trajectory Extraction Code\TrajectoryExtractorN.m
FDCAI.m TrajectoryExtractorN.m +
85
86 % the Trj File
87 - trajectory', 'Trj');
88
89
90 % Create System Objects
91 % Create System objects used for reading the video frames, detecting
92 % foreground objects, and displaying results.
93
94 obj = setupSystemObjects()
95
96 % Initialize Video I/O
97 % Create objects for reading a video from a file, drawing the tracked
98 % objects in each frame, and playing the video.
99
100 % create a video file reader
101 - obj.reader = vision.VideoFileReader('F:\Yusuf ANN File\Converted\ch01_20200202152717_20200303104907.avi');
102
103 % create two video players, one to display the video,
104 % and one to display the foreground mask
105 - obj.videoPlayer = vision.VideoPlayer('Position', [20, 400, 700, 400]);
106 - obj.maskPlayer = vision.VideoPlayer('Position', [740, 400, 700, 400]);
107
108 % Create system objects for foreground detection and blob analysis
109
110 % The foreground detector is used to segment moving objects from
111 % the background. It outputs a binary mask, where the pixel value
112 % of 1 corresponds to the foreground and the value of 0 corresponds
113 % to the background.
114
115 - obj.detector = vision.ForegroundDetector('NumGaussians', 5, ...
116     'NumTrainingFrames', 500, 'MinimumBackgroundRatio', 0.6);
117
118 % Connected groups of foreground pixels are likely to correspond to moving
119 % objects. The blob analysis system object is used to find such groups
120 % (called 'blobs' or 'connected components'), and compute their
121 % characteristics, such as area, centroid, and the bounding box.
122
123 - obj.blobAnalyser = vision.BlobAnalysis('BoundingBoxOutputPort', true, ...
124     'AreaOutputPort', true, 'CentroidOutputPort', true, ...
125     'MinimumBlobArea', 250);
```

Figure 4:5 Screenshot of data extraction trajectory

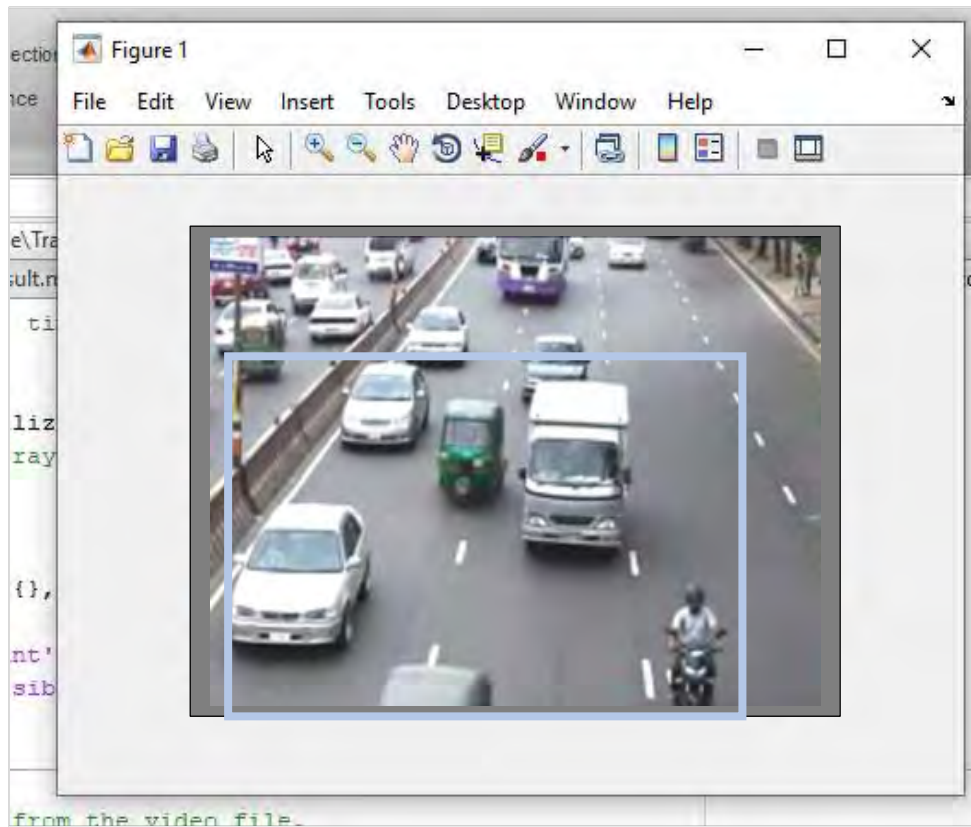


**Figure 4:6 Screenshot of area selection for data extraction**

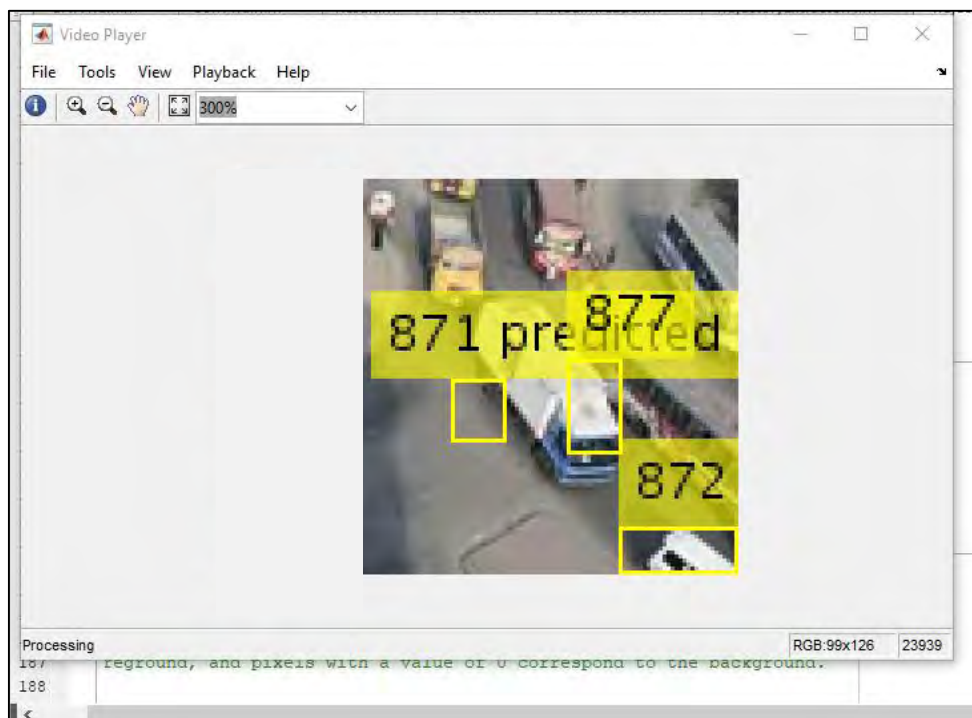


**Figure 4:7 Screenshot of vehicles detection and counting block**



**Figure 4:8 Screenshot of tracked binary image for illumination of vehicles**

#### **4.5 Extracted Data**

From data extraction, the traffic flows were calculated for each of the selected location with speed. The extracted data then aggregated in different level i.e. 20 seconds, 1 min, 2 min, 3 min, 5 min, 6 min. The sample of extracted data is given in Table 4.1 and detail data is given in Appendix A-3.

**Table 4.1 Data collected from study corridor**

<b>Time</b>	<b>Speed (Mile/hr)</b>	<b>Flow (veh/hr)</b>	<b>Density (veh/mile)</b>
3:00:20 PM	22.6	5040	223
3:00:40 PM	18.1	3780	209
3:01:00 PM	23.9	3960	166
3:01:20 PM	18.3	4500	246
3:01:40 PM	21.3	4320	202
3:02:00 PM	20.3	4140	204
3:02:20 PM	24.0	4140	172
3:02:40 PM	20.4	3600	176
3:03:00 PM	21.8	4680	214
3:03:20 PM	18.8	4320	230
3:03:40 PM	25.0	3420	137
3:04:00 PM	25.6	5220	204
3:04:20 PM	28.0	3600	129
3:04:40 PM	25.8	2880	112
3:05:00 PM	15.9	2700	170

## CHAPTER 5

### CALIBRATION RESULTS AND MODEL VALIDATION

#### 5.1 Introduction

Generally, a model development sequence includes: identification of model objectives, formulation of a conceptual model, validation, performance analysis and model application etc. In the model life cycle, validation is probably one of the most important steps, but it is also the most overlooked procedure after the model development. Validation is the task of testing whether the proposed model is an accurate representation of the real world from the perspective of the intended use by referring the model output to experimental observations (Nikolaidis et al., 2005). The model outputs of the stochastic models are usually in forms of distribution functions. The traditional approach in calculating the descriptive statistics such as mean and variance is insufficient when comparing the stochastic outputs to empirical observations.

Measuring the closeness of two sets of distributions has been of great interest to a wide branch of academic and professional communities. The initial impetus to find the distance between two distributions came from the need to conveniently measure the discrepancy/similarity between two distribution functions. Computing distances between distributions is important in many circumstances. This dissertation reviews some probabilistic distance measures to evaluate the closeness/discrepancy between two different sets of distributions to serve the purpose of validating a stochastic model. The work to find the distance between two distributions has been discussed in literature with many possible solutions available (Cortes et al., 2007). There is a multitude of literature existing with a variety of possible solutions to serve the validation purpose of simulation models in general (Lei et al., 1998) and to validate microscopic and macroscopic traffic simulation models (Daiheng et al., 2004). The validation techniques can be categorized as qualitative and quantitative for systems which are observable or not. Qualitative measures include series plot, contour plot, surface plot, diagonal plot, histogram, animation etc (Daiheng et al., 2004). Quantitative statistical measures include mean error (ME), mean absolute error (MAE), mean squared error (MSE), root-mean square error (RMSE), mean percentage error (MPE), mean absolute percentage error (MAPE) etc. The main criticism of these statistical measures is that they are describing “average” behavior (Daiheng et al., 2004). Two totally different stochastic processes can have the same mean error. These measures may fail to satisfy the approximation of the real world

traffic condition of proposed stochastic model. Rao (1975) discussed some ways of validating stochastic models in which two schools of validation methodology are emphasized as the predictive power and the dynamics of the stochastic model. This research focuses on the predictive capability for validating the stochastic model.

## **5.2 Effects of Different Parameters in Proposed Model**

There are a number of options and settings to explore during proposing an ANN model. The illustration of the available options and their effects on a number of modeling aspects is provided in this chapter. For example, experiment was performed to identify the optimal split of data into a training and a testing sample. In addition there four other aspects are the type of optimization algorithm, number of hidden layer, number of epochs and time aggregation level. These aspects are also illustrated here. The developed ANN model is further validated using different dataset and against other conventional models and the results are accumulated in this chapter later. To implement and test the proposed single-input ANN architecture, MATLAB neural net fitting Toolbox from MathWorks was selected as the development tool. This tool offers an environment to build and evaluate neural systems using a graphical user interface (GUI).

### **5.2.1 Effect of Size of Training and Testing Data Sets**

In neural networks, a subset of the sample (training data set) is used to train the neural network. Later, to test the ability of the model to reproduce other realities, the remaining portion of the sample (testing data set) that was not used for model calibration is used as a testing device. In practice, the optimal composition of the original sample (separation of the data into training and testing sets) needs to be known. The effects of different sizes of the training and the testing data sets on goodness of fit value are summarized in Table 5.1. All the results are presented in Appendix A-1 and graphical representation is in Appendix A-2.

For this study, seven different composition of data set for each scenario were considered to assess the effect. With an increase in training dataset, the fitness value ( $R^2$ ) obtained from Equation (5.1) improves as the generated ANN structure is fed with larger number of training dataset to optimize its parameter values. On the other hand, decreasing testing dataset causes the ‘overfitting’ phenomenon to occur. Overfitting is a common problem in ANN model building, which occurs when the data are over trained by ANN. Every data set that is trained using ANN has its maximum number of epochs before overfitting occurs; this causes the

predicted output to be over its accuracy. From Table 5.1, it can be observed 80-20 composition demonstrated the best fit over others. As, 80-20 split of original dataset for training and checking produced best results for all scenarios, this size is adopted as optimum composition for ANN modeling in this thesis.

$$R^2 = 1 - \frac{SS_E}{SS_T} \quad (5.1)$$

**Table 5.1 Effect of different composition of training dataset on fitness of data ( $R^2$  values) for different scenarios**

Scenario type	Training dataset and testing dataset composition						
	50-50	60-40	70-30	75-25	80-20	85-15	90-10
Main line	0.88035	0.88168	0.88059	0.88048	0.88187	0.88187	0.88160
Main line close to off-ramp	0.96259	0.96244	0.96259	0.96220	0.96259	0.96257	0.96246
Main line close to on-ramp	0.95265	0.95275	0.95277	0.95273	0.95285	0.95234	0.95249
Off- ramp	0.95312	0.95417	0.95417	0.95349	0.95417	0.95004	0.95408
On-ramp	0.93673	0.93779	0.93758	0.93418	0.93780	0.93752	0.93665

### 5.2.2 Effect of Hidden Layer Number

Hidden Layer Number determine the shape of the projection of input-output mapping and the parameters of these layer numbers adjusted through the neural system to capture the trend of the empirical data. In this study, four types of hidden layer number were considered. The results for different layer numbers are summarized in Table 5.2 for different scenarios. In all cases, Five hidden layer number achieved the best fitness value ( $R^2$ ) as determined form Equation (5.1). As clustering of a given dataset serves the purpose of discerning its natural classification and generate an incisive representation of the data, clustered based approach reproduces better results in all scenarios

**Table 5.2 Effect of hidden layer number on fitness of data ( $R^2$  values) for different scenarios**

Scenarios	Hidden Layer	2	3	4	5	6
	Main lane		0.87969	0.88136	0.88071	<i>0.88187</i>
Main lane close to off- ramp		0.96197	0.96234	0.96254	<i>0.96260</i>	0.96244
Main lane close to on- ramp		0.95018	0.95244	0.95275	<i>0.95285</i>	0.9528
Off- ramp		0.95277	0.95418	0.95418	<i>0.95418</i>	0.95277
On- ramp		0.93664	0.93739	0.93759	<i>0.93780</i>	0.93751

### 5.2.3 Effect of Training Algorithm

There are several types of training algorithm available such as Bayesian Regularization algorithm (BRA), Scaled Conjugate Gradient algorithm (SCGA), Levenberg-Marquardt algorithm (LMA). In this study three types of algorithm are considered to run the model.

The results of the different algorithm are summarized in Table 5.3 , In all case the Levenberg-Marquardt algorithm(LMA) achieved the best fitness value ( $R^2$ ) as determined equation (5.1). The table presents the result for training and testing dataset 80-20 and hidden layer number 5.



**Table 5.3 Performance comparison among different algorithm to fit the data in terms of fitness value ( $R^2$ )**

<b>Algorithm</b> <b>Scenarios</b>	<b>BR</b>	<b>SCG</b>	<b>LM</b>
Main lane	0.87792	0.87823	<i>0.88187</i>
Main lane close to off- ramp	0.95936	0.96019	<i>0.96259</i>
Main lane close to on- ramp	0.94942	0.95021	<i>0.95285</i>
Off- ramp	0.94143	0.94181	<i>0.95417</i>
On- ramp	0.93191	0.93242	<i>0.93780</i>

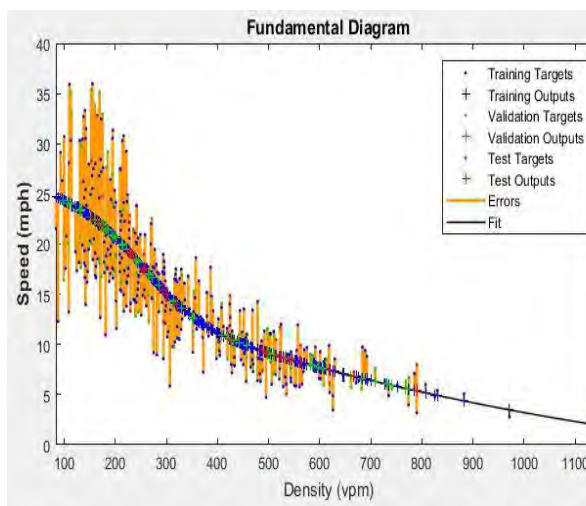
From the above table, it is seen that Levenberg-Marquardt algorithm(LMA) fits best for the data. Moreover, LMA takes less memory than other two algorithms as a results it takes less time to fit.

#### **5.2.4 Effect of Number of Epoch**

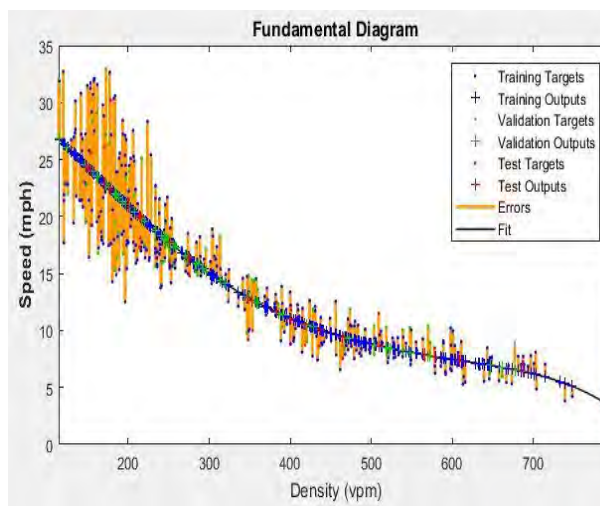
Epoch number controls the number of times the combined execution of back propagation and least square estimation occurs for training dataset. The training process terminates once the designated epoch number or the training goal is achieved. However, the number of epoch should be chosen such that overfitting does not occur. In this thesis, experiments with ANN training on six different types hidden layer were conducted with varying epoch numbers 3, 5, 10 and 100. Analysis shows that no notable variation in results was found ( $R^2$  value varying less than 0.003% on average ). Only a minor change in computation time was noticed if all other parameters were remained same. For example, an average runtime for a 1-year dataset with epoch number 3 was found to be 43.05 seconds, with epoch number 5, runtime increased to be 51.73 seconds and with epoch number 100, the runtime was 87.61 seconds. Later, basing on some of the literatures (Afaq and Rao, 2020), a fixed epoch number 100 is chosen for analysis all through this study.

## 5.2.5 Effects of Time Aggregation Level on Speed-density Relationship

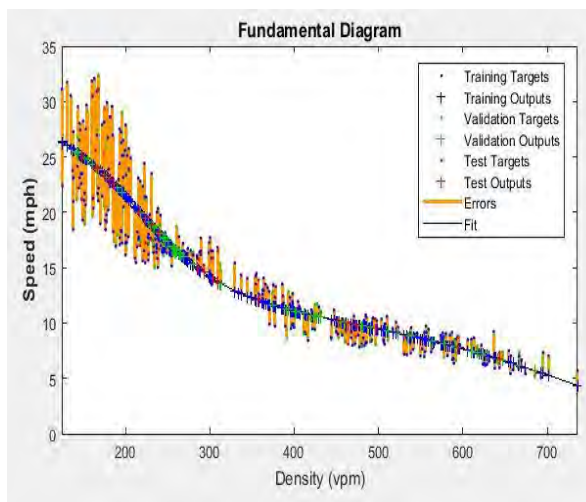
It is still debatable as to what intervals of time aggregation should be chosen when generating the fundamental speed-density relationship. In this section, how the varying time aggregation levels affect the speed-density relationship will be discussed. The raw data is 20 seconds aggregated from which the speed-density relationship from location is widely scattered. To demonstrate how the time aggregation level affects the speed-density relationship, the on-ramp data collected from non-lane based traffic condition is used for this purpose. Data is averaging during a varying number of intervals of time aggregation ranging from 20 seconds, 1, 2, 3, 5, 6 minutes to generate the fundamental speed-density relationship.



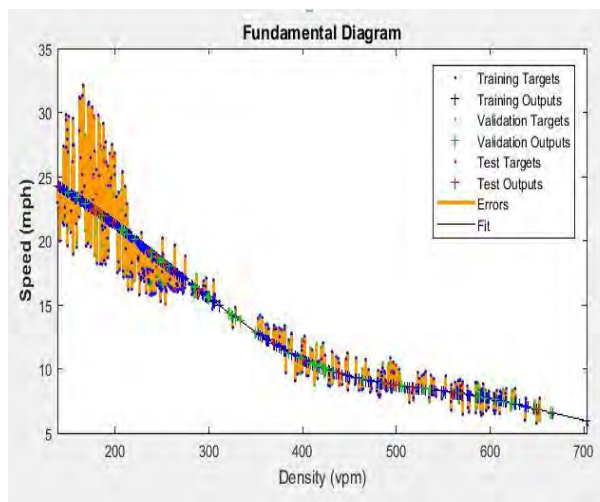
(a) On ramp, 20 seconds



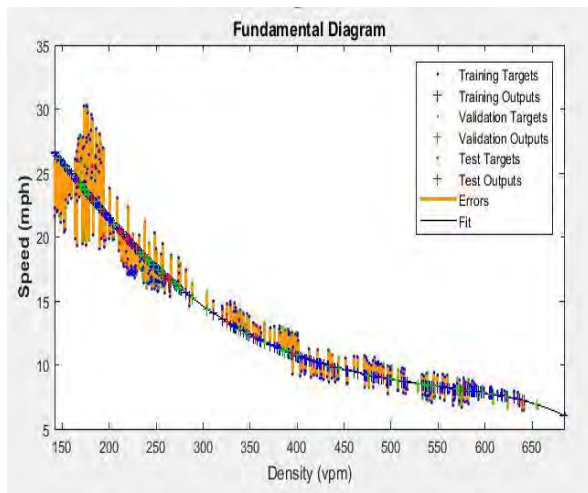
(b) On ramp, 1 minutes



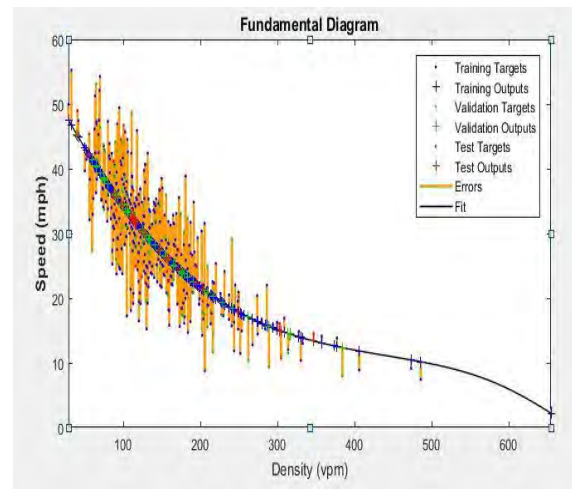
(c) On ramp, 2 minutes



(d) On ramp, 3 minutes



(e) On ramp, 5 minutes



(f) On ramp, 6 minutes

**Figure 5:1 Effect of time aggregation level on speed-density relationship at location on ramp**

From Figure 5.1, it can be seen that as the time aggregation level increases, the empirical speed-density relationship gets thinner and the tail part of the curve has less and less points due to the average. The results of the aggregation level are presented in table 5.4.

**Table 5.4 Effect of different interval of time aggregation**

Aggregation time	R <sup>2</sup> value
20 sec	0.8987
1 min	0.9229
2 min	0.9286
3 min	0.9294
5 min	0.9354
6 min	0.9289

It is obvious that a lower aggregation level such as 20 seconds preserves most of the original data but also keep too much white noise in the speed-density relationship which might deviate the empirical curve from the true relationship.

### 5.3 Model Validation Result

Validation is the indication of how the proposed model replicates system behavior with enough reliability to serve analysis objectives. ANN based speed–density model is fitted from I-80 dataset. In order to test whether the model also fits well with empirical data from other highway scenarios, in total 15 independent datasets (three datasets for each five scenarios) are fitted using the ANN model as shown in Figure 5.2 to Figure 5.6. Five scenarios considered for validation are: (a) Mainline (SC1); (b) Mainline close to off-ramp (SC2); (c) Mainline close to on-ramp (SC3); (d) Off-ramp (SC4); and (e) On-ramp (SC5). SC-1 contains uninterrupted traffic flow having very light amount of data below the speed 20 mph in comparison to other scenarios. SC-2 and SC-3 represent traffic flow influenced by either off-ramp and on-ramp respectively. Furthermore, SC-4 and SC-5 are isolated flows of off-ramp and on-ramp having different characteristics than mainline.

#### 5.3.1 Comparison with Single Regime Models

A graphical representation of the numerical comparison of different model performance in terms of goodness of fit ( $R^2$ ) at various scenarios using testing dataset is plotted in Figure 5.2 to Figure 5.6. The models considered are Greenshields model, Greenberg model, Underwood model, Northwestern model, Pipes-Munjal model, Drew model, ANFIS model and proposed SINN model. All the aforementioned models are included in a single plot to see the effectiveness in capturing the traffic state along with the empirical trend for different scenarios. The results compared to empirical observations show that:

1. There exists a curvature change in the speed-density relationship (see Figure 5.2). However, the relative positions of the points of curvature change (Inflection point) with respect to the  $(v_f, 0)$  and  $(0, \rho_j)$  are not same for all scenarios., where  $v_f$  and  $\rho_j$  are free flow speed and jam density respectively. It can be seen that the inflection point shifts to the left from SC-1 to SC-5. It is due to the origin of instability near the inflection point. This instability occurs due to sudden speed variation caused by heterogeneous driving behavior. It can be seen from Figure 5.2 to Figure 5.6 that only the ANN model captures the exact inflection point in all scenarios. Interestingly, the left part of the inflection point is concave and the other is convex. The left part is partially skewed downward and the right part becomes asymptotic near the zero speed. ANN model can also sense the shift in the inflection point and therefore show different inflection points

for different scenarios. Although, Northwestern model shows the inflection point, the point is not in exactly same position as the empirical one. Other speed–density models cannot capture this kind of trend in data.

**Table 5.5 Performance comparison among different model in estimation of fundamental diagram parameter**

Scenario type	R <sup>2</sup> Value		
	ANFIS	5PL	ANN
Main lane	0.82	0.80	<i>0.88</i>
Main lane close to off- ramp	0.92	0.91	<i>0.96</i>
Main lane close to on- ramp	0.87	0.86	<i>0.95</i>
Off- ramp	0.88	0.87	<i>0.95</i>
On- ramp	0.84	0.84	<i>0.94</i>

The ANN model gives better result from the other model due to the various transfer function which works inside the ANN and optimization algorithm works to minimize the error. Hidden layer number gives the flexibility to fit perfectly to the data set.

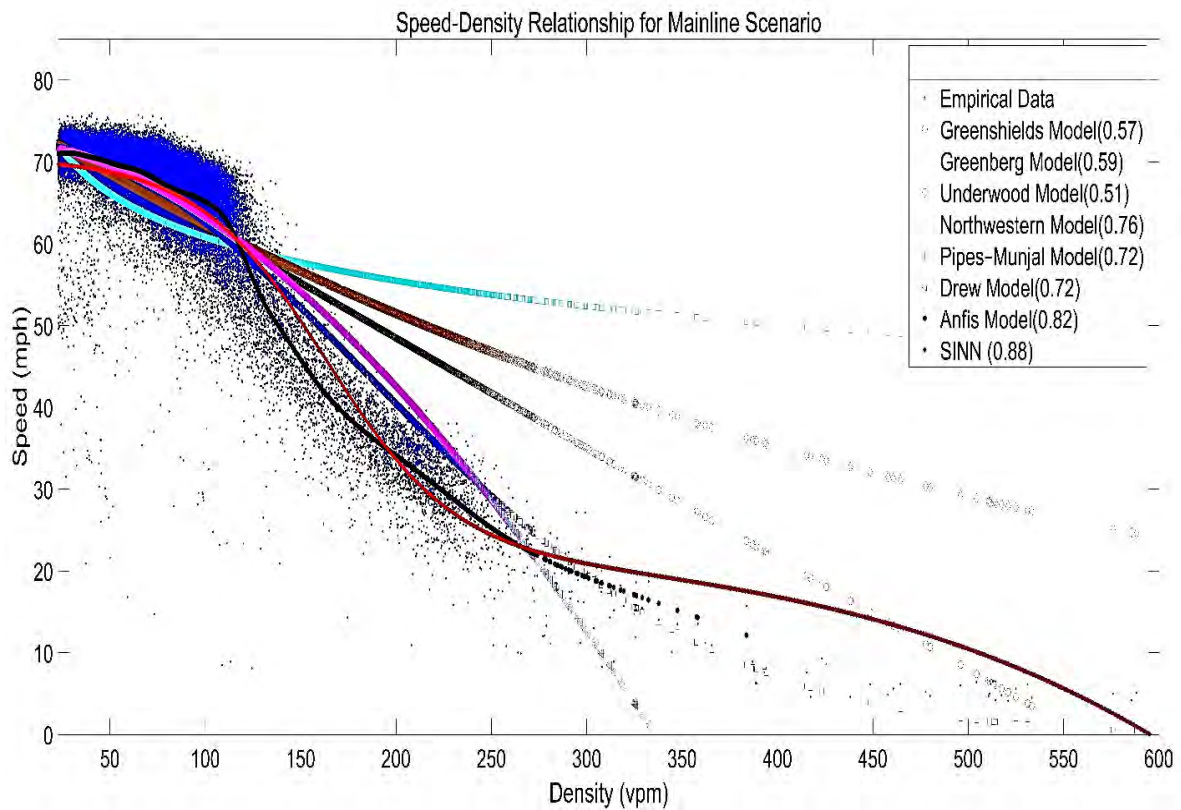


**Figure 5:2 Comparison of different model with proposed model observed from mainline**

2. The proposed ANN model achieved the best goodness-of-fit ( $R^2$ ) in all the scenarios (see Figure 5.2 to Figure 5.5). Although Northwestern, Drew and Pipes-Munjaj models achieve good  $R^2$  value, Greenberg, Greenshields and Underwood perform poorly to capture the trend of empirical data. Greenshields, being a linear model, fails to produce good  $R^2$  as none of locations has data with linear trend. In addition, both Greenberg and Underwood are convex in nature and so these models fail to capture the concave portion of the data. That's why those models are valid in free flow regime, cannot capture the trend perfectly in congested regime. However, the performance of the underwood model increases from SC-1 to SC-5. It is due to decrease in the length of concave part of the curve.

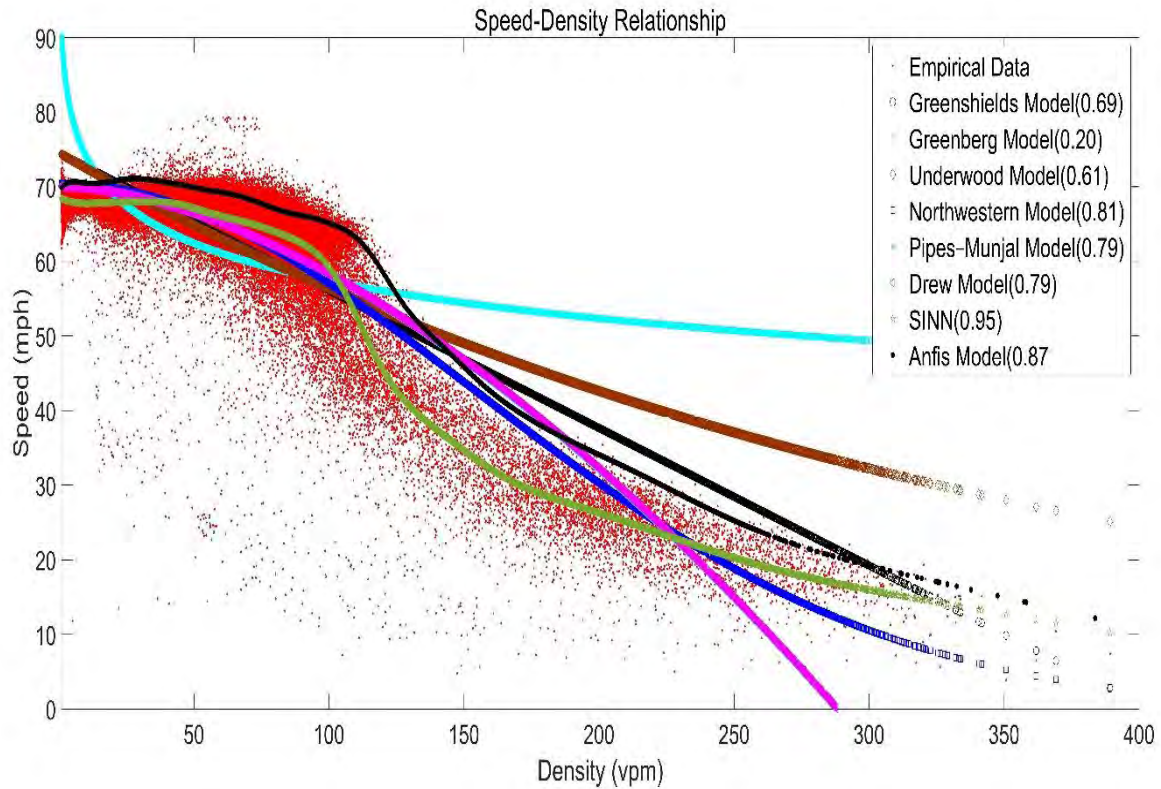


**Figure 5:3 Comparison of different model with proposed model observed from mainline near to on-ramp**

3. Another observation from Figure 5.2 to Figure 5.6 is that ANN generated curve does not have any definite shape, rather its shape changes with the change of scenario of the dataset. In other words, the gradient of the equilibrium curve generated by ANN model is stochastic as it does not have any deterministic gradient. However, other models have a deterministic gradient in nature meaning that they try to fit the traffic dynamics to a definite shape forcing the empirical data into the model without capturing the actual trend



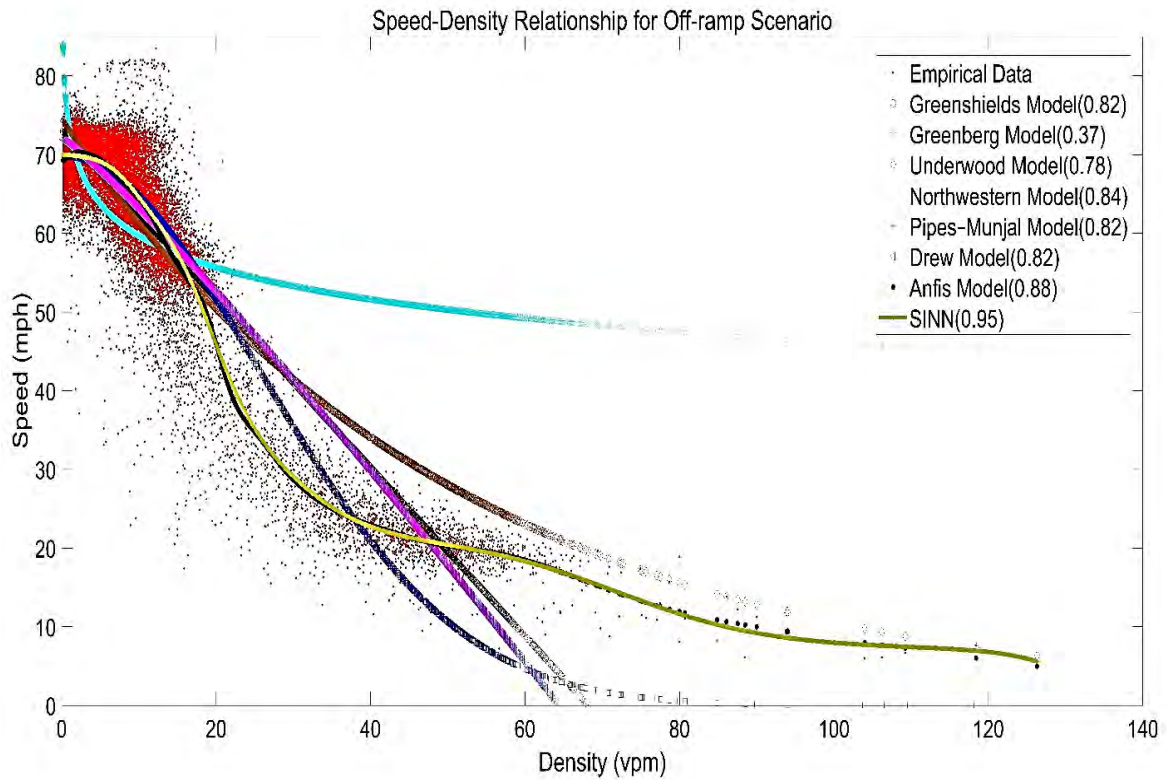


**Figure 5:4 Comparison of different model with proposed model observed from off ramp**

4. Change in shape, orientation and scenarios of the transition region in speed–density is observed from SC-1 to SC-5. Interestingly, the proposed ANN model has captured all the changes perfectly, whereas the other models have failed to capture the changes. The superimposed effect of premise parameters from different hidden layer enables the ANN model to capture the curvature of the transition region. On the other hand, consequent parameters determine the target gradient of the superimposed curvature.



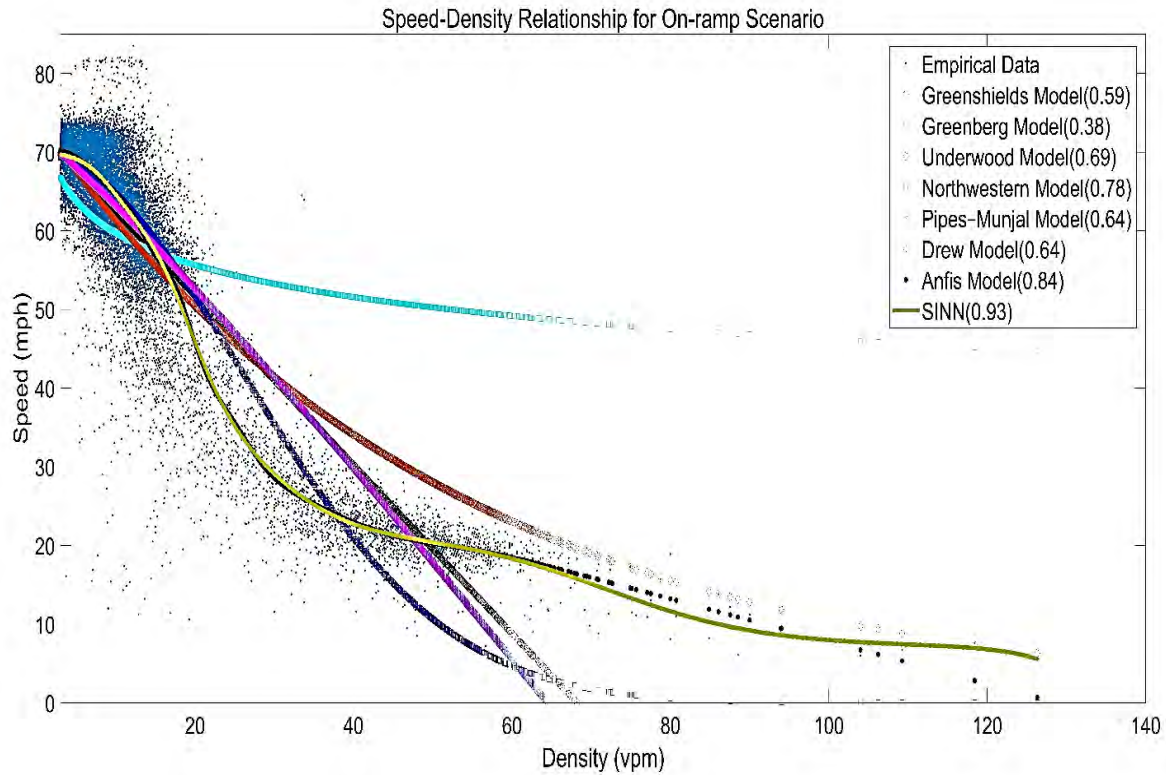


**Figure 5.5 Comparison of different model with proposed model observed from on-ramp**

In order to demonstrate the proposed ANN model's efficacy in estimation of FD parameters, we consider the 5-parameter logistic speed–density model (5PL) of (Wang, 2010) and ANFIS model of (Hadiuzzman et al., 2018). Table 5.5 lists the comparison of performance of the ANN model in estimation of the FD parameters with the 5PL model and ANFIS model. The results reveal that both models produce similar result in parameter estimation as well as achieve good  $R^2$  value for all five highway scenarios but ANN model achieve higher  $R^2$  value than rest of two model. In addition, ANN model provides estimation of jam density which 5PL model cannot determine.

### 5.3.2 Comparison with Multi-Regime Models

An illustrative numerical performance comparison with Multi-Regime models at SC-2 is plotted in Figure 5.6. Additionally, the goodness-of-fit values for different location are provided in Table 5.5. The Multi-Regime models considered in this research work are the Edie model and Two-Regime Linear model. Analysis shows that Edie and Two-Regime Linear model have performed well and achieved goodness-of-fit value 0.80 and 0.79, respectively, for mainline near to off-ramp scenarios. However, the ANN model has achieved the maximum

goodness-of-fit value (0.94) and has outperformed them. The existence of estimable breakpoint allows the multi-regime models to reduce the residual while performing the regression. However, it forcefully fits the data into the predefined shapes identical to the single regime models. Thus it also inherits the limitations of the single regime models such as inability to capture the transition point, the inflection point, and the gradient of the empirical data. In contrast, the proposed ANN model is able to address these limitations; therefore, the ANN model performed best.

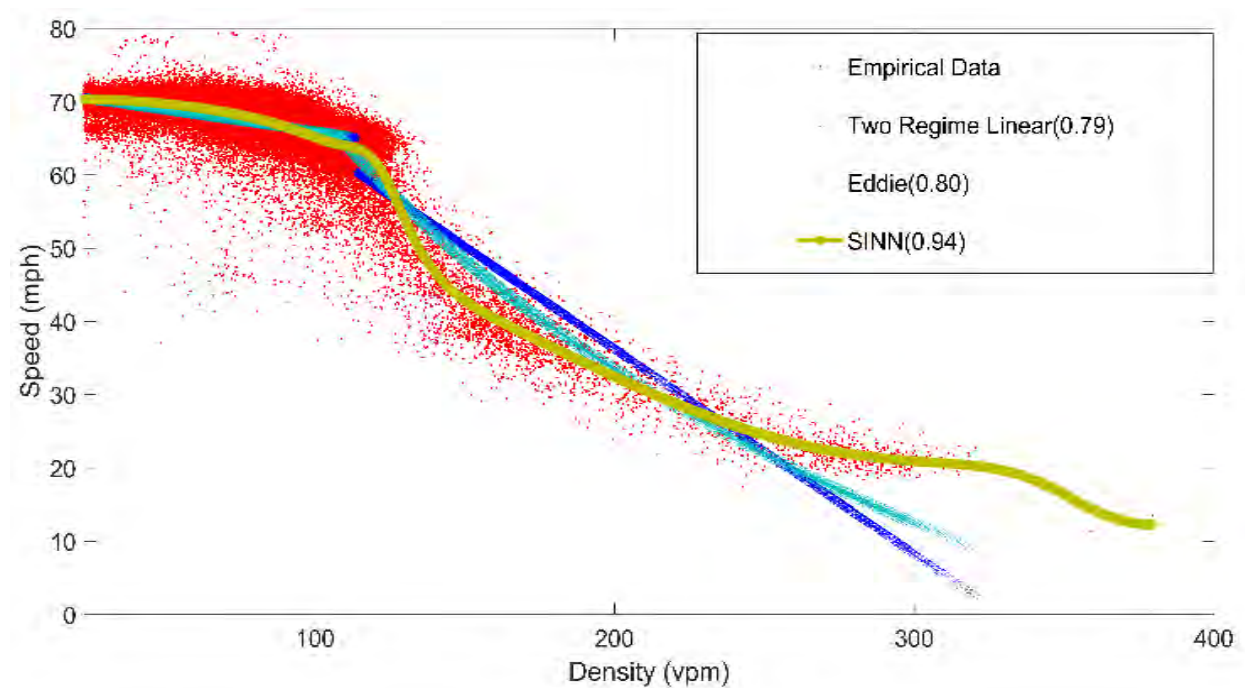
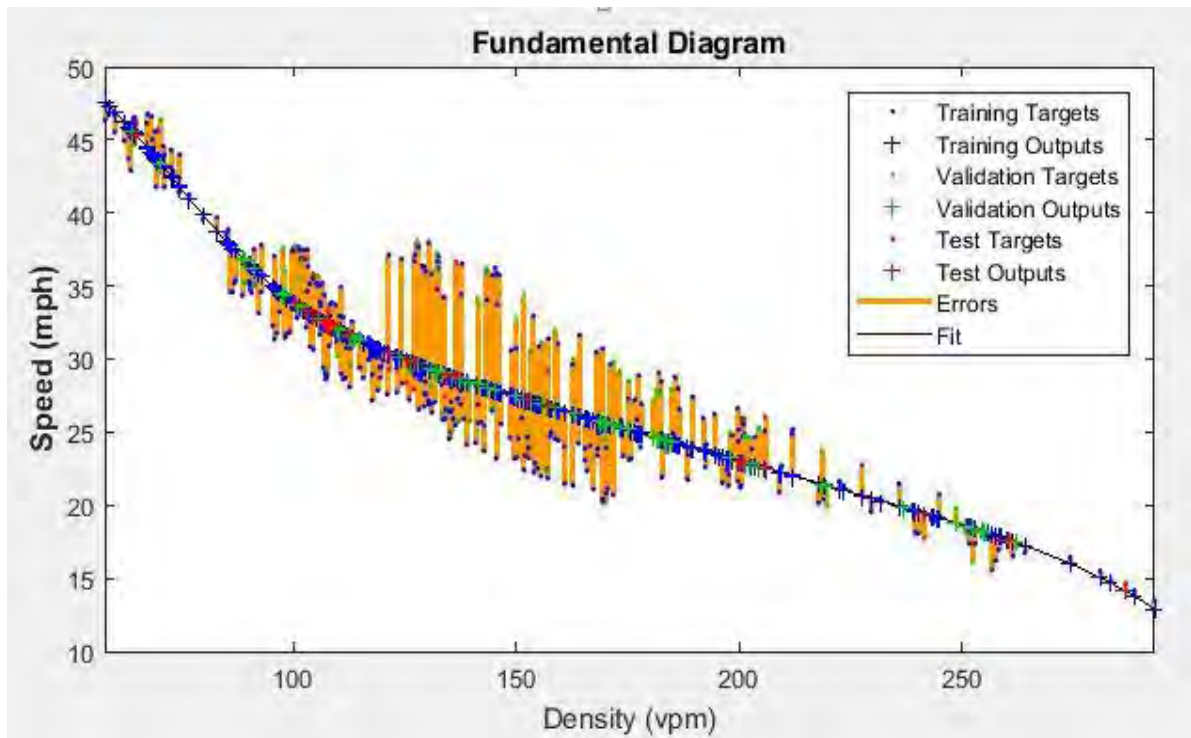


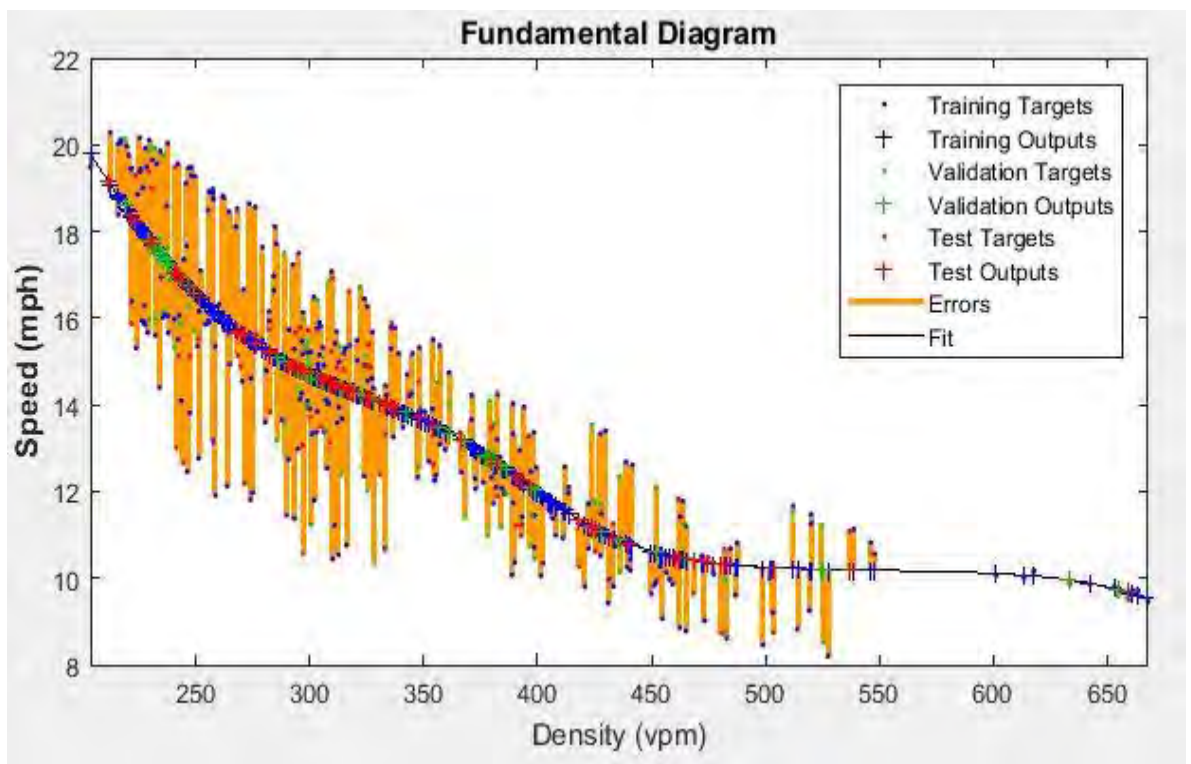
**Figure 5:6 Graphical representation of different model performances at I-80 on- mainline near to off-ramp**

#### **5.4 Proposed Model Performance for Non-Lane Based Traffic Condition**

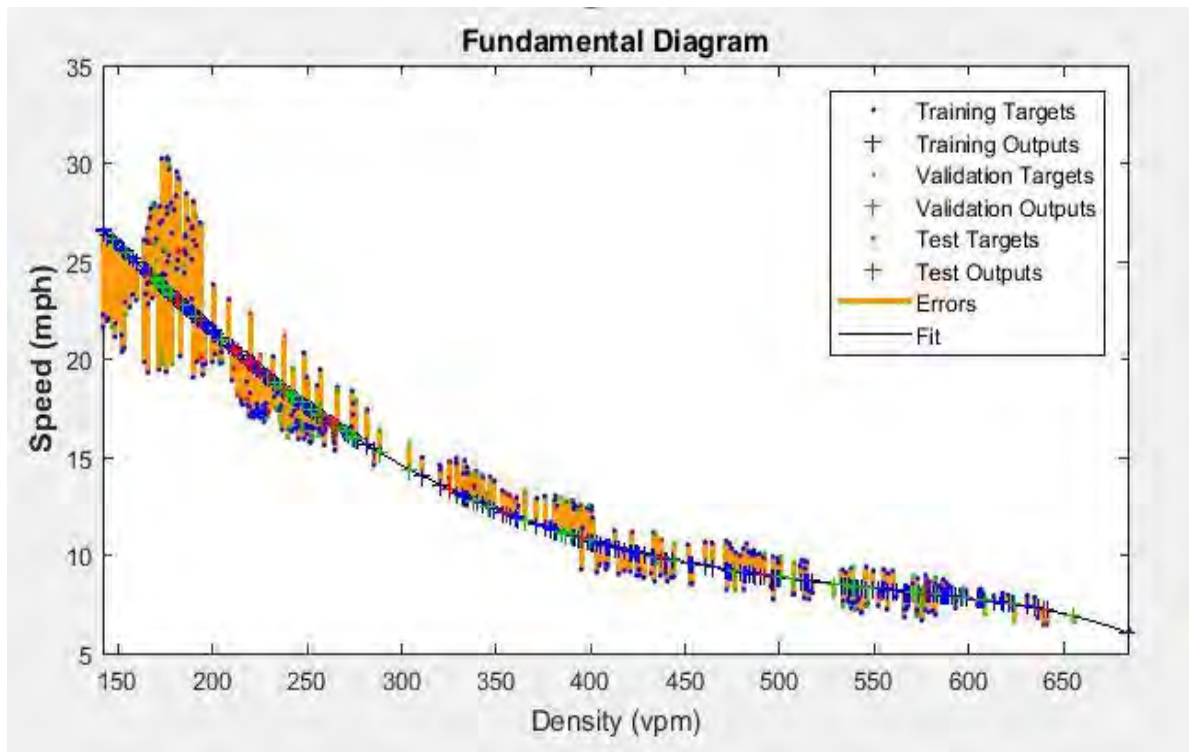
Data collected from five locations along the study corridor (see Figure 4.1) to know how the proposed model perform in non-lane based heterogeneous traffic condition. Five scenarios are considered so that the proposed model can perform in all type of highway geometry. All the scenarios are performed in hidden layer number five, data split 80-20 training and testing respectively, optimization algorithm is chosen Levenberg-Maquardt.



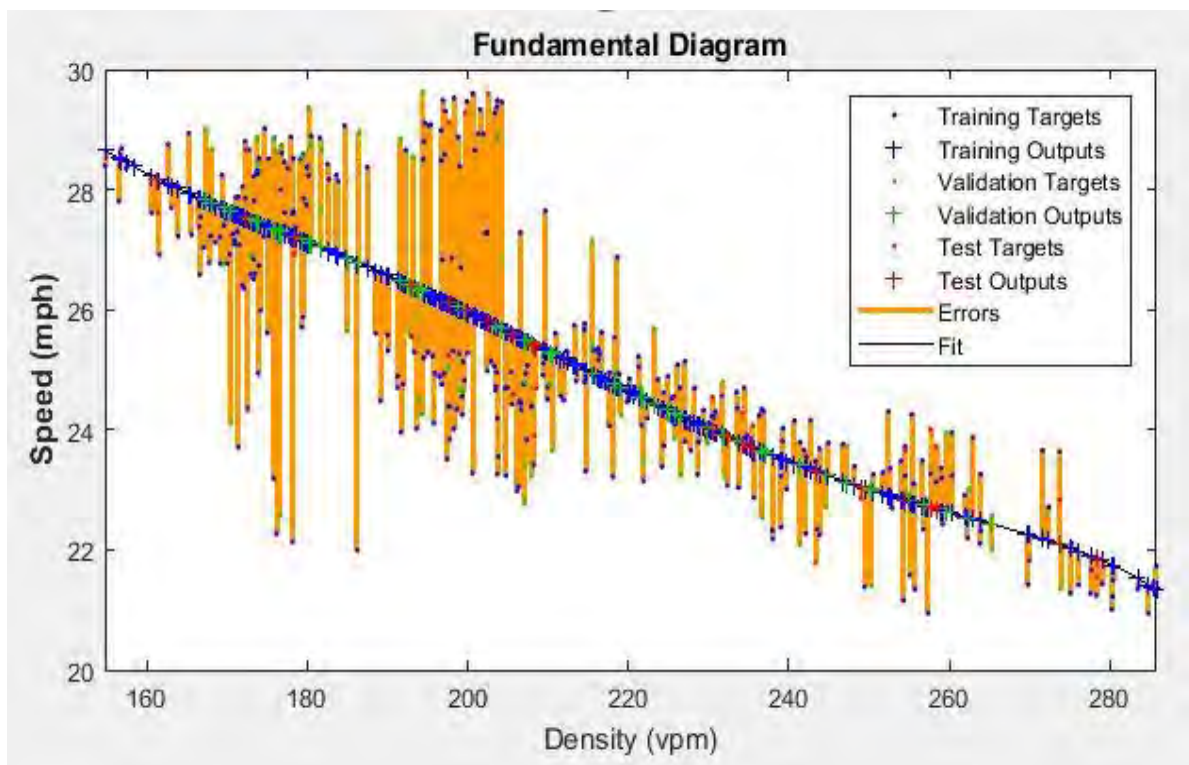
(a)



(b)

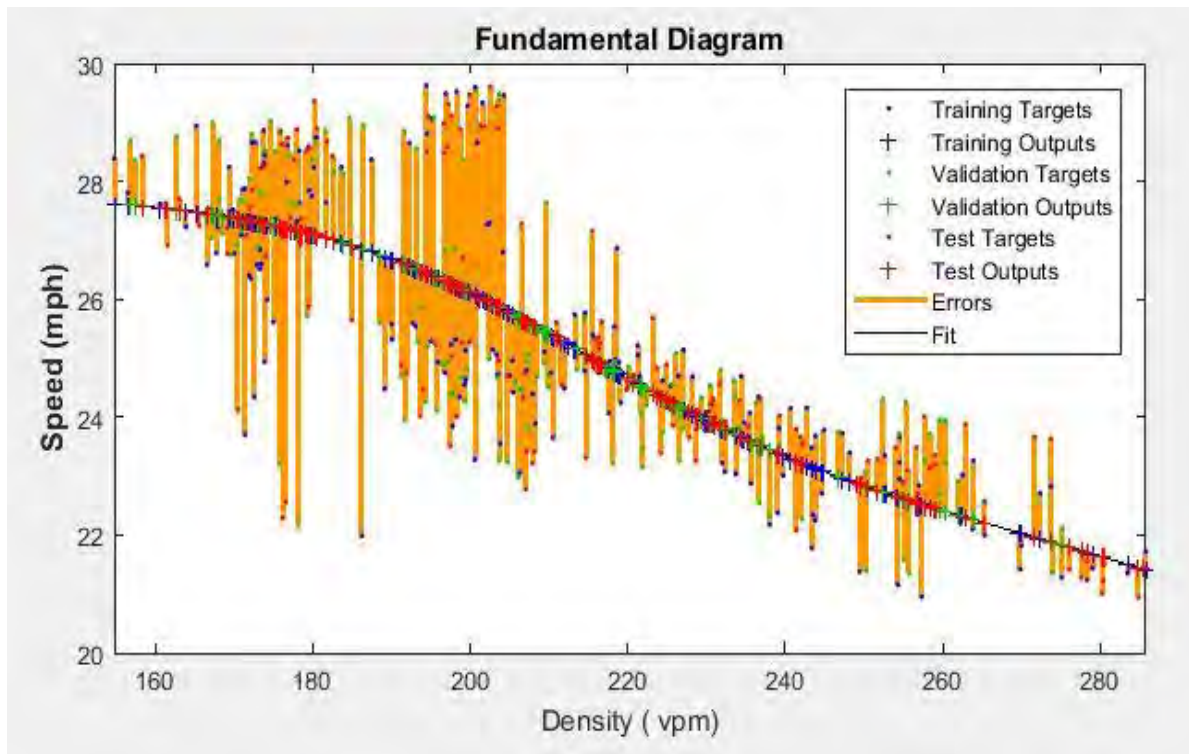


(c)



(d)





(e)

**Figure 5:7 Graphical representation of proposed model performance for non-lane based heterogeneous traffic at (a) main line close to on- ramp; (b) off- ramp; (c) on- ramp; (d) main line close to off- ramp; and (e) main line**

From the above Figure 5.7(a) to Figure 5.7(e), it can be concluded that on-ramp scenario and mainline close to on-ramp scenario shows better fit in speed–density relation. It is also noticed that mainline data get dispersed most. We have already seen from previous section that mainline close to on-ramp scenario and mainline close to off-ramp scenario performs well in case of lane based homogeneous traffic. But homogeneous traffic data performs better than the heterogeneous traffic data in terms of goodness of fit. This happens due to the randomness of the driver behavior, speed dynamics. From, this above discussion, it is evident that speed-density relationship performs well in stochastic manner. The performance of five scenarios for non-lane based heterogeneous traffic condition data is listed in Table 5.6.

**Table 5.6 Performance evaluation of the proposed model for non-lane based heterogeneous traffic condition**

<b>Scenario</b>	<b>R<sup>2</sup> Value</b>
Main lane	0.79016
Main lane close to off- ramp	0.82296
Main lane close to on- ramp	0.88191
Off- ramp	0.85032
On- ramp	0.93543

From the above Table 5.6, it can be seen that the performance of data collected from on-ramp yields better goodness of fit. It is also noticed that the proposed function performs well in all scenarios of non-lane based heterogeneous traffic condition.

## CHAPTER 6

### CONCLUSION AND RECOMMENDATION

#### 6.1 Introduction

In this chapter, a brief research summary is presented to provide a general picture of this thesis work and research findings, and future research directions are suggested.

Fundamental diagrams (FDs) have been a subject of wide-ranging study due to its significance in both the design of traffic facilities, and for the control of traffic operations. Traditional speed-density models attempt to fit the traffic dynamics to a definite shape (i.e. logarithmic, exponential, and exponential to the quadratic and various forms of polynomials) rather than capture the variations in drivers' behavior caused by the shockwave in the transition zone. In addition, they fail to acknowledge the effect of different geometrical patterns of the roadway (i.e., on-ramp/off-ramp on a freeway) on the shape of the speed–density fundamental diagram. This study proposes the application of the Artificial Neural Network (ANN) in developing a new saturation-based approach for modeling equilibrium speed-density relationship to overcome the well-known drawbacks of the traditional models. Proposed single input ANN architecture are calibrated over five different highway scenarios. These scenarios represent different driving behavior and consist of main lane, main lane with interruption from off-ramp, main lane with interruption from on-ramp, off- ramp and on- ramp.

We have applied the ANN in modeling equilibrium speed- density relationship because of its efficacy in being shape-flexible. ANN provides shape flexibility incorporating two factors: (a) number of hidden layer; and (b) proportion of training and testing sample. Among these, hidden layer number provide the required curvature to the speed–density fundamental diagram.

A number of options (i.e. optimal split of data into an estimation sample and a validation sample, selection of suitable hidden layer) offered by ANN are illustrated using data from I-80 near Berkeley. Levenberg-Marquardt algorithm has been used to optimize the parameters within the ANN structure. The study results show that with an increase in training dataset, the fitness value improves as fed with larger number of input-output data pairs to optimize its parameter values. It is observed that 80-20 split of original dataset for training and checking produced best results for all scenarios. For hidden layer number, five hidden layer number gives the best project the trend of the speed-density relationship in all scenarios. Model results show

that with increasing number of number of hidden layer, fitness of data ( $R^2$ -value) improves but decreases after five hidden layer so these improvements in results are imperceptible.

## 6.2 Key Findings

If one keyword can be used to characterize this thesis, it would be “stochastic”. What additional benefits can be obtained beyond a deterministic speed-density model? What traffic phenomena can be captured or explained if a stochastic speed-density relationship is applied to transportation problems? The first question essentially leads to the research on why a stochastic speed-density model is needed, and the second question leads to the performance of a stochastic speed-density model. Before discussing the benefits and performance of the stochastic speed-density model, it should know how to develop a stochastic speed-density model. In this thesis, the stochastic speed-density model is developed through a random traffic speed function.

The major results of this dissertation can be summarized as follows.

A comprehensive analysis of empirical speed-density relationship is provided. The empirical speed-density observations come from the 5 detectors installed on bed test I-80, Berkeley to represent the lane based homogeneous traffic and 5 video cameras are installed along the study corridor to represent the non-lane based heterogeneous traffic. From those dataset 3 speed-density curves are observed on basic highway segments and 2 empirical curves collected from on-ramps/off-ramps. The time aggregation level for these empirical observations is chosen 5 minutes from the analysis. The structured uncertainty embedded in this relationship is mainly caused by the behaviors of different driver populations.

A speed-density relationship is proposed through an iterative nonlinear curve fitting procedure: Levenberg-Marquardt algorithm. The saturation speed-density relationship with a varying number of parameters balances the empirical accuracy and mathematical elegance. It has been verified that the proposed speed-density model matches the empirical observation well by tracking the average behavior (i.e. mean) faithfully. A finer analysis of how the different different training percentage affects the shape and range of the empirical speed-density relationship is also performed and the results revealed that the lower the training percentage, the more deviation the empirical wide-scattering plot is. A varying number of training percentage is chosen to investigate their effects on the speed-density relationship. The results



indicate that a higher training percentage can plot the graph more accurately up to a certain percentage. Some useful information will be averaged out in this process and the variance of traffic speed will be reduced.

Several transfer function is proposed to fit the empirical data. Among them the best fit saturation function is chosen based on the goodness of fit ( $R^2$ ).

The data is split in different composition like 50-50, 60-40, 70-30, 75-25, 80-20, 85-15, 90-10 in training and testing data set respectively. Among the above composition the 80-20 split division gives better results in terms of goodness of fit ( $R^2$ ).

Hidden layer number gives flexibility of the speed-density curve for fitting this curve properly. Four types of hidden layer number are considered to effect of layer. Hidden layer number 2, 3, 4, 5, 6 is considered during the fitting of the speed-density curve. It is seen from the analysis hidden layer number 5 gives better results.

It is also been examined that the effect of epoch number. But from the analysis it is seen that epoch number effect is very minor which can be negligible.

Three type of optimization algorithm named Bayesian regularization, Scaled conjugate gradient, Levenberg-Marquardt is exercised and it has been seen that Levenberg-Marquardt algorithm performs well. Additionally, it takes less memory and time to fit.

This study also shows the effect of time aggregation level on speed-density relationship. This study analysis the time aggregation 20 seconds, 1, 2, 3, 5, 6 minutes and from this analysis it can be concluded that 5 min minute aggregation level yields better performance.

The proposed model is validated with other prominent existing model i.e. ANFIS, 5 PL model. The study analysis dictates that ANN model performs well than other model. Additionally, ANN gives the flexibility of the curve shape using the hidden layer.

A parametric modeling framework of the heterogeneous traffic speed-density is presented. The term parametric modeling means that all of the information in the experiments is assumed to

be contained in the parameters in model. The heterogeneity is verified by empirical plots of traffic data collected along the study corridor.

The proposed model is further applied to the non-lane based heterogeneous traffic flow stream. It can be concluded that on-ramp scenario and mainline close to on-ramp scenario shows better fit in speed–density relation.

The modeling results of the stochastic speed-density model and its validation is presented. The stochastic modeling result show that the stochastic speed-density model matches the empirical observations better than deterministic ones do. The validation of the stochastic speed-density model is performed by comparing the empirical traffic speed variation at a certain density with the simulated traffic speed variation under the same density. The stochastic speed-density model proposed in this dissertation is mathematically rigorous and computationally efficient. This pursuit helps us better understand how uncertainty/randomness acts in a dynamical traffic system.

### **6.3 Application of Stochastic Speed-Density Model**

Some potential applications of stochastic speed-density model include but are not limited to:

**Stochastic capacity:** Capacity is usually termed as the maximum number of vehicles that a highway link or junction can reasonably carry or accommodate per unit of time under specified conditions. Traditionally, traffic capacity is represented by the number of vehicles (vehs/hr) or passenger car units in a deterministic manner. For example, the highway capacity given in Highway Capacity Manual is a fixed value in different versions of HCM: 1800 pcu/hr/lane (1985), 2000 pcu/hr/lane (1986). This study found that capacity is a dynamic concept and is subject to a varying number of parameters such as number of lanes, road geometric settings and traffic conditions. From the empirical fundamental diagram generated from I-80 Berkeley, the observed capacity from speed-flow relationships indicate that capacity is not a fixed value but a range. The deterministic speed-density model also has deficiencies in representing the dynamic nature, but a stochastic speed-density model can remedy that.

**Transportation Planning:** Capacity consideration is one of the most important steps in transportation planning. As stated earlier, the highway capacity is a dynamic concept and is

subject to a varying number of parameters and weather condition is one of them. We can use this model to predict the capacity drop during the rainy season for planning a city transportation system considering the rainfall effect.

**Highway design:** Capacity determination from the stochastic model can be used for highway design in Bangladesh since the proposed model will work for non-lane based heterogeneous traffic condition. Free-flow speed will be used for limiting the speed for highway and designing the roadway.

**Traffic control management:** Fundamental diagram is an essential for traffic control management. For real time control system, we need real time traffic data which might not be a complete dataset. It is possible to establish fundamental diagram from an incomplete dataset for real time traffic management using the proposed stochastic model. Moreover, we can predict the traffic flow characteristics from these fundamental diagrams and warn the road users by variable message sign (VMS).

**Incomplete data set:** Sometimes it is seen that in a particular roadway full data set is not available. It is difficult to collect both free-flow side and congestion side data. To overcome the unavailability of free-flow side and congestion side data, the proposed model is prepared in a way that it will also work in incomplete data set.

**Tool:** Developed tool can be used for traffic management through intelligent transportation system (ITS). **Fundamental Diagram Calibration using Machine Learning (FRAME)** has a user friendly interface which provides flexibility to calibrate FD model. Aggregated speed-density dataset readable in .xlsx format can be uploaded and analyzed. User can choose various single regime (Greenshields, Greenberg, Underwood, Drew, Pippes-Munjaj, 5 PL logistic) models, multi-regime (Edie and Two Regime Linear model) and data driven (ANFIS) models to fit with the observed data. The tool is capable to generate corresponding fitted FD plots for the models and estimates various FD parameters—critical density, free flow speed and maximum capacity. The  $R^2$  value for the speed-density plot is directly computed and user can understand the fitness of the models. They can evaluate various FD models corresponding to

measured traffic data, estimates FD parameters and conduct comparative study to find the best fitted models for calibration.

#### **6.4 Limitations and Recommendations for Further Research**

Different techniques are available to develop a stochastic speed-density model. Other techniques include Expansion Optimal Linear Estimation (EOLE) and Orthogonal Series Expansion (OSE). Interested readers are referred to (Sudret, 2000) for more details of these two discretization schemes.

Other approaches could be investigated to develop a stochastic speed-density model. Due to the lack of precision of measurements and presence of environmental fluctuations, the effects of prevalent randomness/uncertainty must be dealt with in order to ensure a realistic modeling of speed-density relationship which is recognized as the key to fundamental diagram and transportation engineering studies.

We know that the speed-density relationship is time and location dependent. When the need to transfer the speed-density relationship to other locations comes up, what we should do is to calibrate the set of parameters for these locations.

Future work includes validation and application of the proposed speed-density model. The accuracy and optimality of the LM algorithm could be improved and tested with other correlation functions to further fine-tune the proposed stochastic speed-density model as compared to empirical observations. Though deterministic speed-density relationship models can explain physical phenomenon underlying fundamental diagrams, the stochastic speed-density model could be more accurate and suitable to describe traffic dynamics.

## REFERENCES

- Aerde, M. (1995). Single Regime Speed-Flow-Density Relationship for Congested and Uncongested Highways. *The 74th TRB Annual Conference*. Washington D.C.: Transportation Research Board.
- Afaq, S., and Rao, S. (2020). Significance Of Epochs On Training A Neural Network. *International Journal of Scientific and Technology Research*, 485-488.
- Berry, D. S., and Belmont, D. M. (1951). Distribution of Vehicle Speeds and Travel Times. *Proceedings of Second Berkeley Symposium on Mathematics, Statistics and Probability* (pp. 589-602). Berkeley: University of California press.
- Brilon, W., Geistefeldt, J., and Regler, M. (2005). Reliability of Freeway Traffic Flow : A Stochastic Concept of Capacity. *In Proceedings of the 16th International Symposium on Transportation and Traffic Theory*, (pp. 125-144). College Park, Maryland,.
- Bryson, A. E., and Ho, Y. C. (1969). *Applied Optimal Control*. Waltham: Blaisdell press.
- Castillo, D., and Benitez, J. M. (1995). On the Functional Form of the Speed-Density Relationship-i: General Theory. *Transportation Research Part B* 29, 373-389.
- Chang-Fu, T., Rui, J., and Qing-Song, W. (2007). Phase Diagram of Speed Gradient Model with an On-ramp. *Physica A: Statistical Mechanics and its Applications*, 641-650.
- Cortes, C., Mohri, M., and Rastogi, A. (2007). P-distance and Equivalence of Probabilistic Automata. *International Journal of Foundations of Computer*, 761.
- Daiheng, N., Leonard, J., Angshuman, G., and Billy, W. M. (2004). Systematic Approach for Validating Traffic Simulation Models. *Transportation Research Record* 1876, 20-31.
- Drake, J., Schofer, J., and May, A. (1967). A Statistical Analysis of Speed-Density Hypotheses. *Highway Research Record* 156, 53-87.
- Drew, D. (1968). *Traffic Flow Theory and Control Chapter 12*. McGraw-Hill: McGraw-Hill book Company.

- Dreyfus, S. E. (1962). The Numerical Solution of Variational Problems. *Mathematics annual applied*, 30-45.
- Dreyfus, S. E. (1990). Artificial Neural Networks, Back Propagation and the Kelley-Bryson Gradient Procedure. *Journal of Guidance, Control Dynamics.*, 926-928.
- Eddie, L. C. (1961). Car-following and Steady-state Theory for Non-congested Traffic. *Operation Research* 9, 66.
- Gaddam, H., and Rao, K. (2019). Speed-Density Functional Relationship for Heterogeneous Traffic Data: A Statistical and Theoretical Investigation. *J. Mod. Transport*, 61-74.
- Gavin, H. P. (2020). *The Levenberg-Marquardt Algorithm for Nonlinear Least Squares Curve-fitting Problems*. North Carolina, USA.: Department of Civil Engineering, Duke University.
- Gazis, D. C., Herman, R., and Potts, R. B. (1959). Car-following Theory. *Operations Research* 7, 499-505.
- Greenberg, H. (1959). An Analysis of Traffic Flow. *Operation Research* 7, 79-85.
- Greenshields, B. D. (1935). A Study in Highway Capacity. *Highway Research Board* (pp. 448-477). Highway Research Board.
- Haddiuzzan, M., Haque, N., Rahman, F., Hossain, S., Siam, M., and Qui, T. (2017). Pixel-based Heterogeneous Traffic Measurement Considering Shadow and Illumination Variation. *SIViP*, 1245-1252.
- Hadiuzzman, M., Siam, M., Haque, N., Hossain, T., and Rahman, F. (2018). Adaptive Neuro-Fuzzy Approach for Modeling Equilibrium Speed-Density Relationship. *Transportmetrica A: Transport Science*, 137-162.
- Hall, F. L., Hurdle, V. F., and Banks, J. H. (1992). A Synthesis on Recent Work on the Nature of Speed-Flow and Flow-Occupancy (or Density) Relationships on Freeways. *ransportation Research Record* (pp. 12-18). Transportation Research Record.
- Hebb, D. (1949). *The Organization of Behavior, a Neuropsychological Theory*. New York: John Wiley.

- Hossain, S., Hadiuzzaman, M., Haque, N., Muniruzzaman, M. S., Musabbir, S., and Hasanat, M. (2016). A New Stochastic Macroscopic Model for Heterogeneous Traffic Considering Variable Fundamental Diagram. *TRB 95th Annual Meeting* (pp. 235-253). Washington, D.C: Transportation Research Board.
- Jayakrishnan, R., Tsai, W., and Chen, A. (1995). A Dynamic Traffic Assignment Model with Traffic Flow Relationships. *Transportation Research Part C Vol.3C, No.1*, 51-72.
- Jia, L., Qian-Yong, C., Haizhong, W., and Daiheng, N. (2008). Investigation of LWR Model with Flux Function Driven by Random Free Flow Speed. *Symposium on The Greenshields Fundamental Diagram: 75 Years Later*.
- Jingang, Y., Hao, L., Luis, A., and Roberto, H. (2002). Stability of Macroscopic Traffic Flow Modeling through Wavefront Expansion. *American Control Conference 2* (pp. 1484-1490). American Control Conference 2.
- Kelley, H. J. (1960). Gradient Theory of Optimal Flight Path. *ARS Journal*, 947-954.
- Kerner, B., and Konhauser, P. (1994). Structure and Parameters of Clusters in Traffic Flow. *Physics Revolution E 50*, 54-83.
- Kharoufeh, J. P., and Gautam, N. (2004). Deriving Link Travel-time Distribution via Stochastic Speed Processes. *Transportation Science 38*, 97-106.
- Lei, R., Larry, O., and David, G. (1998). Development and Application of Validation Framework for Traffic Simulation Models. *WSC '98: Proceedings of the 30th conference on Winter simulation* (pp. 1079-1086). Los Alamitos, CA, USA,: IEEE Computer Society Press.
- Li, Y., Li, L., and Li, Z. (2014). Missing Traffic Data: Comparison of Imputation Methods. *Intelligent Transport Systems. 8(1)*, pp. 51–57. IET .
- Lighthill, M., and Whitham, G. (1955). On Kinematic Waves.ii. A Theory of Traffic Flow on Long Crowded Roads. *Royal Society of London Proceedings Series A 229*, 317-345.
- Lu, S., and Jie, Z. (2005). Development of Multi-Regime Speed-Density Relationship by Cluster Analysis. *Transportation Research Record 1934*, 64-71.

- MacNicholas, M. J. (2008). A Simple and Pragmatic Representation of Traffic Flow. *In Symposium on The Fundamental Diagram: 75 years*. Woods Hole, MA: Transportation Research Board.
- May, A. D. (1990). *Traffic Flow Fundamentals*. Prentice Hall, Inc. New Jersey.
- McCulloch, N. S., and Pitts, W. H. (1943). A Logical Calculus of the Ideas Imminent in Nervous Activity. *Bull Mathematics Biophy.*, 115-133.
- Mohamad, S. (2015). *Capacity Models for Multilane Roundabouts and Their Evaluation Using Microscopic Simulations*. United Arab Emirates University.
- Newell, G. F. (1961). Nonlinear Effects in the Dynamics of Car Following. *Operation Research* 9, 209.
- Nikolaidis, E., Ghiocel, D., and Singhal, S. (2005). *Engineering Design Reliability Handbook*. New York: CRC Press.
- Nilsson, N. J. (1965). *Learning Machines: Foundations of Trainable Pattern Classifiers*. New York: McGraw Hill.
- PeMS. (2017, December 21). Retrieved January 17, 2018, from <http://pems.dot.ca.gov/>
- Pipes, L. A. (1967). Car Following Models and the Fundamental Diagram of Road Traffic. *Transportation Research* 1, 21-29.
- Qin, X., and Hani, S. M. (2004). Adaptive Calibration of Dynamic Speed-Density Relations for Online Network Traffic Estimation and Prediction Applications. *Transportation Research Record*, 82-89.
- Rao, T. R. (1975). Validation of Stochastic Models: Some Perspectives. *Journal of the Academy of Marketing Science* 3, 192-199.
- Rouse, and Douglas, I. (1991). Stochastic Modeling of Plant Disease Epidemic Processes. *Handbook of Applied Mycology Soil and Plants*, 192-194.
- Soyster, A. L., and Welson, G. R. (1973). A Stochastic Model of Flow versus Applied to Traffic Flow on Hills. *Highway Research Record* 456, 28-39.



- Sudret, B. A. (2000). *Stochastic Finite Element Methods and Reliability*. California, Berkley: University of California, Berkley.
- Transportation Research Board. (2010). *Highway Capacity Manual*. Washington, DC: Transportation Research Board.
- Underwood, R. (1961). Speed, Volume and Density Relationship: Quality and Theory of Traffic Flow. *Yale Bureau of Highway Traffic* (pp. 141-188). New Haven, Connecticut: Yale Bureau of Highway Traffic.
- Wang, H. (2010). *Stochastic Modelling of Equilibrium Speed-Density Relationship*. Amherst: University of Massachusetts - Amherst.
- Werbos, P. (1974). *Beyond Regression: New Tools for Prediction and Analysis in the Behavioral Sciences*. Harvard: Harvard University Press.
- Wong, G. C., and Wong, S. C. (2002). A Multi-class Traffic Flow Model an Extension of LWR Model with Heterogeneous Drivers. *Policy and Practice 36* (pp. 827-841). Transportation Research Part A.

**APPENDIX A-1: RESULTS OF THE PROPOSED MODEL**

### 1. Results for data used from main line

(%)			Hidden Layer	R <sup>2</sup> -value			
Training	Validation	Testing		Training	Validation	Testing	All
50	15	35	3	0.88091	0.87698	0.88379	0.88135
			5	0.87709	0.88642	0.88225	0.88035
	20	30	3	0.86855	0.86788	0.87402	0.87006
			4	0.87754	0.87823	0.88678	0.88044
			5	0.87641	0.87109	0.87477	0.8749
	25	25	2	0.87615	0.86866	0.86991	0.87279
			3	0.88129	0.88819	0.87439	0.88135
			4	0.88041	0.87926	0.88131	0.88035
			5	0.88091	0.87698	0.88379	0.88135
			10	0.87709	0.88642	0.88225	0.88035
60	10	30	1	0.86579	0.86576	0.874	0.86818
			2	0.87079	0.86263	0.86488	0.86825
			3	0.88174	0.88317	0.87679	0.88039
			4	0.87346	0.87656	0.87327	0.87372
			5	0.87928	0.88392	0.88163	0.88044
			10	0.889	0.87501	0.87082	0.88247
	15	25	2	0.8764	0.87595	0.88957	0.87969
			3	0.88095	0.88345	0.8769	0.88029
			5	0.88234	0.87941	0.87688	0.88058
	20	20	4	0.88319	0.87351	0.88005	0.88071
			5	0.88099	0.88377	0.88178	0.88168
	70	5	25	3	0.87917	0.88447	0.88347
4				0.87587	0.86289	0.87314	0.87464
5				0.87795	0.87559	0.88718	0.88018
10		20	3	0.8802	0.87129	0.88546	0.88039
			4	0.86974	0.86663	0.87282	0.87008
			5	0.88086	0.87688	0.88157	0.88059
15		15	2	0.88183	0.88375	0.86417	0.87969
			3	0.88298	0.86784	0.88665	0.88136
			4	0.8729	0.86896	0.87466	0.8726
	5		0.87996	0.87814	0.88505	0.88046	
80	5	15	4	0.87366	0.87746	0.88014	0.8748
			5	0.88225	0.88304	0.87303	0.88091
	10	10	3	0.88125	0.86074	0.89095	0.88031

**1. Results for data used from main line (Contd.)**

(%)			Hidden Layer	R <sup>2</sup> -value			
Training	Validation	Testing		Training	Validation	Testing	All
80	10	10	4	0.87962	0.88197	0.88352	0.88029
			5	0.88165	0.88321	0.88232	0.88187
90	5	5	3	0.88125	0.87056	0.87437	0.88044
			4	0.88035	0.88456	0.87308	0.88018
			5	0.88283	0.87451	0.86503	0.88161

**2. Results for data used from mainline close to off-ramp**

(%)			Hidden Layer	R <sup>2</sup> -value			
Training	Validation	Testing		Training	Validation	Testing	All
50	15	35	3	0.96118	0.96138	0.96434	0.96234
			4	0.96205	0.96224	0.96332	0.96254
			5	0.9623	0.96048	0.96389	0.9626
	20	30	4	0.96238	0.96081	0.96262	0.96215
			5	0.96303	0.96167	0.9625	0.9626
			3	0.96334	0.9612	0.96111	0.96226
	25	25	4	0.9623	0.96177	0.9625	0.96222
			5	0.96299	0.96146	0.96281	0.96258
			3	0.9615	0.96177	0.96348	0.96215
60	10	30	5	0.96389	0.96181	0.96454	0.96326
			3	0.96203	0.96122	0.9636	0.9623
	15	25	4	0.96215	0.96248	0.96226	0.96222
			5	0.9632	0.96279	0.9624	0.96281
			2	0.96242	0.96185	0.96114	0.96205
	20	20	3	0.96191	0.96246	0.96338	0.96232
			5	0.96197	0.96299	0.96324	0.96244
			3	0.96248	0.96081	0.96224	0.96234
	70	5	25	5	0.96236	0.96181	0.96234
3				0.96201	0.9637	0.96277	0.96234
10		20	5	0.96289	0.96018	0.96277	0.9626
			3	0.96205	0.96266	0.96338	0.96234
15		15	5	0.96258	0.96258	0.96234	0.96254
			3	0.96234	0.96464	0.9615	0.96234
80	5	15	3	0.96234	0.96464	0.9615	0.96234

**2. Results for data used from mainline close to off-ramp (Contd.)**

(%)			Hidden Layer	R <sup>2</sup> -value			
Training	Validation	Testing		Training	Validation	Testing	All
80	5	15	3	0.96234	0.96464	0.9615	0.96234
			5	0.96244	0.96016	0.96256	0.96234
	10	10	3	0.96207	0.96332	0.96303	0.96228
			4	0.96256	0.96044	0.96395	0.96248
			5	0.96293	0.96171	0.96065	0.9626
90	5	5	3	0.95993	0.9584	0.95494	0.95962
			4	0.96279	0.96368	0.95625	0.96254
			5	0.96222	0.96248	0.96631	0.96246

**3. Results for data used from mainline close to on-ramp**

(%)			Hidden Layer	R <sup>2</sup> -value			
Training	Validation	Testing		Training	Validation	Testing	All
50	15	35	3	0.94895	0.95556	0.95164	0.9509
			4	0.95238	0.95246	0.95248	0.95242
			5	0.95135	0.95431	0.95359	0.95262
			6	0.95263	0.95262	0.95277	0.95267
			7	0.9523	0.95072	0.95396	0.95265
	20	30	3	0.95215	0.94967	0.95205	0.95162
			5	0.95402	0.95129	0.95111	0.95262
			6	0.95181	0.94965	0.95603	0.95267
			7	0.95226	0.95221	0.95342	0.9526
	25	25	3	0.95148	0.95254	0.95082	0.9516
			4	0.95129	0.95441	0.95392	0.95275
			5	0.95303	0.95482	0.94981	0.95265
			6	0.95295	0.95066	0.95252	0.9526
60	10	30	3	0.95271	0.9524	0.95047	0.95201
			4	0.95248	0.95637	0.95121	0.9525
			5	0.95383	0.94893	0.95135	0.95263
			6	0.95295	0.95066	0.95252	0.9526
	15	25	3	0.95125	0.94985	0.95064	0.9509
			4	0.9531	0.95029	0.95269	0.9526
			5	0.95275	0.95357	0.95088	0.95242
			6	0.95303	0.95014	0.95394	0.95281
20	20	3	0.95158	0.95363	0.94986	0.95164	

### 3. Results for data used from mainline close to on-ramp (Contd.)

(%)			Hidden Layer	R <sup>2</sup> -value			
Training	Validation	Testing		Training	Validation	Testing	All
60	20	20	4	0.95172	0.9524	0.95482	0.9525
			5	0.95156	0.95469	0.95441	0.95275
			7	0.95297	0.95281	0.95127	0.9526
			9	0.95098	0.95596	0.95414	0.95262
70	5	25	3	0.95285	0.95142	0.9515	0.95244
			5	0.95347	0.95213	0.95068	0.95273
			7	0.95162	0.95061	0.9558	0.95262
			8	0.95275	0.95545	0.95183	0.95267
	10	20	4	0.95228	0.95193	0.95137	0.95207
			5	0.9523	0.95541	0.95322	0.95277
			7	0.95236	0.95262	0.95394	0.95269
	15	15	4	0.95185	0.95566	0.95304	0.95262
			5	0.95224	0.95183	0.95517	0.95265
			6	0.95297	0.94926	0.95451	0.95263
			7	0.95201	0.95558	0.95324	0.95275
	80	5	15	4	0.95156	0.95242	0.9547
5				0.95344	0.95221	0.94918	0.95273
10		10	3	0.95086	0.95396	0.95547	0.95162
			5	0.95263	0.95191	0.95541	0.95285
			7	0.95326	0.95074	0.95162	0.95285
90	5	5	3	0.95238	0.9542	0.95267	0.9525
			5	0.95239	0.95459	0.95676	0.95263
			7	0.95148	0.95254	0.95082	0.9516

#### 4. Results for data used from off-ramp

(%)			Hidden Layer	R <sup>2</sup>			
Training	Validation	Testing		Training	Validation	Testing	All
50	15	35	3	0.95508	0.95357	0.95312	0.95418
			5	0.95412	0.95494	0.95646	0.95506
			6	0.95652	0.95287	0.95373	0.955
			7	0.95453	0.94949	0.95201	0.95291
	20	30	5	0.9549	0.95435	0.95283	0.95418
			6	0.95547	0.95478	0.95457	0.95508
			7	0.95414	0.95643	0.95578	0.9551
	25	25	3	0.95433	0.95353	0.95449	0.95416
			5	0.95414	0.9547	0.95731	0.95508
7			0.95373	0.95551	0.95793	0.95523	
60	10	30	4	0.95326	0.95643	0.95279	0.95344
			5	0.9549	0.95004	0.95137	0.95336
			6	0.9531	0.95449	0.95154	0.95277
			7	0.95357	0.95195	0.95613	0.95418
	15	25	4	0.95289	0.95713	0.95549	0.95418
			5	0.95185	0.95566	0.95304	0.95262
			7	0.95359	0.95291	0.95369	0.95351
	20	20	5	0.95386	0.95388	0.95535	0.95418
			6	0.95441	0.95619	0.956	0.95508
			8	0.95441	0.95363	0.95459	0.95429
			10	0.95513	0.95418	0.95465	0.95484
	70	5	25	4	0.95211	0.94819	0.95187
5				0.95449	0.95402	0.95273	0.95402
10		20	5	0.95361	0.95654	0.95502	0.95418
			7	0.95299	0.95556	0.95482	0.95361
15		15	5	0.95215	0.95353	0.95125	0.95222
			7	0.95472	0.95772	0.95418	0.9551
80	5	15	3	0.95279	0.95541	0.95426	0.95314
			4	0.95469	0.94897	0.95297	0.95416
			5	0.95402	0.95811	0.94979	0.95359
			6	0.95217	0.9539	0.95361	0.95248
			7	0.95328	0.95408	0.95443	0.95349
			8	0.95504	0.95396	0.95556	0.95508
	10	10	3	0.95447	0.95459	0.95154	0.95418
			4	0.95345	0.95359	0.95016	0.95314

**4. Results for data used from off-ramp (Contd.)**

(%)			Hidden Layer	R <sup>2</sup>			
Training	Validation	Testing		Training	Validation	Testing	All
80	10	10	5	0.95455	0.95117	0.954	0.95418
90	5	5	3	0.95148	0.94983	0.9539	0.95152
			4	0.95398	0.94873	0.96111	0.95408
			5	0.95508	0.95357	0.95312	0.95418



## 5. Results for data used from on-ramp

(%)			Hidden Layer	R <sup>2</sup>			
Training	Validation	Testing		Training	Validation	Testing	All
50	15	35	3	0.93867	0.94074	0.93404	0.93739
			4	0.93978	0.93443	0.93559	0.93751
			5	0.93551	0.9385	0.93762	0.93671
	20	30	3	0.93648	0.9372	0.93685	0.93673
			5	0.93821	0.93499	0.93941	0.94018
			7	0.93633	0.94005	0.93613	0.93664
	25	25	4	0.93631	0.93786	0.93896	0.93735
			5	0.93753	0.93844	0.93669	0.93685
			7	0.93439	0.93751	0.94055	0.93671
60	10	30	2	0.93594	0.94005	0.93687	0.93664
			3	0.9372	0.93381	0.93699	0.93679
			4	0.93567	0.93652	0.93884	0.93669
			5	0.93633	0.94005	0.93613	0.93664
	15	25	4	0.93813	0.93673	0.9376	0.9378
			5	0.93536	0.93602	0.93693	0.94024
			6	0.93631	0.93404	0.93939	0.93673
	20	20	5	0.93586	0.93751	0.93462	0.93579
			6	0.93826	0.93499	0.9384	0.93764
70	5	25	3	0.93879	0.94389	0.93262	0.93751
			4	0.93753	0.93941	0.93821	0.9384
			5	0.93822	0.93519	0.93536	0.93737
	10	20	3	0.93739	0.94028	0.93687	0.93759
			4	0.93629	0.94018	0.93768	0.93749
			5	0.93594	0.93764	0.93848	0.93664
	15	15	4	0.93689	0.93762	0.94069	0.93759
			5	0.93726	0.93693	0.93898	0.93768
			6	0.93846	0.93462	0.93586	0.93751
80	5	15	3	0.93602	0.93579	0.94024	0.93666
			5	0.93795	0.93688	0.93575	0.93678
	10	10	3	0.93662	0.93391	0.93852	0.93675
			4	0.93726	0.92268	0.93503	0.93753
			5	0.93813	0.93178	0.93436	0.93771
90	5	5	3	0.9365	0.9371	0.93852	0.93664
			4	0.9303	0.93528	0.96491	0.93704
			5	0.93664	0.93853	0.93709	0.93766

**APPENDIX A-2: GRAPHICAL REPRESENTATION OF MODEL  
PERFORMANCE**

# Graphical representation of proposed model for lane based homogeneous traffic

## Fundamental Diagram

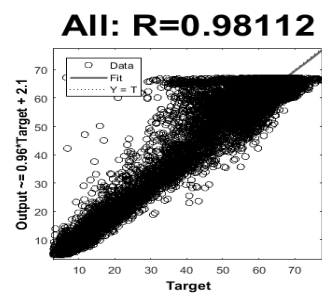
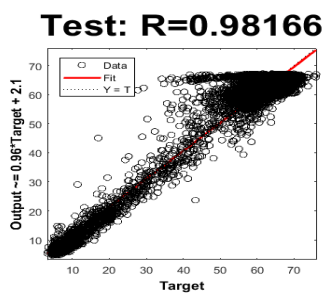
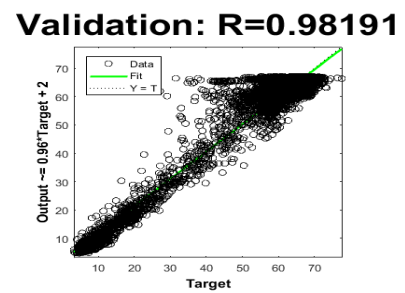
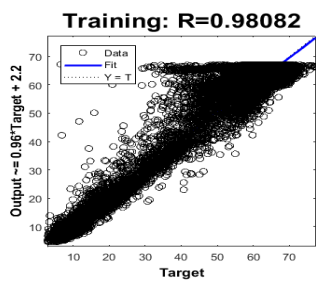
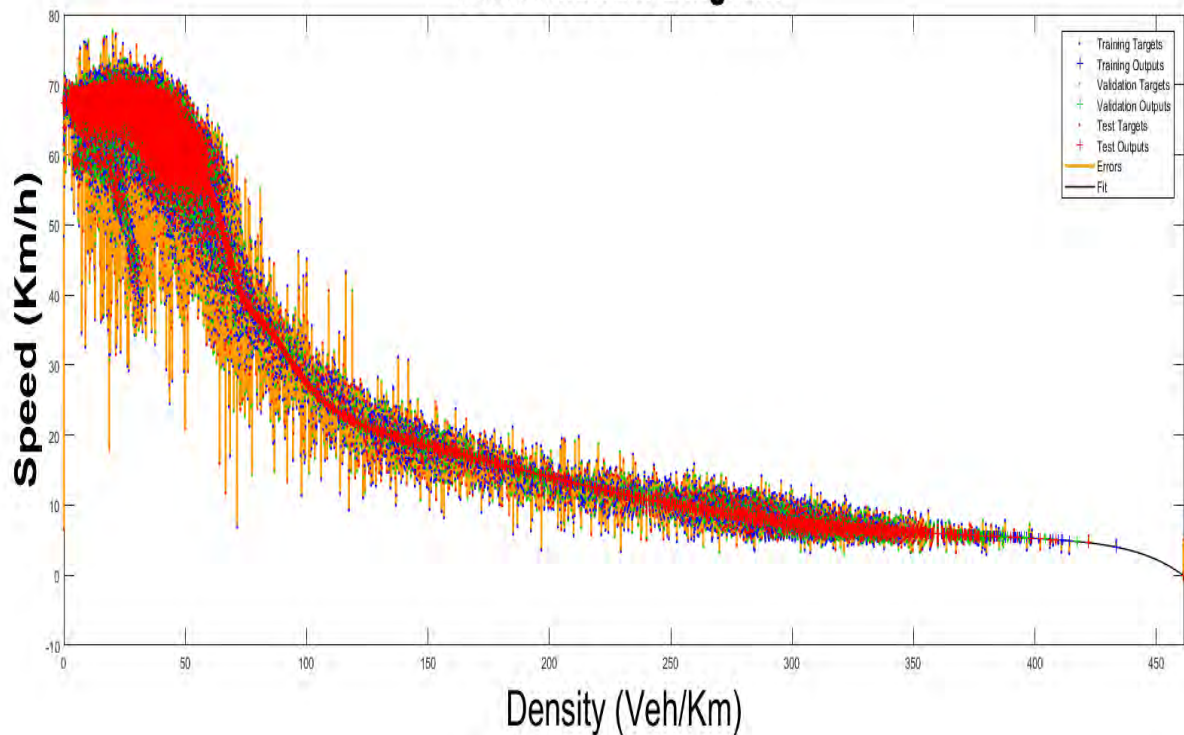
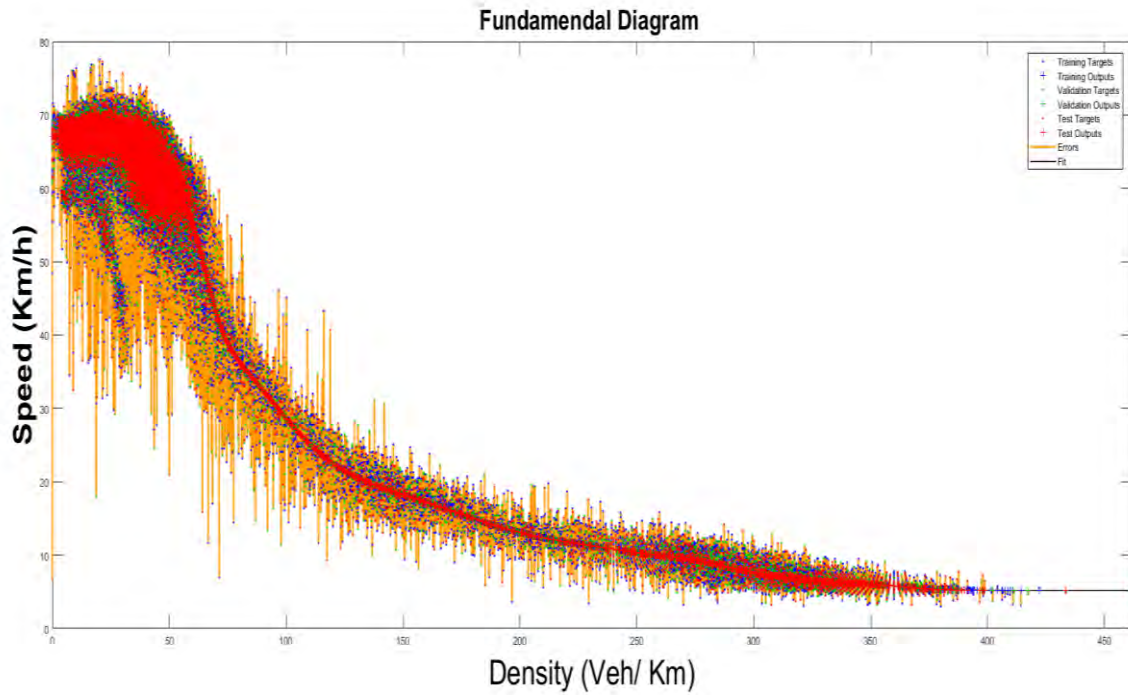
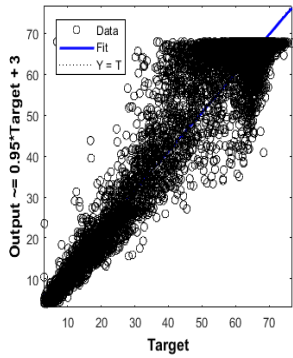


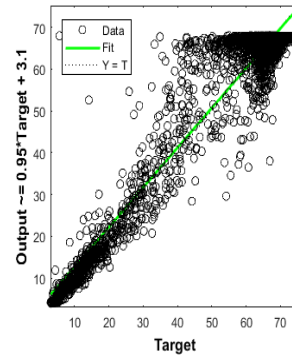
Figure: Performance of 55-25 data split with hidden layer 5 at mainline close to off-ramp



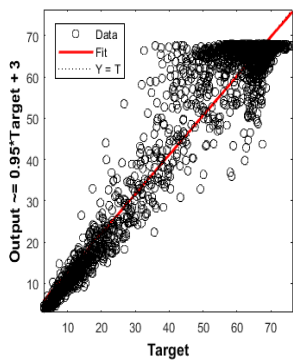
**Training: R=0.97651**



**Validation: R=0.97299**



**Test: R=0.97672**



**All: R=0.97605**

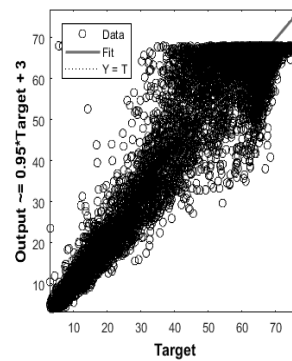
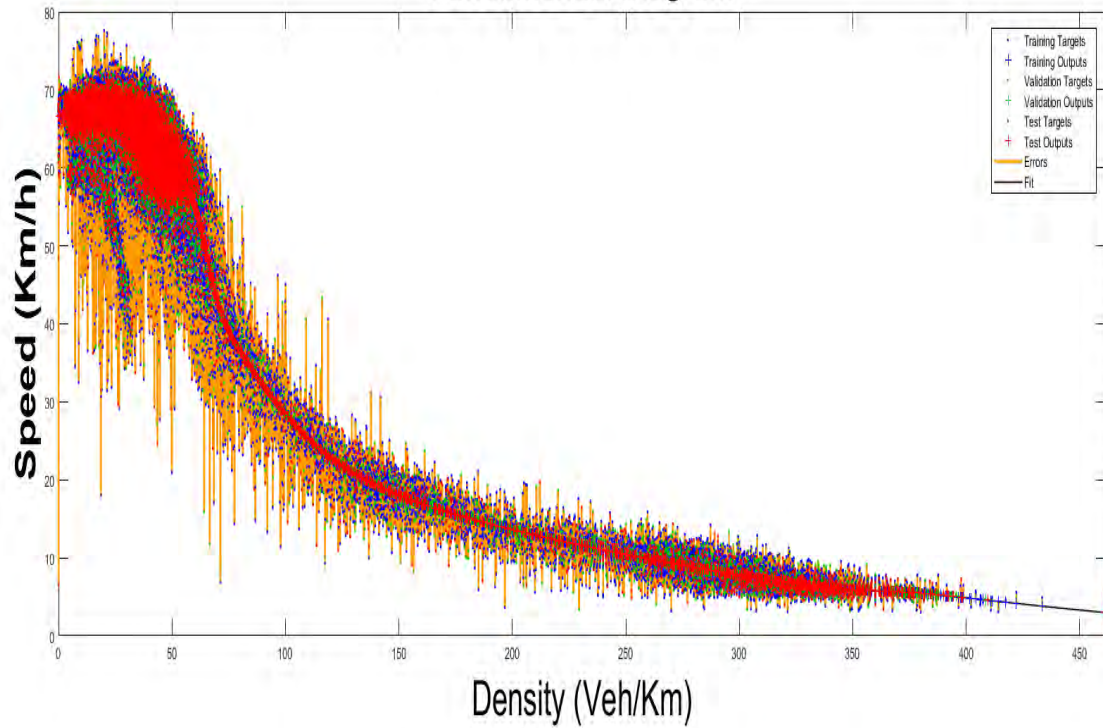
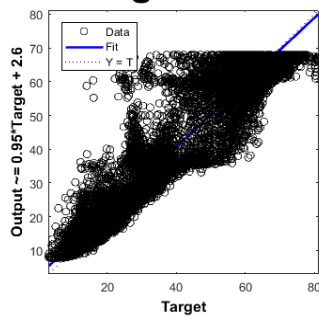


Figure: Performance of 55-25 data split with hidden layer 10 at mainline close to off-ramp

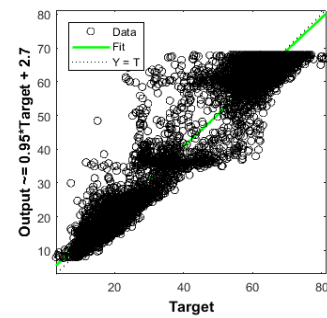
## Fundamental Diagram



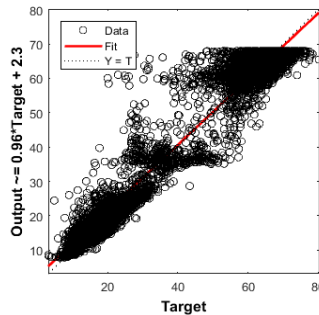
**Training: R=0.97657**



**Validation: R=0.97495**



**Test: R=0.97872**



**All: R=0.97656**

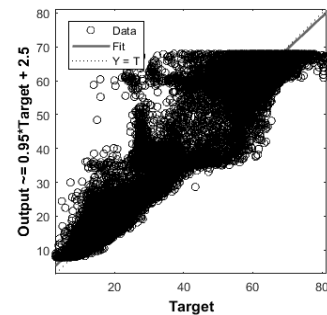
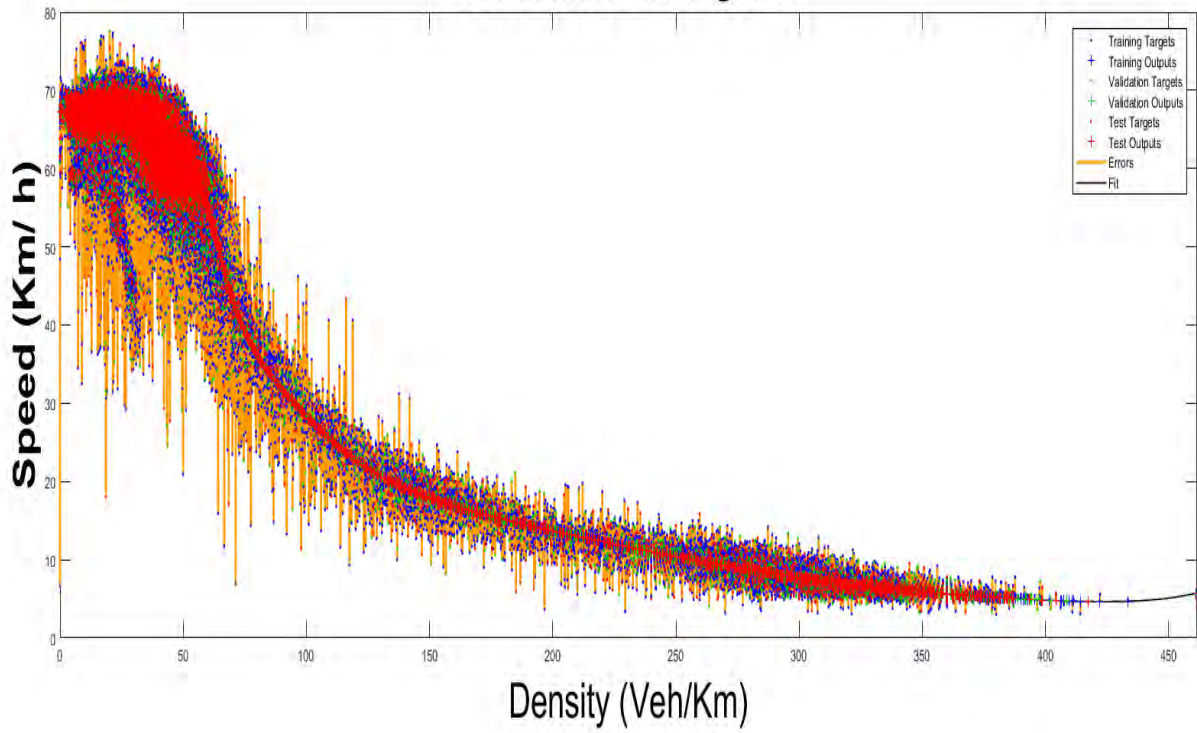
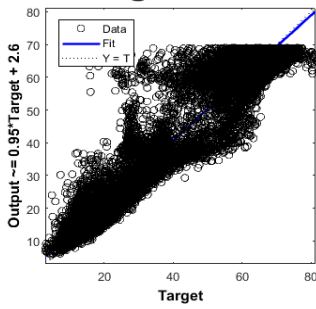


Figure: Performance of 65-20 data split with hidden layer 5 at mainline close to off-ramp

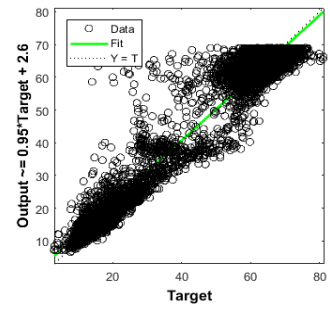
# Fundamental Diagram



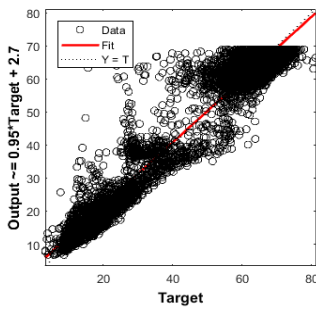
**Training: R=0.97671**



**Validation: R=0.97732**



**Test: R=0.97693**



**All: R=0.97683**

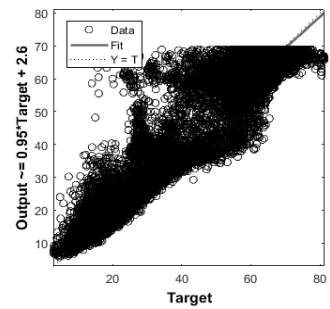
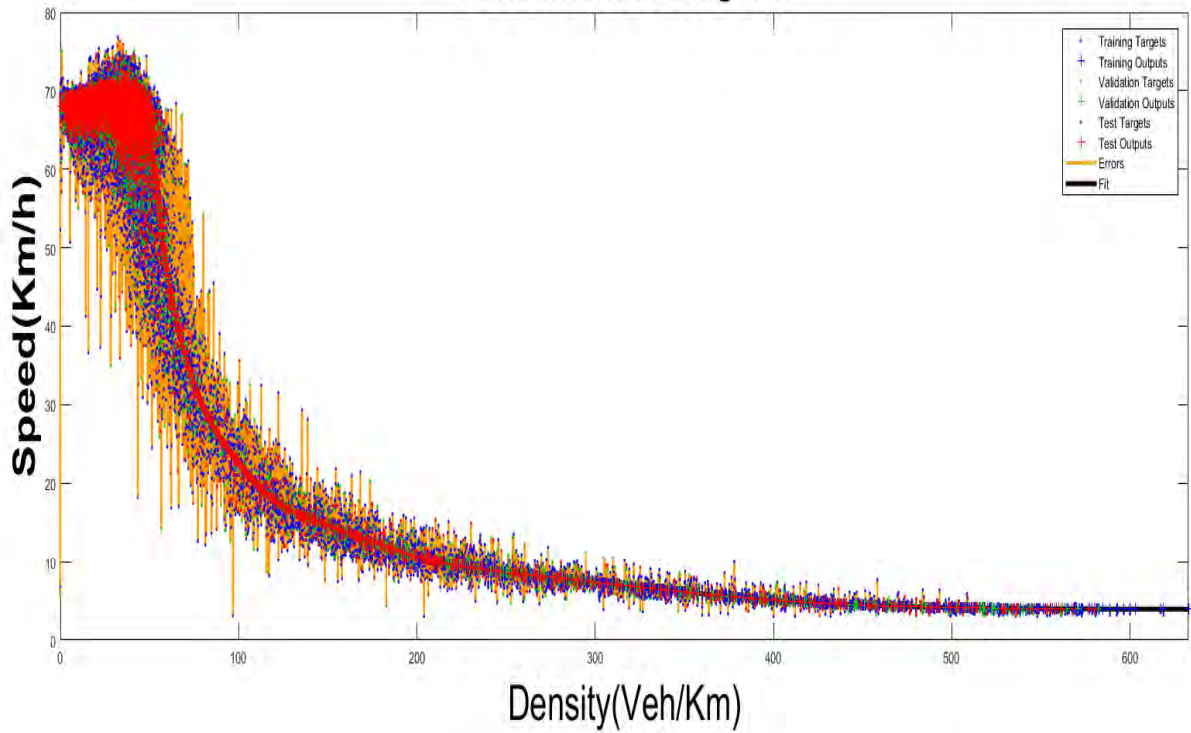


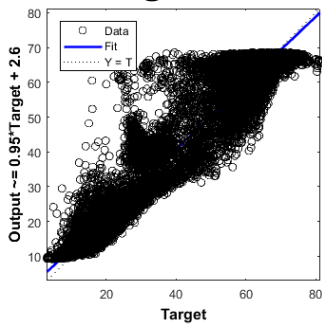
Figure: Performance of 75-15 data split with hidden layer 5 at mainline close to off-ramp



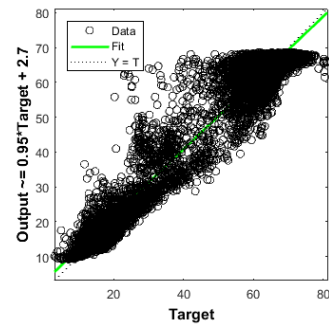
# Fundamental Diagram



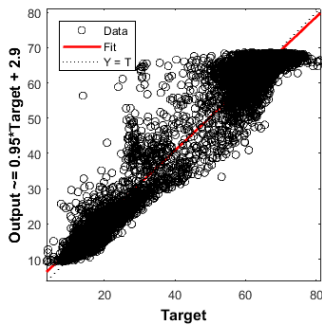
**Training: R=0.9759**



**Validation: R=0.97569**



**Test: R=0.97303**



**All: R=0.97543**

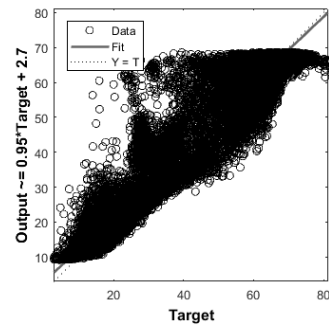
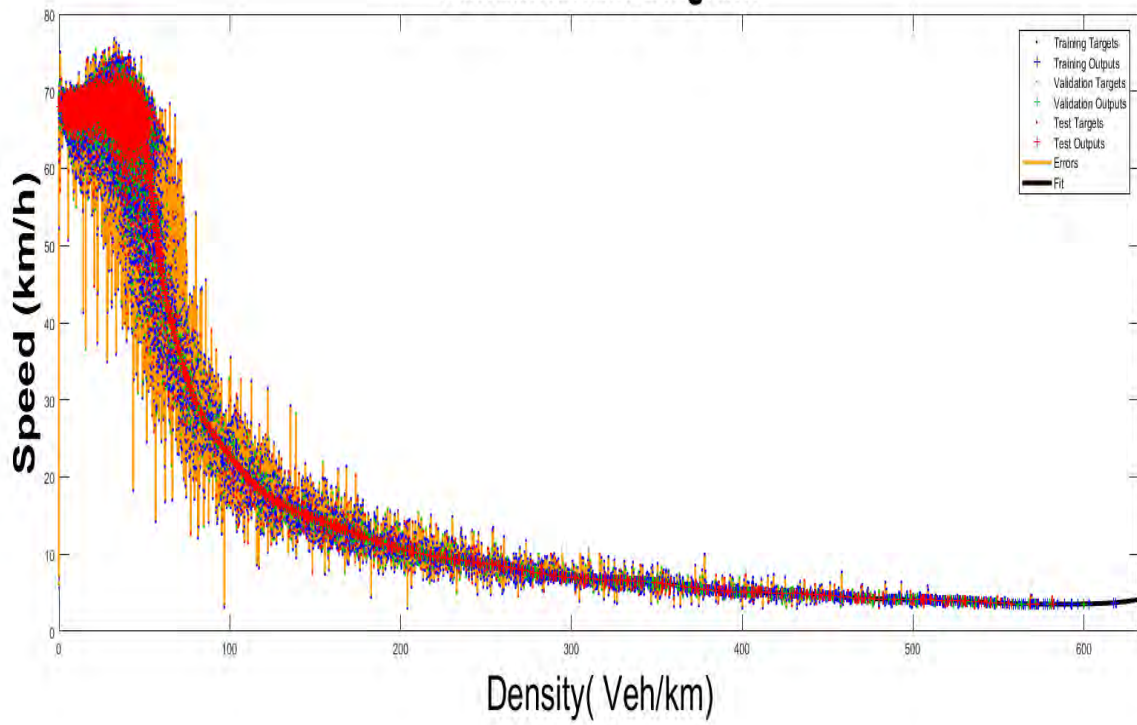
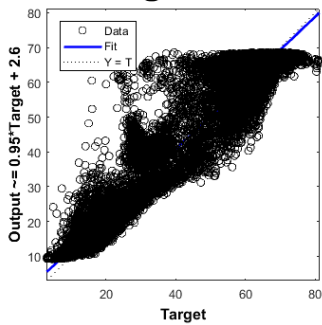


Figure: Performance of 75-15 data split with hidden layer 5 at mainline close to on-ramp

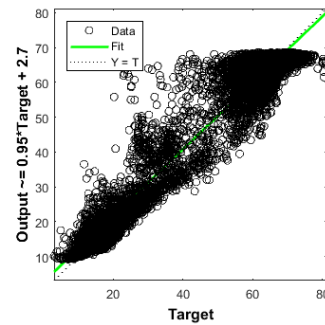
# Fundamental Diagram



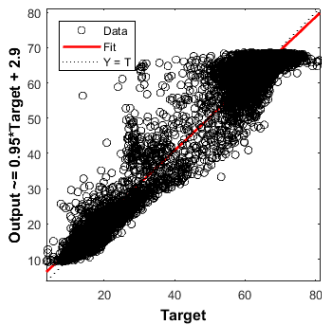
**Training: R=0.9759**



**Validation: R=0.97569**



**Test: R=0.97303**



**All: R=0.97543**

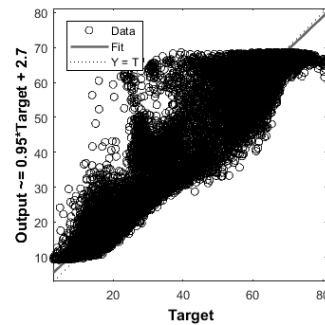
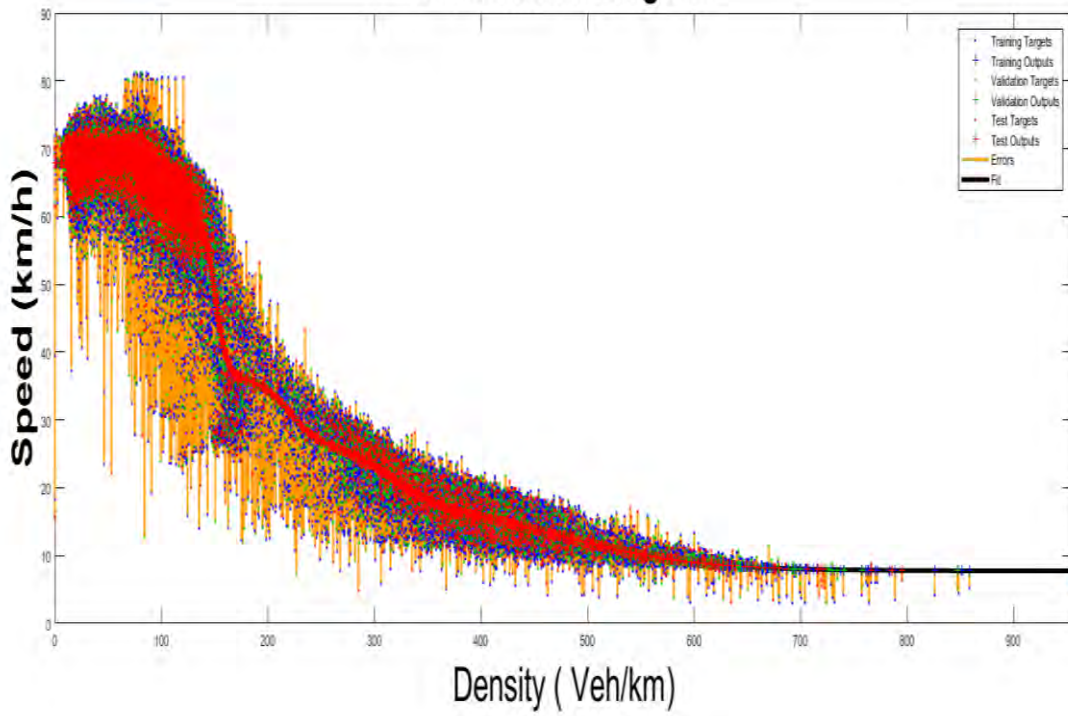


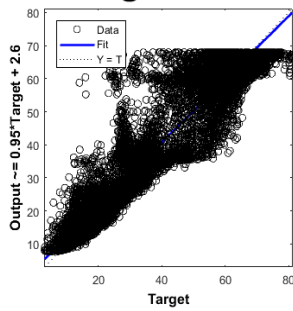
Figure: Performance of 75-15 data split with hidden layer 10 at mainline close to on-ramp



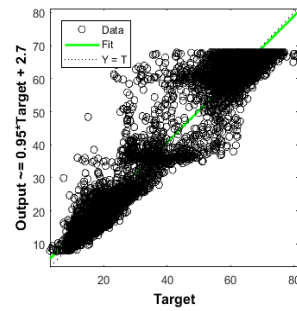
# Fundamental Diagram



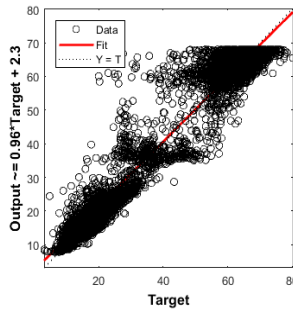
**Training: R=0.97657**



**Validation: R=0.97495**



**Test: R=0.97872**



**All: R=0.97656**

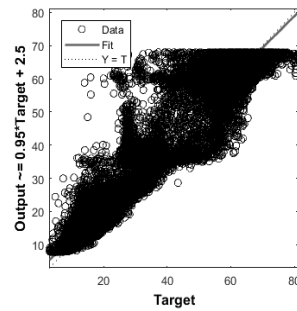
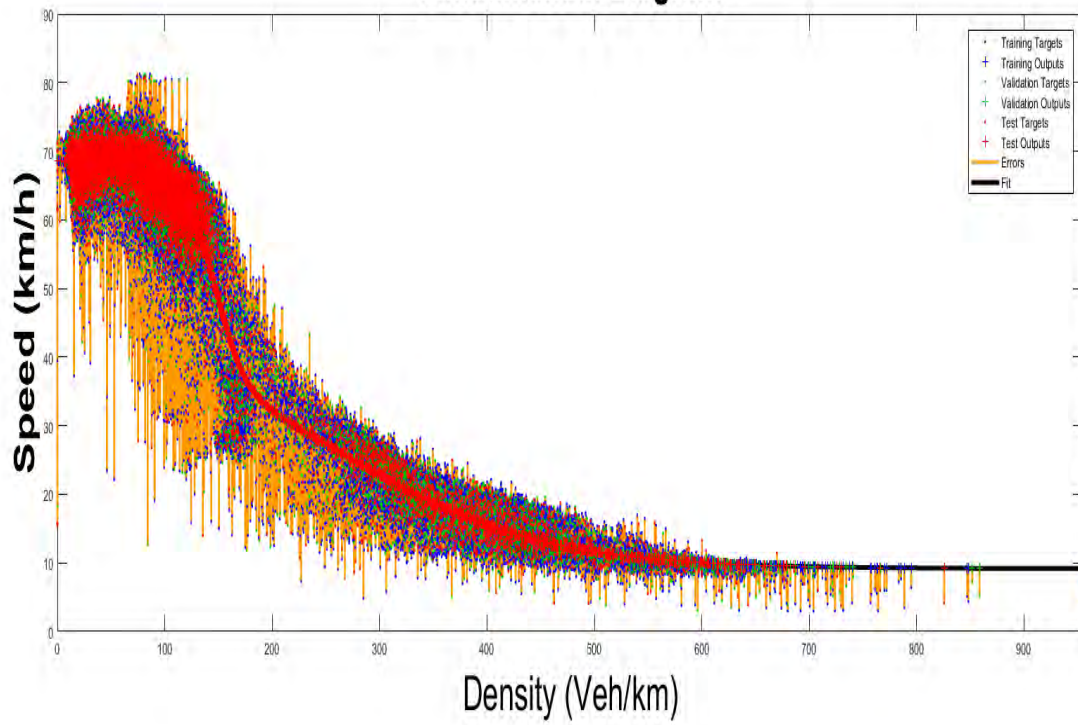
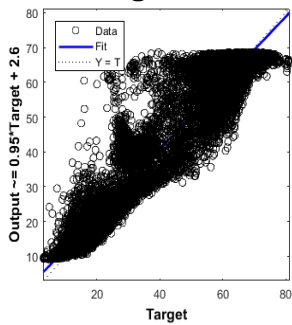


Figure: Performance of 65-20 data split with hidden layer 5 at off-ramp

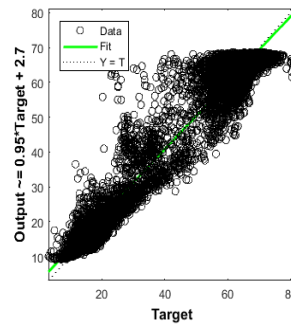
# Fundamental Diagram



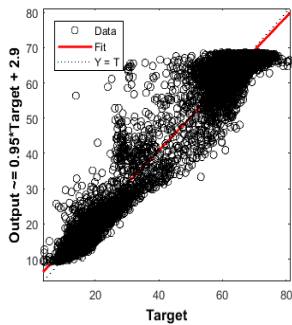
**Training: R=0.9759**



**Validation: R=0.97569**



**Test: R=0.97303**



**All: R=0.97543**

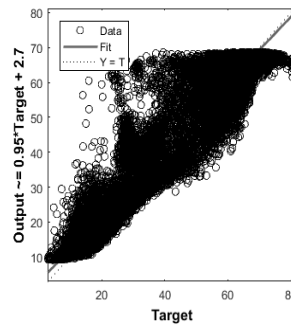
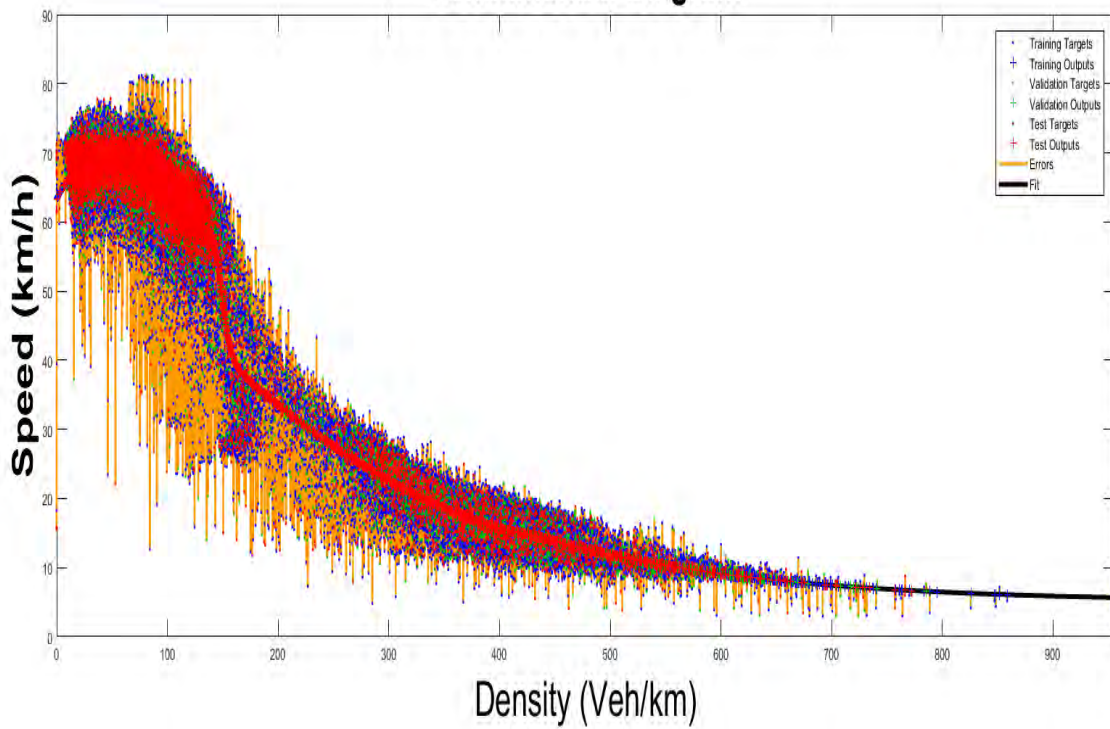
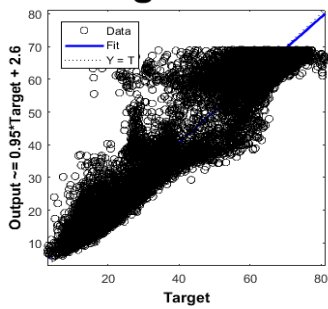


Figure: Performance of 65-20 data split with hidden layer 2 at off-ramp

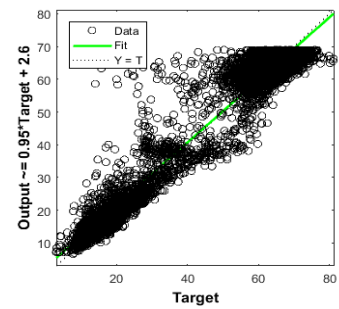
## Fundamental Diagram



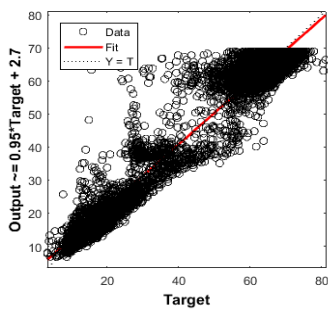
**Training: R=0.97671**



**Validation: R=0.97732**



**Test: R=0.97693**



**All: R=0.97683**

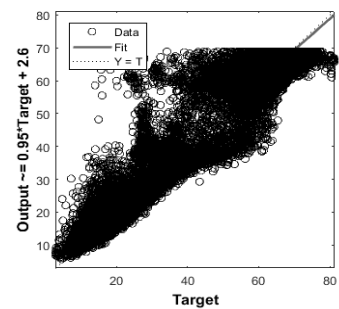


Figure: Performance of 70-15 data split with hidden layer 5 at off-ramp

## Graphical representation of proposed model for non-lane based heterogeneous traffic

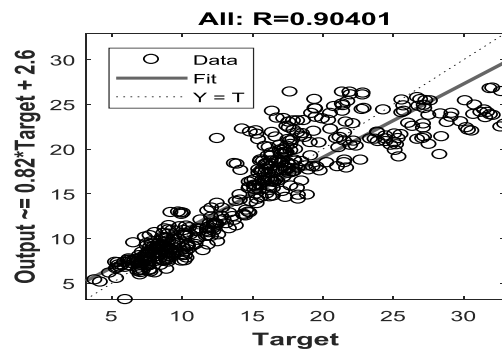
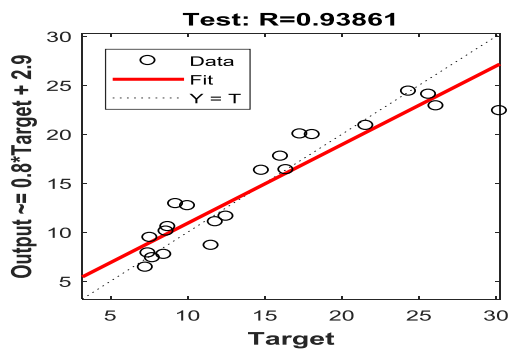
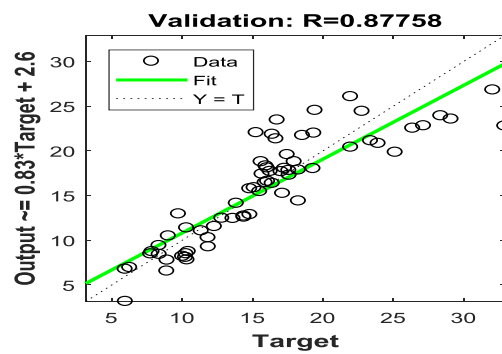
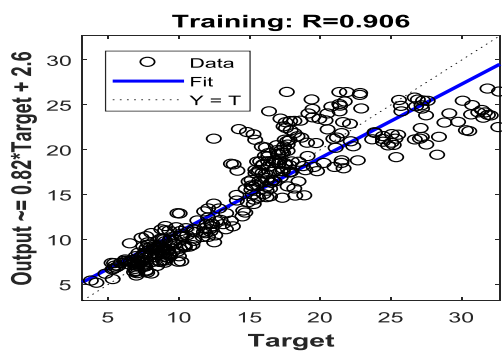
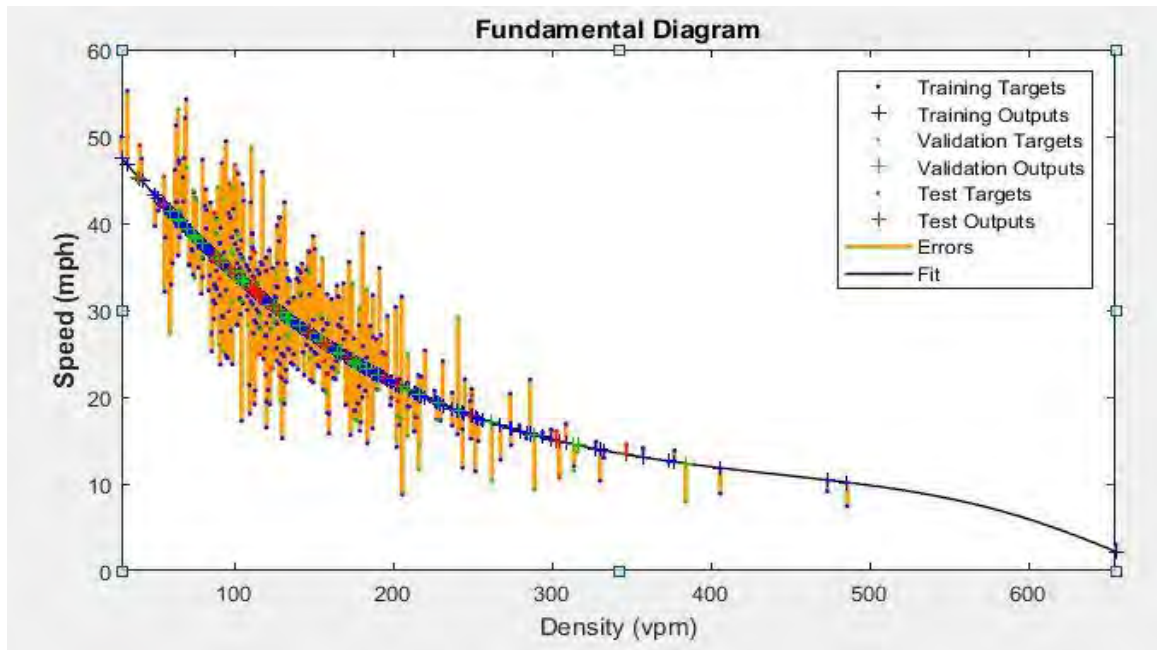


Figure: Performance of 75-15 data split with hidden layer 5 at mainline close to off-ramp

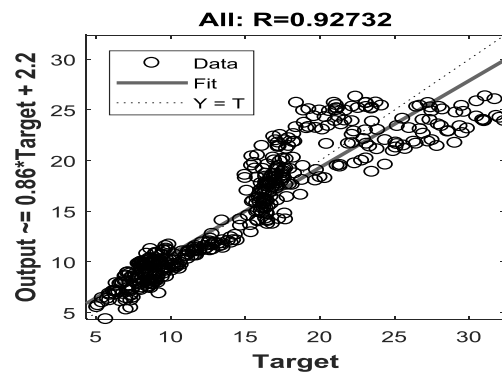
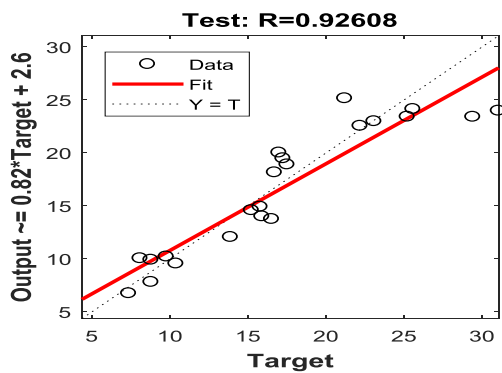
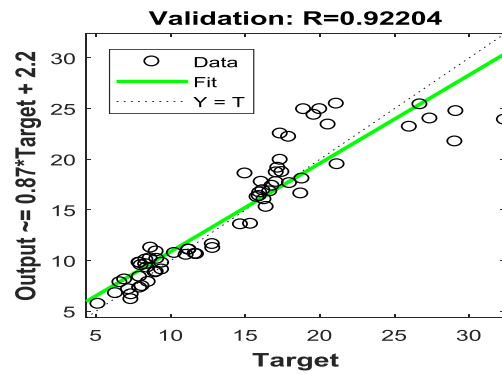
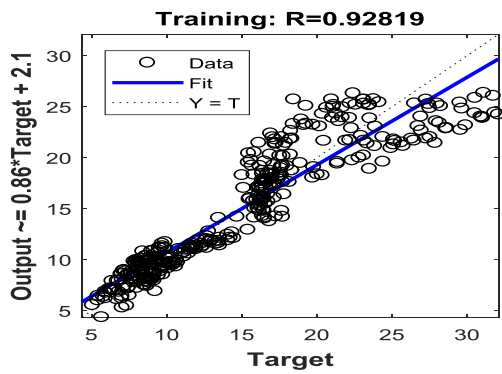
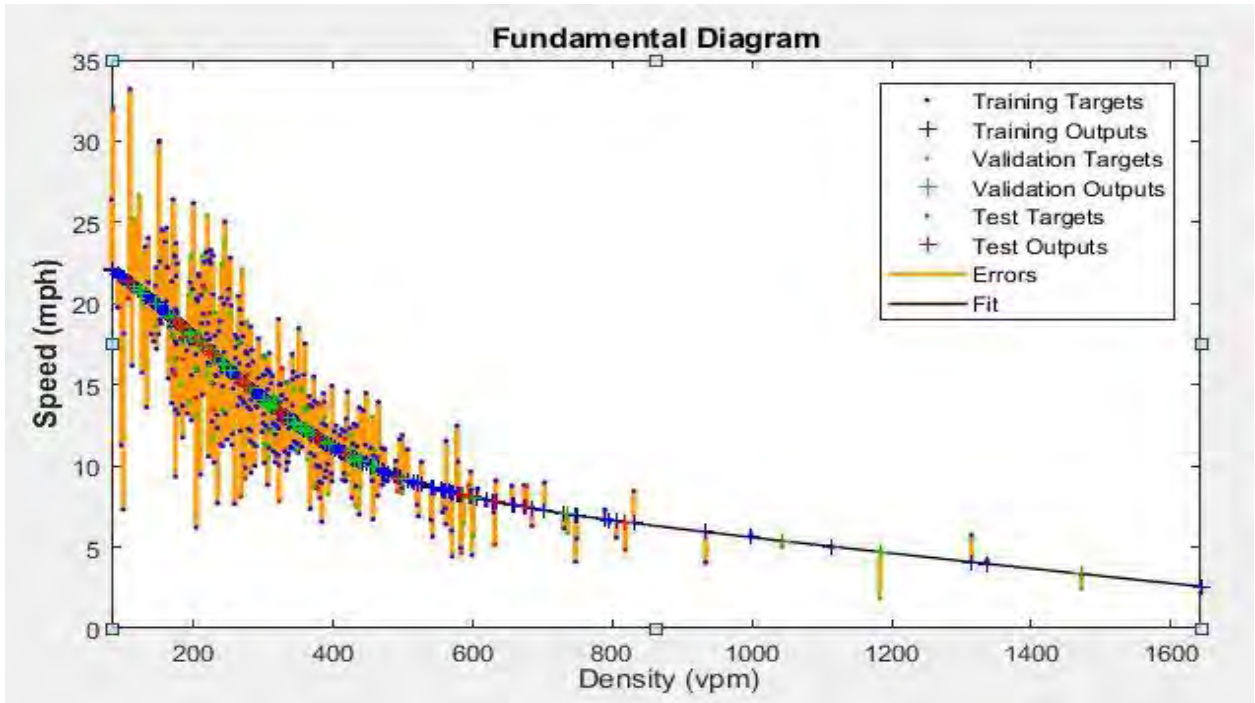


Figure: Performance of 75-15 data split with hidden layer 5 at off-ramp



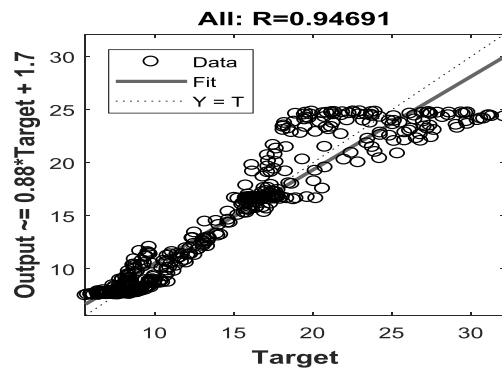
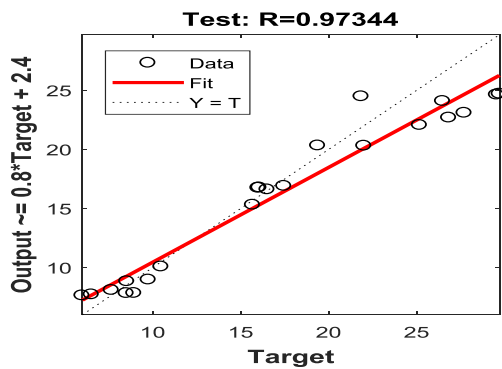
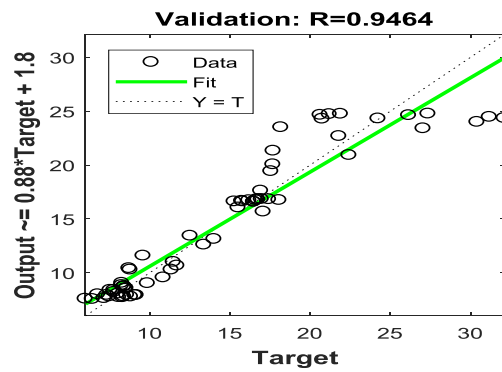
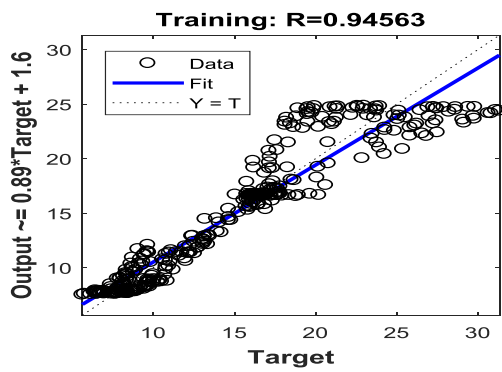
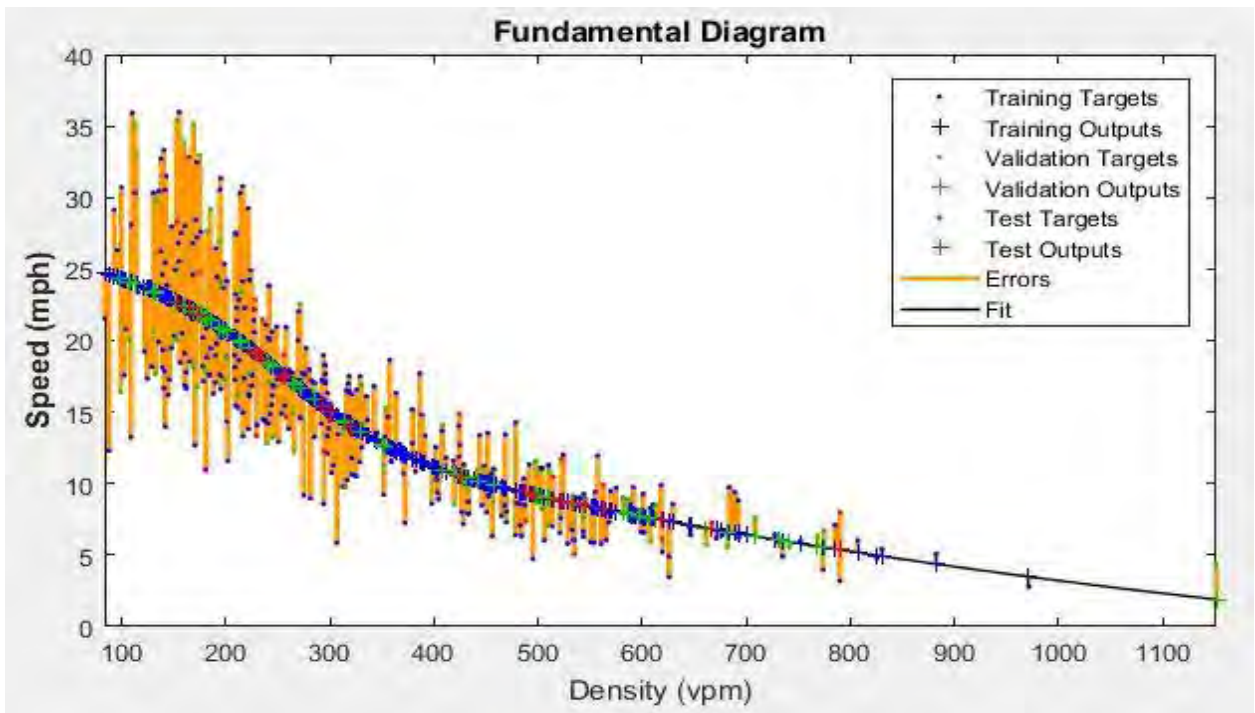


Figure: Performance of 75-15 data split with hidden layer 5 at mainline close to on-ramp

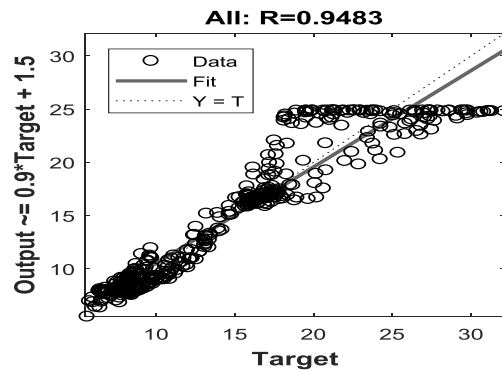
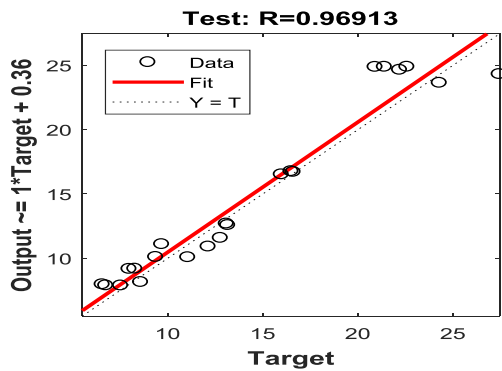
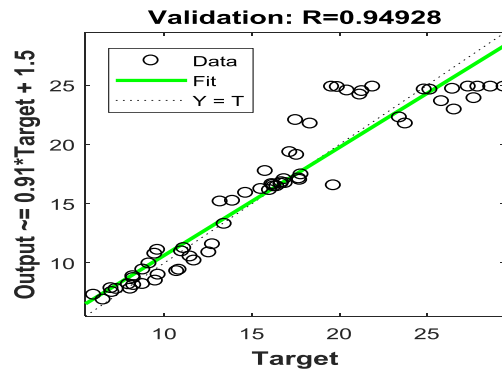
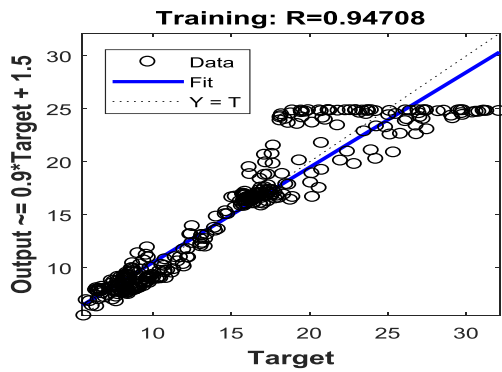
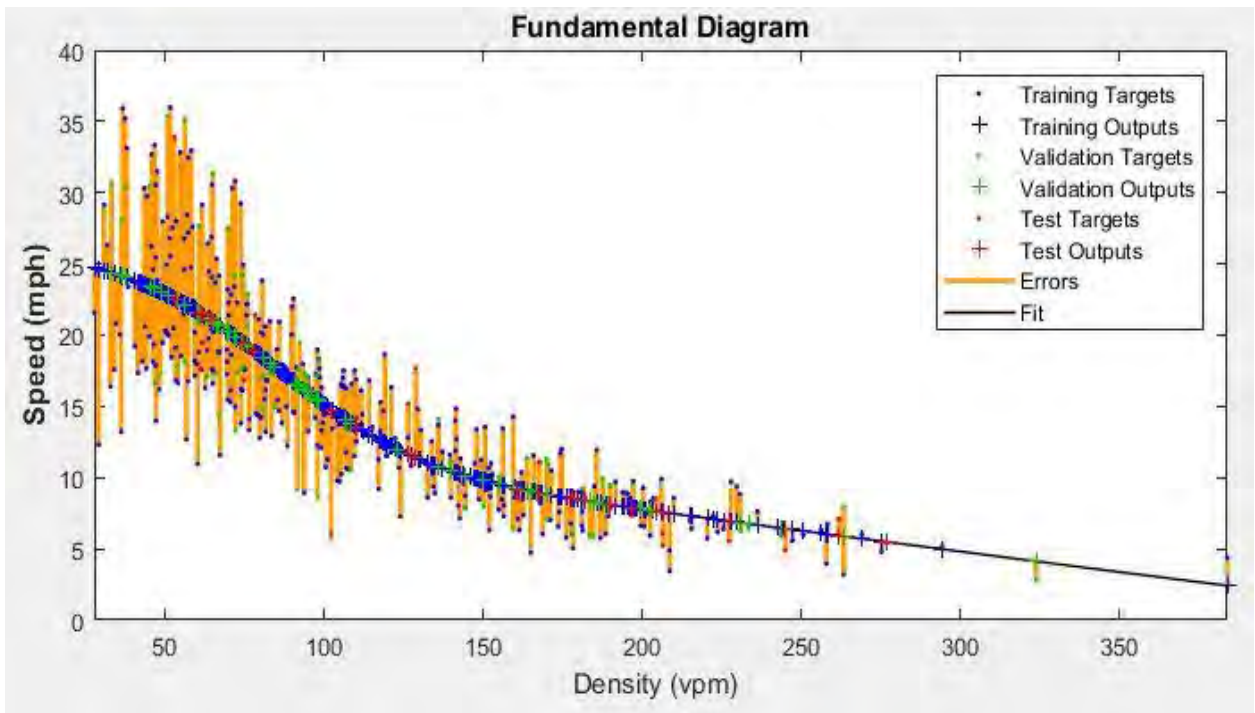


Figure: Performance of 75-15 data split with hidden layer 5 at mainline close to on-ramp

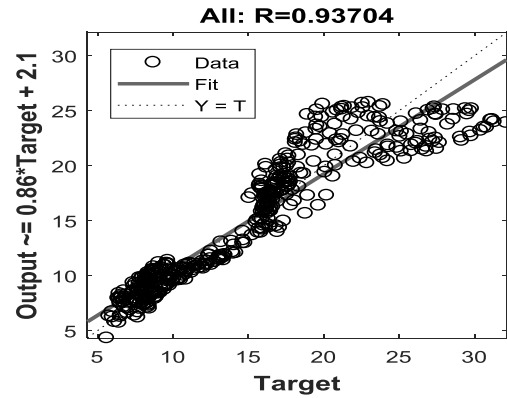
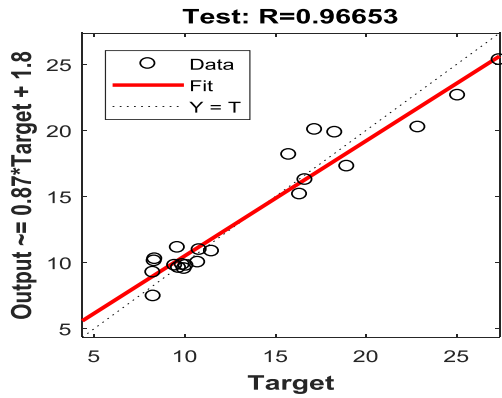
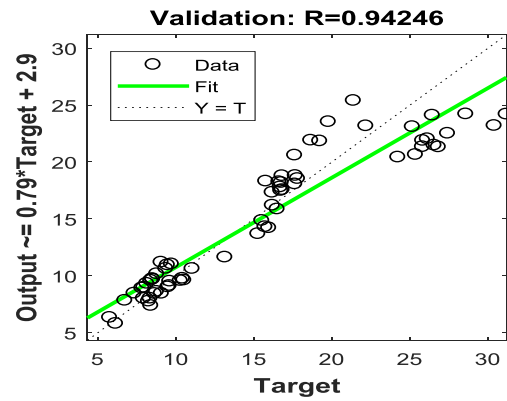
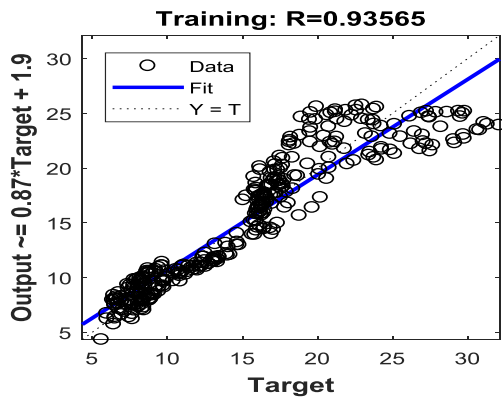
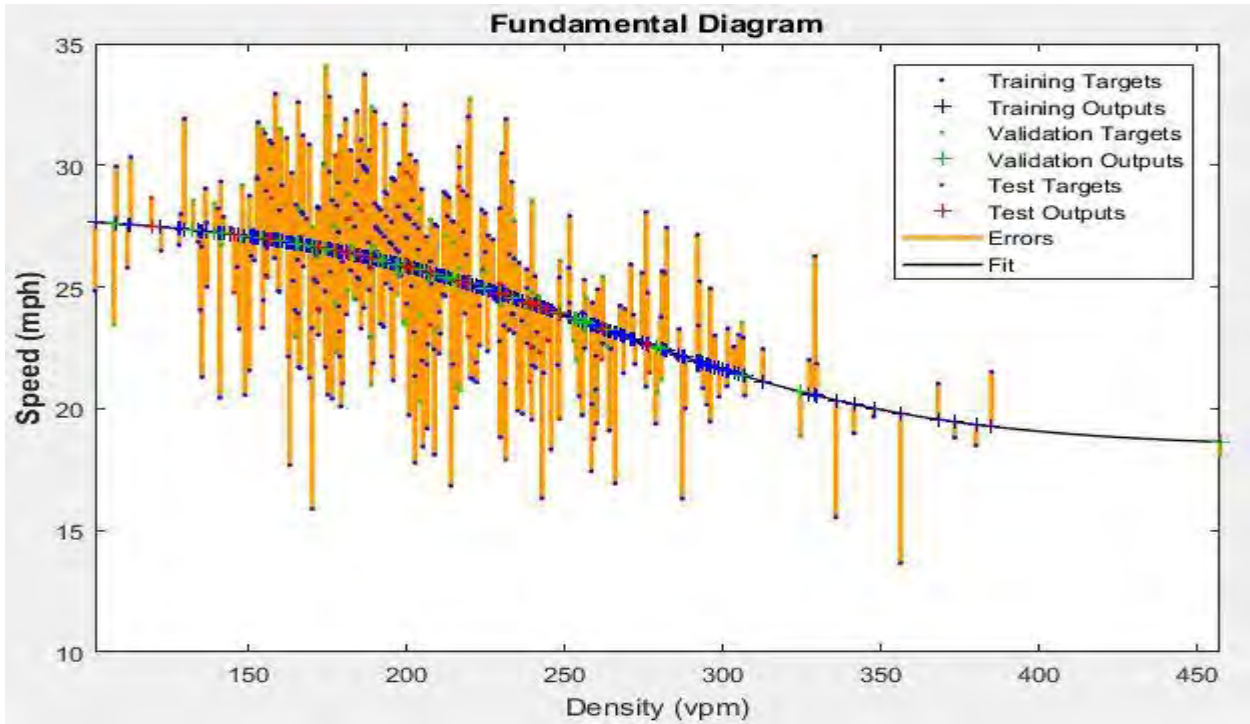


Figure: Performance of 75-15 data split with hidden layer 5 at mainline close to on-ramp



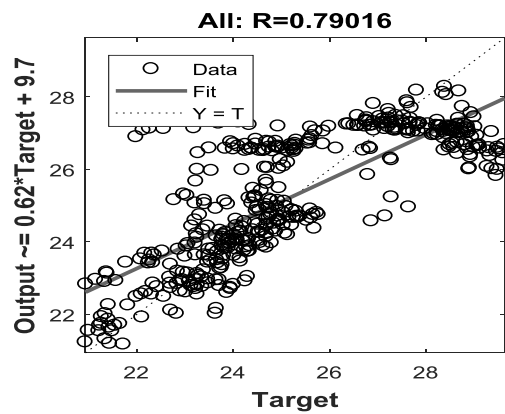
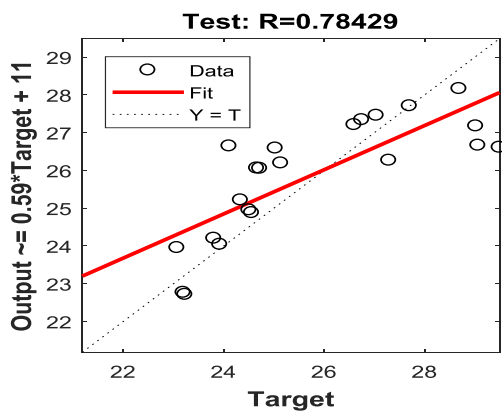
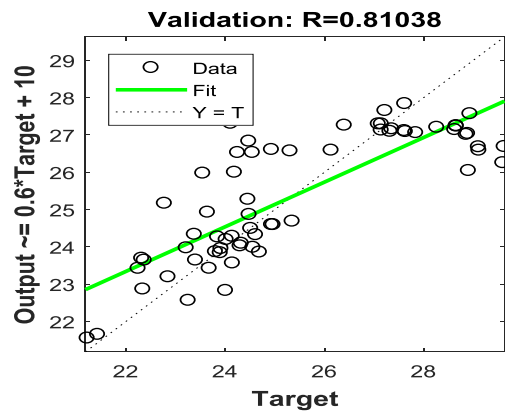
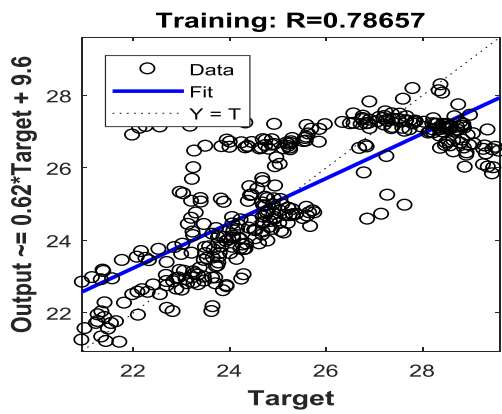
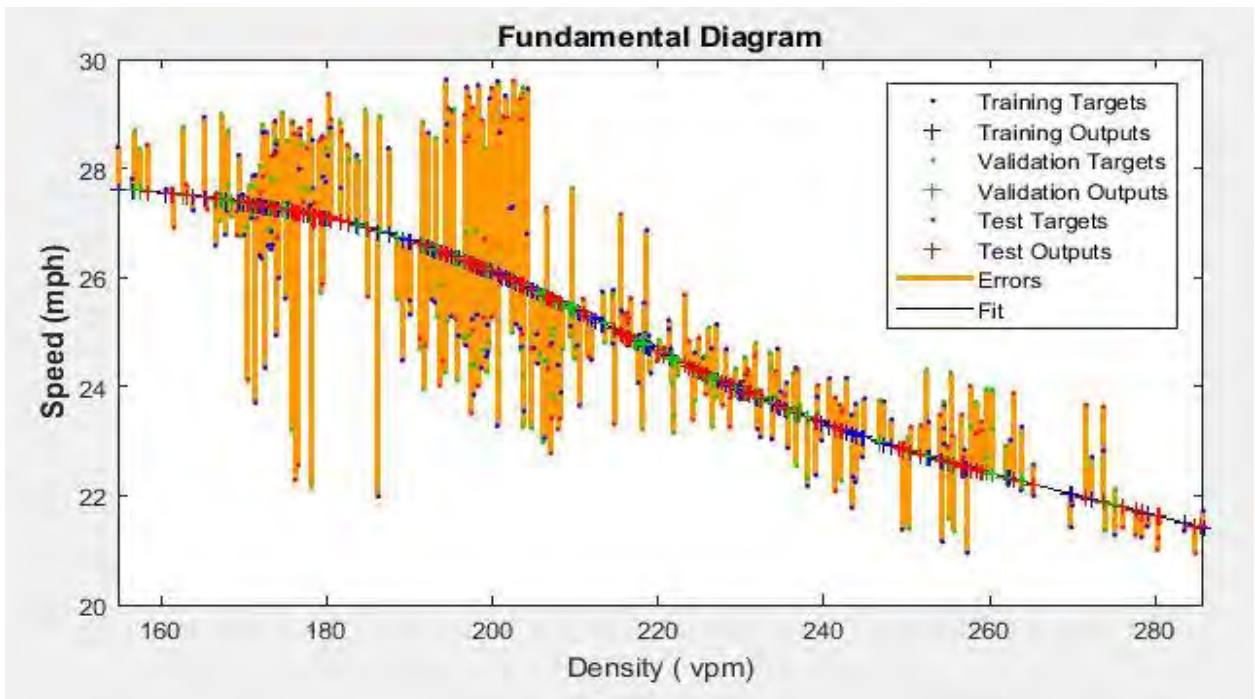


Figure: Performance of 75-15 data split with hidden layer 5 at mainline

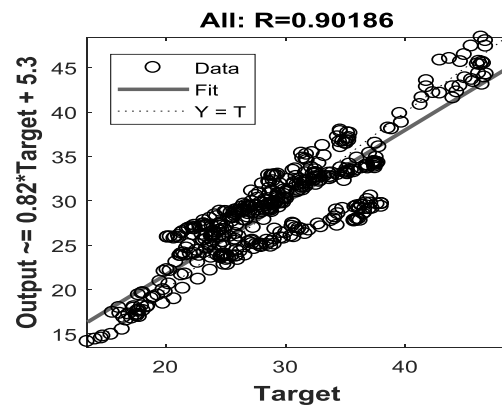
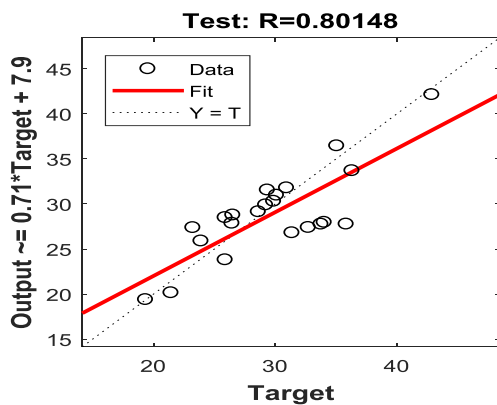
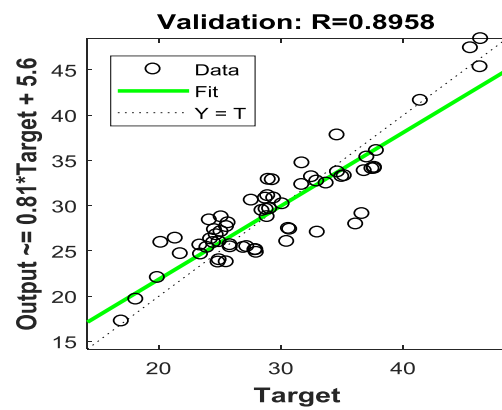
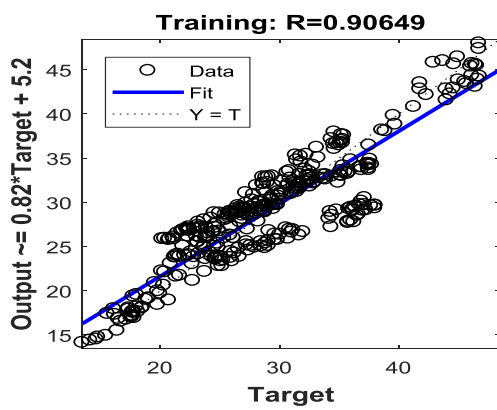
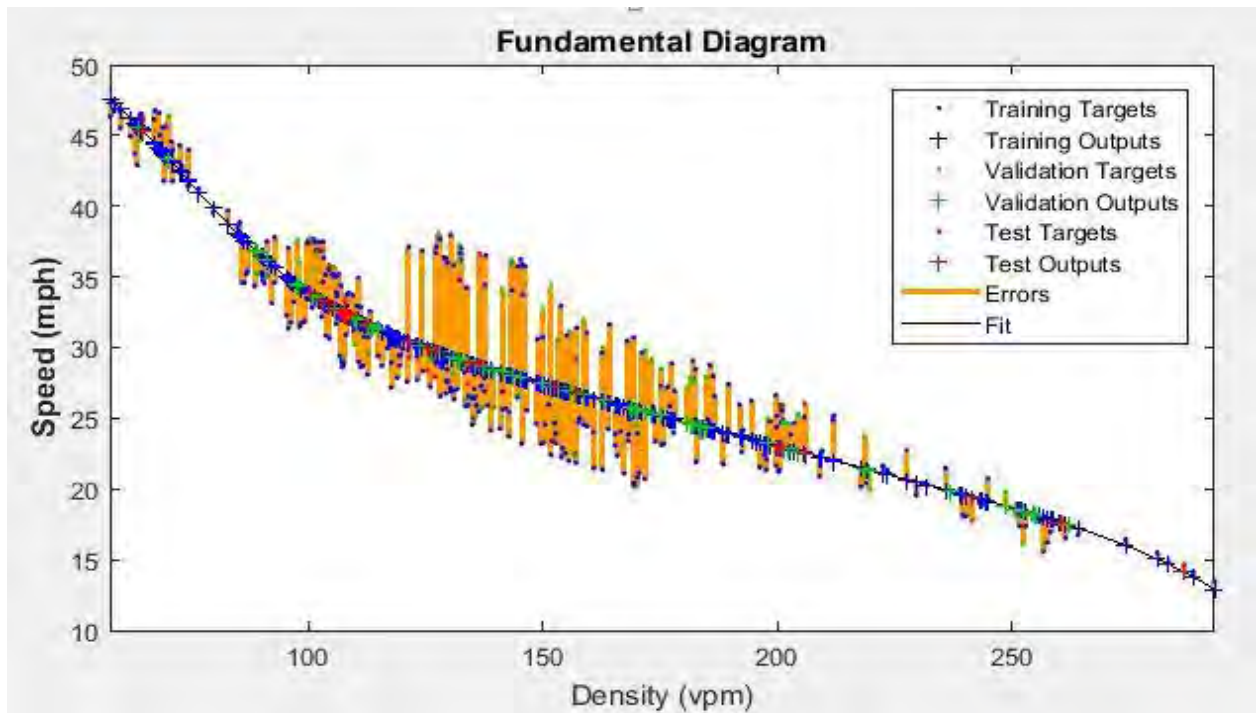


Figure: Performance of 75-15 data split with hidden layer 5 at mainline close to off-ramp

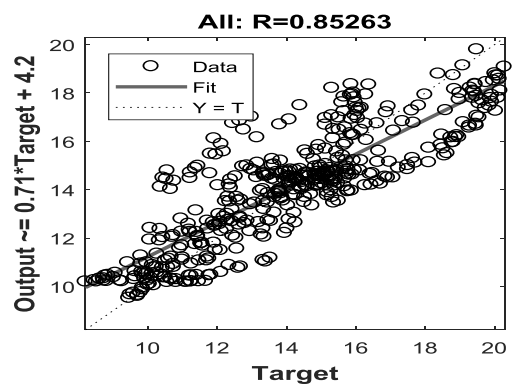
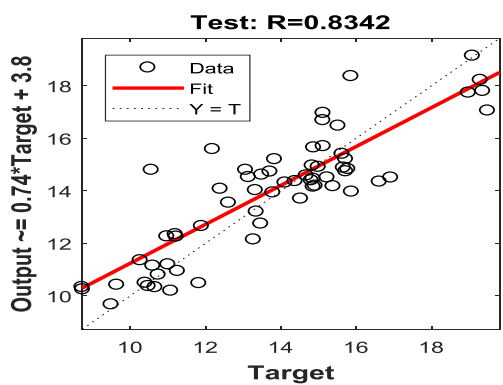
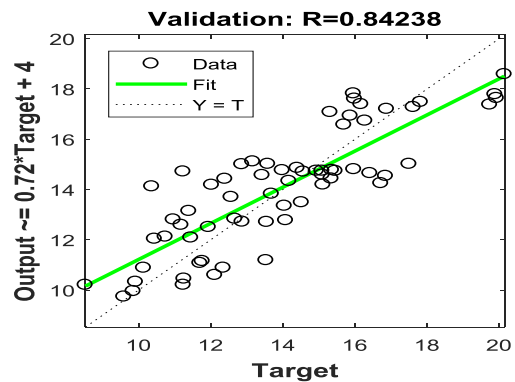
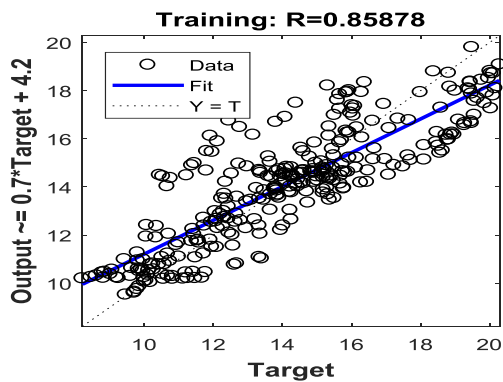
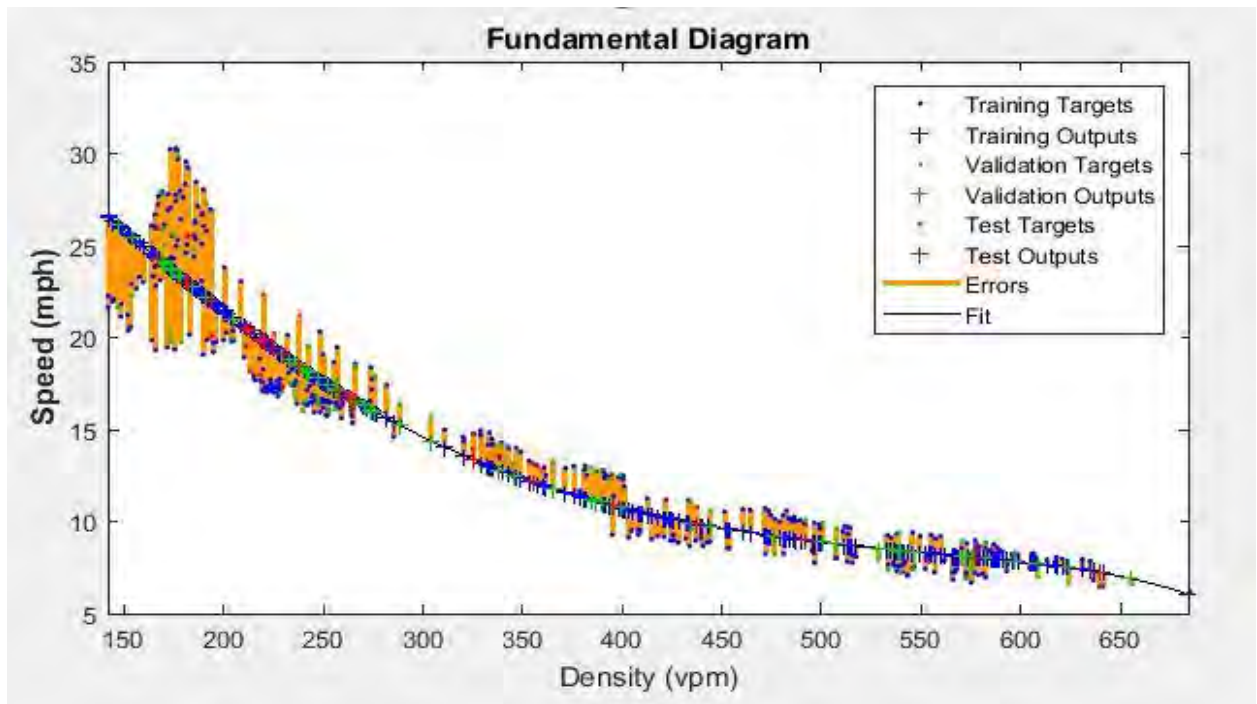


Figure: Performance of 75-15 data split with hidden layer 5 at mainline

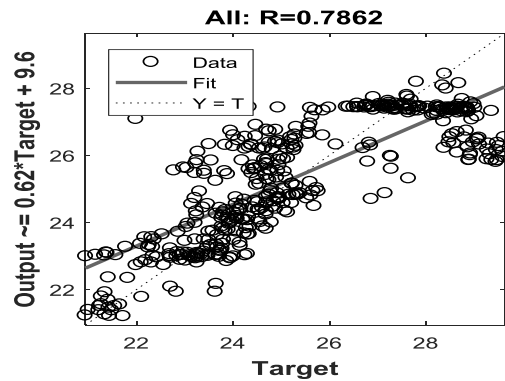
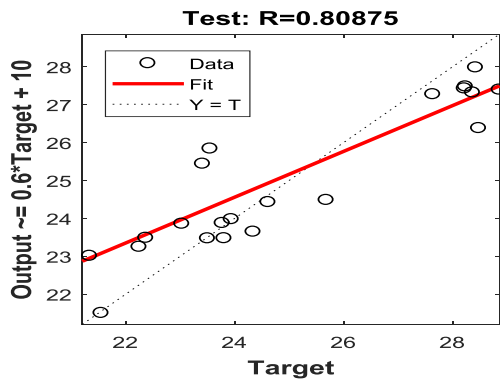
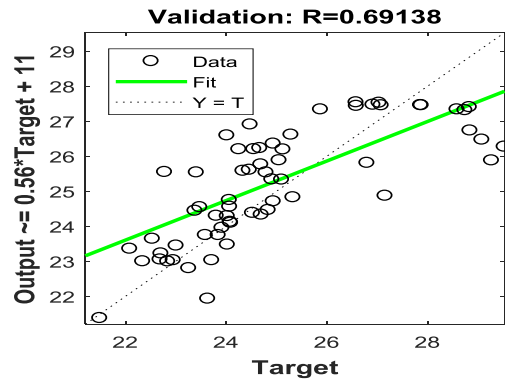
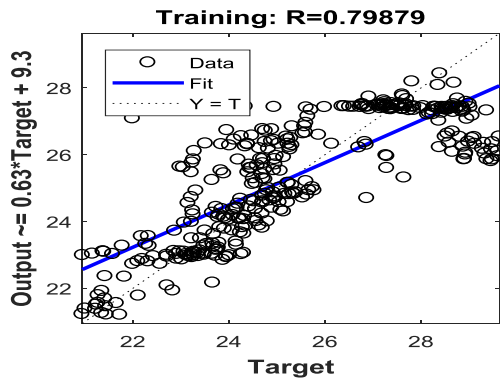
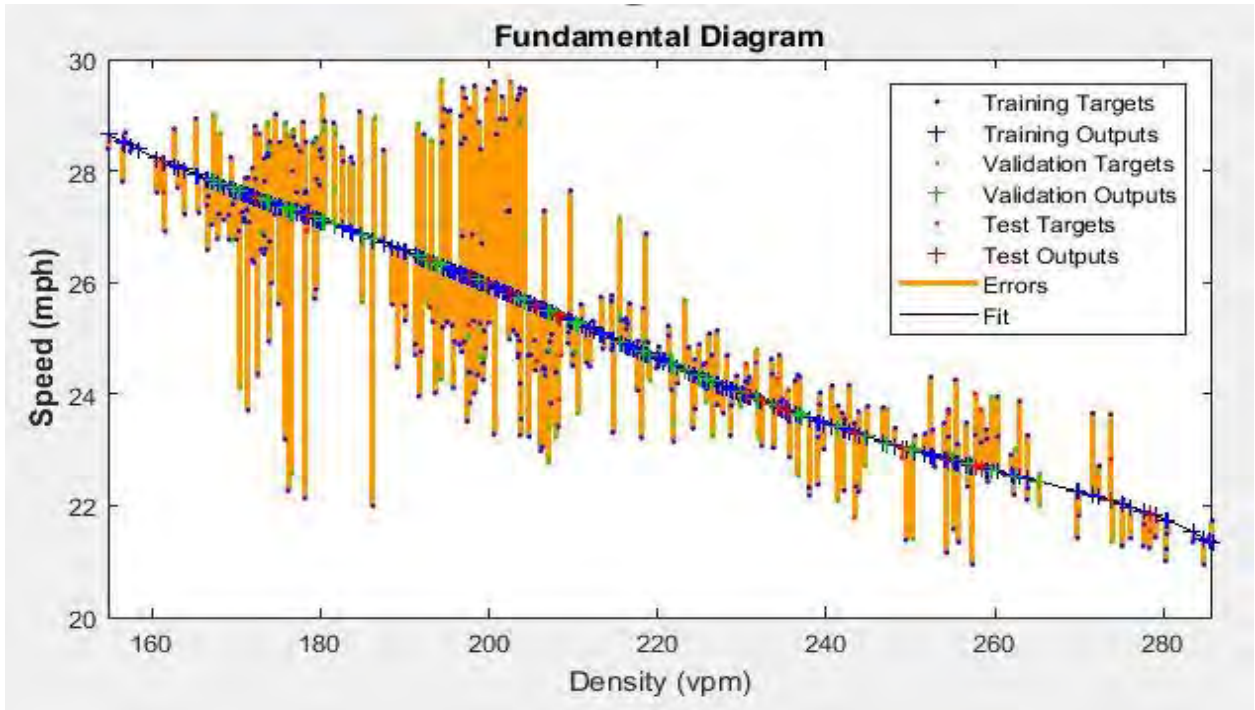


Figure: Performance of 75-15 data split with hidden layer 5 at mainline

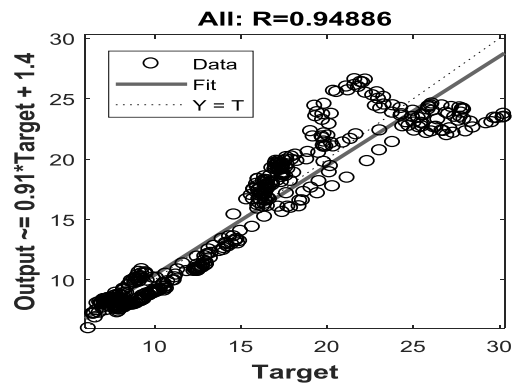
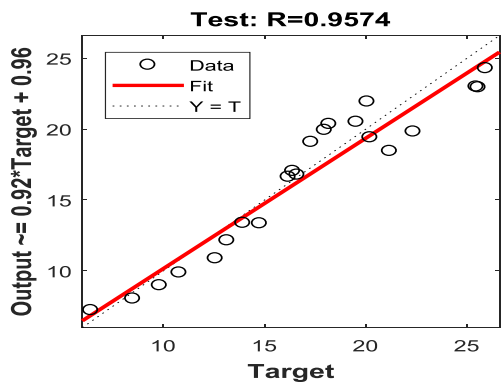
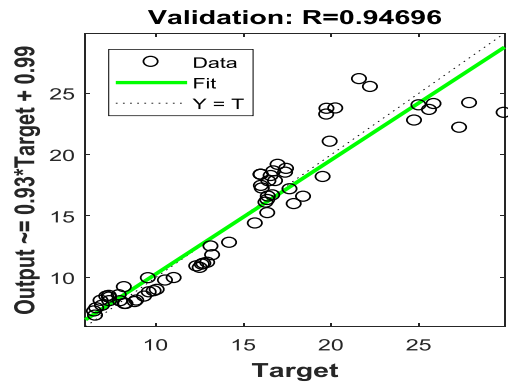
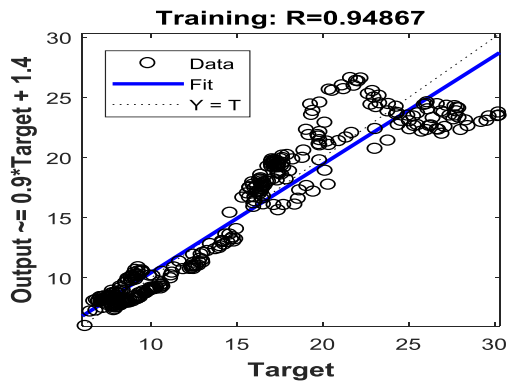
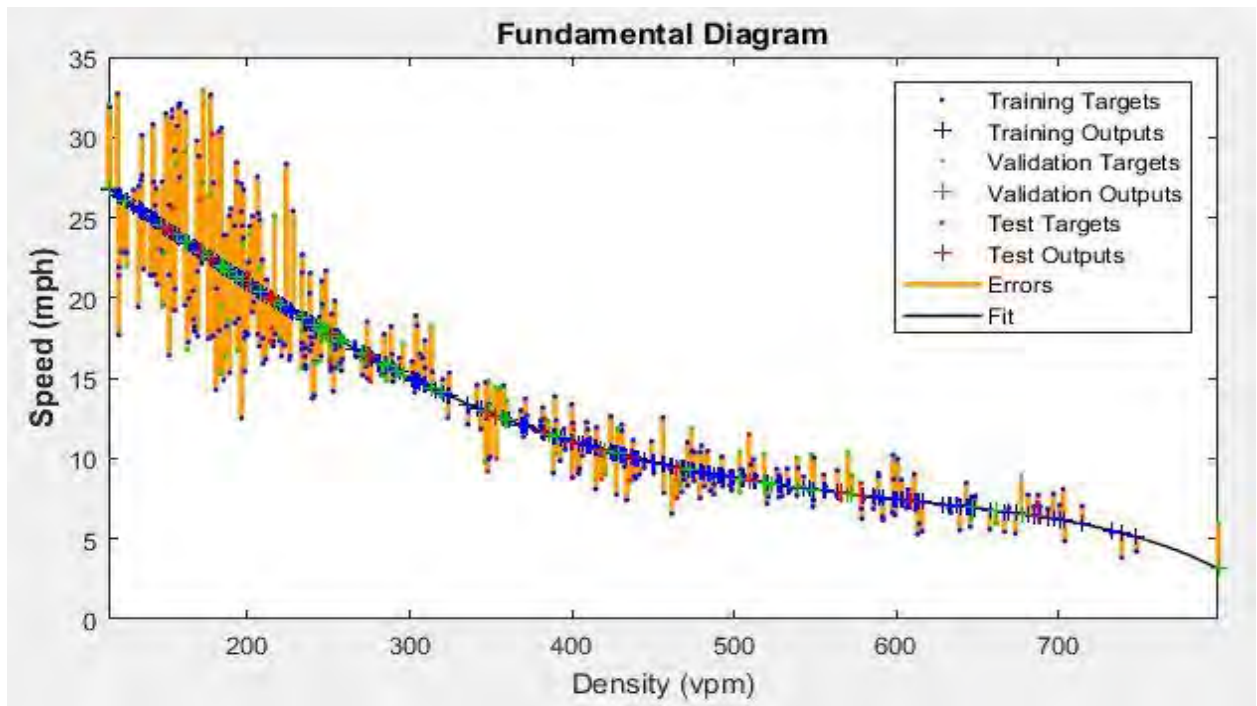


Figure: Performance of 75-15 data split with hidden layer 5 at on-ramp

## **APPENDIX A-3: EXTRACTED TRAFFIC DATA**



**Table: Extracted Data for time interval 20 second**

<b>Speed (Mile/hr)</b>	<b>Flow (veh/hr)</b>	<b>Density (veh/mile)</b>
16.3	3060	188
19.3	2700	140
17.3	3600	209
12.5	4140	331
14.7	4680	319
17.2	3060	178
17.0	5400	318
14.7	3780	258
15.3	5400	353
15.9	4680	295
17.6	4860	276
18.6	6660	357
13.3	3780	285
17.6	3960	225
15.5	3780	244
14.9	3780	254
18.0	3240	180
17.2	4860	282
17.0	4860	285
17.5	3420	195
18.3	5400	295
14.6	3960	272
17.9	2520	141
14.7	5220	356
17.5	5580	318
13.9	4140	299
14.5	3420	236
18.5	3060	165
16.1	5400	335
17.8	2880	162
14.1	3240	230
17.2	4680	271
16.4	5220	318
18.1	3780	209
15.6	4500	288
14.4	3420	237
17.2	5040	294
14.8	3600	243
17.0	4500	265
17.3	3420	198
17.6	3240	184
16.4	4680	285
17.3	4320	250
17.6	3240	184
16.3	5220	321
16.6	3240	195

<b>Speed (Mile/hr)</b>	<b>Flow (veh/hr)</b>	<b>Density (veh/mile)</b>
14.3	3420	238
16.5	4500	274
17.7	4680	264
20.1	2160	108
18.2	2340	129
14.6	3960	271
18.2	4500	247
18.8	3420	182
16.2	3600	222
17.3	2160	125
18.3	5400	296
17.0	5040	296
17.9	4680	261
18.6	3960	213
17.3	5040	292
17.8	3960	223
17.3	2520	146
17.6	3960	225
16.3	4860	298
18.8	3780	201
18.8	3780	201
16.3	5940	364
16.8	2880	172
15.0	3240	216
16.9	4140	245
19.1	3060	160
16.8	5760	343
13.8	4500	327
14.2	4140	292
17.6	4500	256
16.1	3600	223
12.3	1080	88
16.2	3960	245
17.4	3780	218
13.2	3240	245
14.8	5760	389
20.2	3600	178
15.4	3960	256
16.6	5400	326
17.1	4140	242
14.5	4860	336
15.0	3960	265
16.1	3420	212
16.8	4140	246
8.7	4320	499
5.0	2700	535
8.5	5220	613



**Table: Extracted Data for time interval 1 min**

<b>Speed (Mile/hr)</b>	<b>Flow (veh/hr)</b>	<b>Density (veh/mile)</b>
17.6	3120	179
16.4	3480	226
14.8	4140	286
14.8	3960	276
16.3	4380	272
16.3	4080	251
15.7	4860	310
15.3	4620	302
16.3	4980	308
17.4	5400	309
16.5	5100	306
16.5	4800	289
15.5	3840	251
16.0	3840	241
16.1	3600	226
16.7	3960	239
17.4	4320	249
17.3	4380	254
17.6	4560	259
16.8	4260	254
16.9	3960	236
15.7	3900	256
16.7	4440	272
15.3	4980	324
15.3	4380	284
15.6	3540	233
16.4	3960	245
17.5	3780	221
16.0	3840	242
16.4	3600	221
15.9	4380	273
17.3	4560	266
16.7	4500	272
16.1	3900	245
15.7	4320	273
15.5	4020	258
16.3	4380	267
16.4	3840	235
17.3	3720	216
17.1	3780	222
17.1	4080	239
17.1	4080	240
17.0	4260	252
16.8	3900	234
15.7	3960	252

<b>Speed (Mile/hr)</b>	<b>Flow (veh/hr)</b>	<b>Density (veh/mile)</b>
15.8	3720	236
16.2	4200	259
18.1	3780	215
18.7	3060	167
17.6	2820	169
17.0	3600	216
17.2	3960	233
17.7	3840	217
17.5	3060	176
17.3	3720	214
17.5	4200	239
17.7	5040	284
17.9	4560	256
17.9	4560	255
17.9	4320	243
17.4	3840	220
17.5	3480	198
17.1	3780	223
17.6	4200	241
18.0	4140	233
18.0	4500	255
17.3	4200	246
16.0	4020	251
16.2	3420	211
17.0	3480	207
17.6	4320	249
16.6	4440	276
14.9	4800	320
15.2	4380	292
16.0	4080	257
15.3	3060	189
14.9	2880	185
15.3	2940	184
15.6	3660	236
15.1	4260	284
16.1	4200	271
16.8	4440	274
17.4	4320	253
16.4	4500	275
16.0	4800	301
15.5	4320	281

**Table: Extracted Data for time interval 2 min**

<b>Speed (Mile/hr)</b>	<b>Flow (veh/hr)</b>	<b>Density (veh/mile)</b>
16.2	3540	227
16.3	3930	249
15.5	4110	269
15.2	4410	293
15.8	4500	287
16.3	4530	280
16.5	5130	309
15.9	4860	304
16.4	4890	299
16.4	4620	280
16.3	4470	273
16.3	4200	257
16.1	3900	245
16.7	4080	245
16.7	3990	240
17.2	4260	249
17.1	4290	252
17.1	4170	245
16.7	4230	257
16.7	4350	263
16.1	4470	280
15.5	4140	270
16.2	3990	253
15.9	4470	285
16.4	4080	253
15.8	3690	238
16.4	3780	233
16.7	4080	247
16.6	4200	254
16.6	4050	246
16.0	4140	259
16.5	4440	270
16.1	4260	265

<b>Speed (Mile/hr)</b>	<b>Flow (veh/hr)</b>	<b>Density (veh/mile)</b>
16.2	4140	256
16.0	4080	254
16.4	3870	237
16.7	4080	245
16.7	3960	237
17.2	3900	228
17.1	4020	237
17.0	3990	236
16.4	4020	246
16.4	3990	244
16.5	4050	246
16.9	3870	233
17.2	3390	201
16.9	3510	214
17.5	3690	215
17.9	3510	200
17.7	3330	193
17.2	3330	196
17.2	3840	224
17.6	4020	228
17.6	4050	230
17.6	4140	235
17.7	4380	247
17.8	4680	263
17.6	4200	238
17.7	4020	227
17.5	4050	233
17.5	4020	231
17.8	3810	216
17.5	4140	239
17.4	4200	243
17.0	4080	242
17.1	3960	233
17.1	3840	226

<b>Speed (Mile/hr)</b>	<b>Flow (veh/hr)</b>	<b>Density (veh/mile)</b>
16.8	4170	250
16.4	3930	244
16.0	4140	264
16.4	4350	270
16.3	4260	267
15.1	3930	255
15.0	3630	238
15.6	3510	220
15.5	3360	212
15.0	3570	235
15.7	3570	227
16.2	4050	255
16.3	4290	269
16.2	4350	273
16.4	4620	288
16.5	4320	267
15.8	4290	273
16.0	4320	271
14.7	4140	300
12.7	3900	349
11.7	3960	395
10.8	3810	403
9.1	3750	456
8.2	3870	485
7.8	3630	478
8.3	3750	461
8.7	3810	444
8.1	3840	480

**Table: Extracted data for time interval 3 min**

<b>Speed (Mile/hr)</b>	<b>Flow (veh/hr)</b>	<b>Density (veh/mile)</b>
16.0	3980	255
16.0	4160	267
15.8	4400	282
15.9	4740	298
16.0	4700	293
16.3	4620	283
16.2	4700	290
15.9	4520	283
16.3	4460	274
16.5	4400	266
16.6	4420	265
16.6	4260	256
16.6	4120	249
16.7	4140	248
16.8	3980	239
16.7	4140	251
17.0	4340	258
16.5	4440	272
16.2	4280	266
16.4	4080	253
16.2	4300	269
16.2	4020	254
16.1	3940	249
16.0	4180	264
16.2	4180	259
16.3	3980	247
16.5	4020	246
16.5	4020	246
16.3	4240	260
16.2	4040	250
16.1	4220	262
16.5	4240	258
16.5	4080	248
16.5	4020	245
16.4	4080	249
16.6	3940	238
16.8	4140	247
16.8	3940	236
16.7	3920	236
16.7	3920	237
16.7	4060	244
17.0	3940	235
17.2	3680	218
16.9	3640	220
16.9	3780	227

<b>Speed (Mile/hr)</b>	<b>Flow (veh/hr)</b>	<b>Density (veh/mile)</b>
17.2	3580	212
17.2	3620	215
17.5	3480	202
17.7	3580	205
17.6	3620	208
17.4	3900	225
17.4	4080	235
17.7	4200	237
17.7	4140	234
17.5	4040	230
17.7	4080	231
17.6	4380	250
17.6	4200	239
17.8	4060	229
17.6	4200	240
17.4	4080	236
17.2	3880	227
17.1	3900	230
17.3	3960	231
17.2	4160	244
16.9	4120	248
16.4	4160	258
16.3	4240	264
16.2	3980	248
15.7	3780	239
15.9	3860	242
15.9	3820	239
15.3	3840	248
15.1	3840	254
15.8	3740	237
15.9	3720	233
15.8	3820	241
15.9	3880	243
16.2	4300	271
16.0	4300	273
15.9	4260	272
16.3	4360	272
15.6	4200	285
13.9	4100	324
13.1	4240	364
12.4	3980	363
11.1	3860	394
10.8	3860	404
9.8	3740	425
8.9	3740	449
8.3	3900	479
8.0	3780	483

**Table: Extracted data for time interval 5 min**

<b>Speed (Mile/hr)</b>	<b>Flow (veh/hr)</b>	<b>Density (veh/mile)</b>
16.2	4236	265
16.1	4284	269
16.0	4320	272
16.0	4404	277
16.3	4452	274
16.5	4368	266
16.6	4524	273
16.4	4428	270
16.6	4344	263
16.6	4332	263
16.7	4392	264
16.4	4344	266
16.2	4128	258
16.5	4080	250
16.4	4176	257
16.6	4116	252
16.5	4080	250
16.5	4176	256
16.4	4200	259
16.5	4128	253
16.3	4200	260
16.1	4068	256
16.3	4140	257
16.1	4212	264
16.2	4164	258
16.2	4020	250
16.4	3960	242
16.6	4044	246
16.5	4128	251
16.6	3984	241
16.5	4140	252
16.7	4140	249
16.5	4056	247
16.5	4008	244
16.4	4068	248
16.7	3912	236
17.0	3840	229
16.8	3768	227
17.0	3828	228
17.2	3756	222
17.1	3768	224
17.1	3696	220
17.2	3744	220
17.2	3792	223
17.2	3888	229



<b>Speed (Mile/hr)</b>	<b>Flow (veh/hr)</b>	<b>Density (veh/mile)</b>
17.4	3804	221
17.4	3924	228
17.6	3960	227
17.7	3828	218
17.7	3780	216
17.4	3960	228
17.5	4056	233
17.7	4044	228
17.6	4140	236
17.5	4104	236
17.4	4080	235
17.4	4212	243
17.4	4056	234
17.4	4104	237
17.1	4092	242
16.8	4104	247
16.9	4068	245
16.8	4044	245
16.4	3948	241
16.3	3948	242
16.4	3876	237
16.0	3840	240
15.8	3972	252
16.0	3816	240
15.9	3888	245
16.0	4032	253
16.1	4032	252
15.7	4152	264
15.6	4032	259
15.8	3960	251
16.0	3960	248
15.4	3948	265
14.6	3888	285
14.4	4164	320
13.9	4104	325
13.2	4056	346
13.1	4164	357
12.5	3972	362
11.7	3960	379
11.4	4068	396
10.7	3924	410
10.1	3924	424

**Table: Extracted data for time interval 6 min**

<b>Speed (Mile/hr)</b>	<b>Flow (veh/hr)</b>	<b>Density (veh/mile)</b>
16.3	4190	261
16.3	4290	266
16.2	4330	269
16.3	4430	274
16.4	4420	271
16.6	4300	261
16.4	4420	271
16.4	4430	271
16.4	4450	273
16.4	4340	266
16.5	4250	259
16.4	4280	262
16.4	4070	252
16.4	4040	249
16.4	4080	251
16.5	4160	255
16.6	4160	253
16.5	4230	259
16.3	4150	256
16.4	4160	257
16.2	4170	259
16.1	4120	258
16.3	4090	254
16.3	4130	256
16.4	4100	252
16.4	4030	248
16.6	3980	242
16.7	4080	247
16.5	4090	248
16.5	3980	243
16.4	4070	249
16.6	4150	251
16.7	4010	242
16.8	3850	231
16.6	3860	235
16.8	3860	233
17.0	3860	229
17.0	3780	225
17.1	3700	219
17.2	3750	221
17.2	3840	226
17.2	3920	230
17.3	3880	226
17.3	3920	229

<b>Speed (Mile/hr)</b>	<b>Flow (veh/hr)</b>	<b>Density (veh/mile)</b>
17.3	3960	231
17.4	3810	221
17.4	3850	223
17.5	3930	226
17.7	3890	222
17.7	3840	219
17.5	4050	233
17.4	4080	235
17.5	4040	232
17.4	4020	232
17.4	4000	231
17.4	4120	238
17.2	4250	249
17.0	4180	249
17.0	4150	246
16.9	4090	244
16.6	3930	237
16.5	3870	235
16.5	3860	234
16.3	3900	240
16.1	4000	249
16.3	3930	242
16.2	3940	245
16.0	4030	252
16.1	3930	246
15.9	4040	255
15.9	4080	257
15.9	4040	256
15.8	4100	260
15.3	4020	269
14.8	3920	281
14.5	3980	298
14.1	3900	302
13.5	3870	319
13.5	4080	337
12.9	4020	349
12.4	4000	361
12.3	4130	376
11.8	3990	384
11.2	4020	399